Fundação
para a Ciência
e a Tecnologia

Assessing the indirect costs of flooding as a traffic disruption on urban mobility

Fereshteh Jafari Shahdani

UMinho | 2026

Universidade do Minho
Escola de Engenharia

Fereshteh Jafari Shahdani

Assessing the indirect costs of flooding as a traffic disruption on urban mobility

April 2026

Universidade do Minho
Escola de Engenharia

Fereshteh Jafari Shahdani

Assessing the indirect costs of flooding as a traffic disruption on urban mobility

Doctoral thesis

Civil engineering

Work performed under the supervision of:
Jose Campos e Matos
Paulo Ribeiro
Stephen Birkinshaw

April 2026

Copyright and Terms of Use for Third Party Work.

This dissertation reports on academic work that can be used by third parties as long as the internationally accepted standards and good practices are respected concerning copyright and related rights.

This work can thereafter be used under the terms established in the license below.

Readers needing authorization conditions not provided for in the indicated licensing should contact the author through the RepositóriUM of the University of Minho

License granted to users of this work:



Atribuição-NãoComercial-SemDerivações
CC BY-NC-ND

https://creativecommons.org/licenses/by-nc-nd/4.0/

ACKNOWLEDGMENTS

The completion of this doctoral degree signifies the fulfilment of a goal that began five years ago. This journey, marked by a spectrum of emotions ranging from excitement to frustration, has been an arduous yet rewarding path. It is with deep appreciation that I acknowledge the invaluable support and guidance provided by many people throughout this endeavour.

First and foremost, I would like to express my gratitude to my supervisors at the University of Minho, José Matos and Paulo Ribeiro. Your trust and mentorship gave me a valuable opportunity to be part of a stimulating research environment. I am also deeply thankful to my supervisor Stephen Birkinshaw from Newcastle University, for his encouragement and generous support throughout my academic journey.

I should also acknowledge the financial support provided by national funds through the Portuguese Foundation for Science and Technology (FCT), via the Ph.D. grant 2020.06035.BD. Additionally, I acknowledge the support from Traffic and Accident Data Unit of the UK for sharing essential data for the case studies, which were fundamental in developing this thesis.

My eternal gratitude is extended to my parents, my siblings, and their families who have continually buoyed me with their emotional support and encouragement, even from afar. Your unwavering faith has been my pillar of strength.

Finally, I wish to convey my profound thanks to my soulmate, Mohammad. Walking on this Ph.D. path alongside you has been an adventure, replete with challenges yet filled with joy and love. This accomplishment is wholeheartedly dedicated to my entire family.

STATEMENT OF INTEGRITY

I hereby declare having conducted this academic work with integrity. I confirm that I have not used plagiarism or any form of undue use of information or falsification of results along the process leading to its elaboration. I further declare that I have fully acknowledged the Code of Ethical Conduct of the University of Minho.

University of Minho, 05 04 2026



RESUMO

Esta tese investiga a resiliência das redes de transporte em condições de inundação, com foco na região de Tyne and Wear, no Reino Unido. Através da integração de modelação hidrodinâmica de cheias (CityCAT) com simulação microscópica de tráfego (SUMO), o estudo quantifica os impactos indiretos das inundações nos sistemas de transporte de passageiros e de autocarros. São analisados diferentes cenários de cheia (eventos de 1 em 10, 1 em 50 e 1 em 100 anos) para captar a variabilidade da severidade da perturbação. Os resultados mostram aumentos significativos nos tempos de viagem, efeitos de desvio de rotas e ineficiências em toda a rede, mesmo sob inundações moderadas. Destaca-se a vulnerabilidade dos sistemas de autocarros, que, mesmo assumindo uma frota totalmente eletrificada, continuam a gerar custos indiretos consideráveis devido a atrasos no serviço e perdas de tempo dos passageiros. A validação com dados observados de tráfego e contagem de autocarros confirma a fiabilidade da metodologia integrada. A tese sublinha a importância de considerar os impactos multimodais e alerta que ignorar os sistemas de autocarros no planeamento da resiliência pode levar à subestimação dos custos socioeconómicos. Em suma, o trabalho apresenta uma metodologia robusta para a avaliação da resiliência e fornece contributos relevantes para políticas de transporte, medidas de adaptação e planeamento futuro das redes face a condições meteorológicas extremas.

Palavras-chave: CityCAT; Custos indiretos; Inundações; Redes de autocarros; Resiliência dos transportes; Simulação de tráfego; SUMO; Tyne and Wear.

ABSTRACT

This thesis investigates the resilience of transportation networks under flood conditions, with a focus on the Tyne and Wear region in the United Kingdom. Integrating hydrodynamic flood modelling (CityCAT) with mesoscopic traffic simulation (SUMO), the research quantifies the indirect impacts of flooding on both passenger and bus transport systems. The analysis considers multiple flood scenarios (1-in-10, 1-in-50, and 1-in-100-year events) to capture a range of disruption severities. Results reveal significant increases in travel times, rerouting effects, and network-wide inefficiencies, even under moderate flooding. Particular emphasis is placed on the vulnerability of bus systems, which, despite assumptions of fleet electrification, continue to generate considerable indirect costs due to service delays and passenger time losses. Validation using observed traffic and bus count data demonstrates the reliability of the integrated framework. The thesis highlights the importance of accounting for multimodal impacts and proposes that overlooking bus systems in resilience planning may lead to underestimation of socio-economic costs. Overall, the study provides a robust methodology for resilience assessment and offers insights for transport policy, adaptation, and future network planning under extreme weather conditions.

KEYWORDS: Bus networks; CityCAT; Flooding; Indirect costs; SUMO; Traffic simulation; Transport resilience; Tyne and Wear.

TABLE OF CONTENTS

ACKNOWLEDGMENTS ..... **vii**

RESUMO ..... **ix**

ABSTRACT ..... **xi**

TABLE OF CONTENTS ..... **xiii**

LIST OF TABLES ..... **xvii**

LIST OF FIGURES ..... **xix**

LIST OF ABBREVIATIONS AND SYMBOLS ..... **xxi**

1. Introduction **1**

1.1. Background and motivation 1

1.2. Aim and objectives 3

1.2.1. Principal Objective 4

1.2.2. Secondary Objectives 4

1.3. Research Questions 5

1.4. Thesis outline and overview 5

1.5. Supplementary scientific contributions 6

1.5.1. Journal Publications 7

1.5.2. Conference Publications 7

1.5.3. Technical reports 8

2. State of the art in assessing the flooded road networks' indirect **9**

2.1. Introduction 9

2.2. Flood types and hydrological models 12

2.2.1. Flood types 12

2.2.2. Hydrological models 13

2.3. Traffic models 17
2.3.1. Graph-based methods 17
2.3.2. Simulation method 19
2.4. Flood and traffic models integration 23
2.5. Flood Impacts on Bus Transport Networks 25
2.6. Flooded network resilience indicators and improvement methods 28
2.6.1. Pre-event phase: mitigation 31
2.6.2. During hazard: relief 33
2.6.3. Post-event phase: restoration 35
2.7. Key findings and conclusion 36
3. Methodological framework 39
3.1. Introduction 39
3.2. Flood modelling 40
3.2.1. CityCAT Model Overview 41
3.2.2. Model Input Data 41
3.2.3. Flood Scenarios Design 42
3.2.4. Flood Model Outputs for Integration 43
3.3. Integration of Flood and Traffic Models 43
3.3.1. Consideration of Vehicle Types and Multimodal Interactions 46
3.4. Traffic Modelling 46
3.4.1. SUMO Overview 47
3.4.2. Model Input Data 48
3.4.3. Route Assignment 50
3.4.4. Flood Impact Implementation 51
3.4.5. Simulation Outputs 52
3.5. Indirect costs of disruption 52

3.5.1. Time Cost and Network-Wide Delay 52
3.5.2. Emission Cost 53
3.6. Resilience Assessment 54
3.6.1. Flood Return Period Classification 57
3.6.2. Definition of Performance Metrics 57
3.6.3. Threshold Definition and Compliance Matrix 61
3.6.4. Resilience Index Calculation 62
3.6.5. Overall Resilience Calculation of the network 63
4. traffic indirect costs quantification in tyne and wear region 65
4.1. introduction 65
4.2. Case Study overview: Tyne and Wear Region, UK 66
4.3. Scenario setup 79
4.4. Flood impacts on road infrastructure 79
4.5. Flood impact on trips 83
4.6. Traffic Indirect costs 87
4.7. Integration Tool verification and results Validation 89
4.7.1. Verification and validation of CityCAT and SUMO outputs 89
4.7.2. Validation of the integration tool 92
4.7.3. Spatial correlation analysis 94
4.7.4. Sensitivity to the rainfall intensity 96
4.8. conclusion 99
5. resilience assessment and mitigation measures 103
5.1. Introduction 103
5.2. Resilience quantification 103
5.3. Most critical parts of the network 108

5.4. Indirect costs reduction and Resilience improvement by mitigation measures 110

5.5. Conclusion 111

6. Conclusions 113

6.1. Introduction 113

6.2. Contributions to research domain 114

6.3. Synthesis of Findings 115

6.4. Conclusions 116

6.5. Limitations and Future Work Suggestions 118

7. Bibliography 121

LIST OF TABLES

Table 2.1. Causes and impacts of different flood types. 12
Table 2.2. Static inundation maps used in recent flooded road network resilience studies. 14
Table 2.3. Key characteristics of simulation levels 20
Table 2.4. Flood depth-disruption models. 25
Table 2.5. Indicators used in resilience assessments. 30
Table 2.6. Models for resource transportation and evacuation routes. 34
Table 3.1. GTFS dataset files. 50
Table 3.2. Flood Return Period Classification based on Pregnolato *et al.* [55] according to 57
Table 3.3. Performance metrics thresholds adopted from Arango *et al.* [107] for 61
Table 4.1. Scenarios setting..... 79
Table 4.2., Indirect traffic cost of 1-in-100 synthetic scenario in the main roads of Tyne. 87
Table 4.3. Correlation analysis results..... 95
Table 4.4. Indirect traffic cost of 1-in-10 and 1-in-50 synthetic scenarios on the main roads. 99
Table 5.1. Performance matrix for Tyne and Wear main roads network for cars at the hour 104
Table 5.2. Compliance matrix for Tyne and Wear main roads network for cars at the hour 104
Table 5.3. Performance matrix for Tyne and Wear main roads network for buses at the hour 104
Table 5.4. Compliance matrix for Tyne and Wear main roads network for buses at the hour 104
Table 5.5. The assessment of road link criticality is based on the severity of the hazard 109
Table 5.6. Results of the mitigation scenarios 110
Table 6.1. Research gaps identified from literature and how this study addressed them115

LIST OF FIGURES

Figure 1.1. Thesis outline. 6
Figure 2.1. Interaction between 1D and 2D models [2]. 16
Figure 2.2. Transportation network graph and adjacency matrix. 18
Figure 2.3. From macroscopic to mesoscopic and microscopic model. 20
Figure 2.4. Comparing example of transportation network performance with and without. 32
Figure 3.1. Methodological framework of this thesis. 40
Figure 3.2. Integration tool to translate the flood model outputs into the sumo readable files. 45
Figure 3.3. Relationship between floodwater depth and the maximum allowed speed. .. 45
Figure 3.4. Resilience assessment methodology for a flooded network at each time step. 55
Figure 3.5. Metric's level based on user's serviceability for resilience assessment..... 56
Figure 4.1. Location of the Tyne and Wear region, UK. 67
Figure 4.2. Main roads which consist 5.7% of the whole road network in the Tyne and Wear. 68
Figure 4.3. Process of preparing the road and bus network in this study for the Tyne and Wear..... 71
Figure 4.4. Network processing workflow for the main roads in Tyne and Wear region, UK. 71
Figure 4.5. Traffic counters on main roads in 2012 and 2023 in Tyne and Wear region, UK. 73
Figure 4.6. Running vehicles over time in the main roads network of Tyne and Wear region 73
Figure 4.7. Selected rainfall station's location. 74
Figure 4.8. 15-minute recorded rainfall in five stations during the Toon Monsoon. 76
Figure 4.9. Rainfall profile applied for each synthetic scenario. a) 1 in 10 year-2 hours ... 78
Figure 4.10. Peak water depth on roads in Tyne and Wear region during the 1-in-100-year 80

Figure 4.11. Maximum Speed reduction on roads in Tyne and Wear region during the 1-in-100 80
Figure 4.12. Road length and percentage of closed or speed-reduced roads over the flooding 82
Figure 4.13. Speed change percentage distribution of the 1-in-100-year synthetic flood scenario 83
Figure 4.14. Simulation state over time and trip information of 1-in-100 flood scenario.. 84
Figure 4.15. (a) Total trip duration and (b) total trip route length per departure hour..... 86
Figure 4.16. Matching the closed and reduced speed roads from simulation and the real90
Figure 4.17. Comparison between the traffic flow on 28 June 2023 from traffic modelling 92
Figure 4.18. Comparison between the disrupted flow of the Toon Monsoon event on 28 June 94
Figure 4.19. Road length and percentage of closed roads or speed-reduced roads..... 98
Figure 5.1. Evolution of network resilience metrics for car users 105
Figure 5.2. Evolution of network resilience metrics for bus users 105
Figure 5.3. Overall resilience of the network over time..... 107
Figure 5.4. Critical Roads for cars and buses in Tyne and Wear main roads network. 109

LIST OF ABBREVIATIONS AND SYMBOLS

CBN — Complex Bilayer Network

CityCAT — City Catchment Analysis Tool

CML — Coupled Map Lattice

DTM — Digital Terrain Model

DUA — Dynamic User Assignment

EWM — Entropy Weight Method

GSI — Green Stormwater Infrastructure

GIS — Geographic Information System

GTFS — General Transit Feed Specification

IFHI — Index of Flood Hazard Intensity

IPCC — Intergovernmental Panel on Climate Change

ITS — Intelligent Transportation Systems

KPI — Key Performance Indicator

MFP — Mixed Flows in Pipes

MTR — Mass Transit Railway

NPV — Net Present Value

RI — Resilience Index

SUMO — Simulation of Urban MObility

TADU — Traffic and Accident Data Unit

TRADS — Traffic Information Database

UAVs — Unmanned Aerial Vehicles

UFRI — Urban Flood Resilience Index

VSS — Variable Speed Sign

CHAPTER 1

INTRODUCTION

1.1. BACKGROUND AND MOTIVATION

Flooding, driven by climate change and urbanization, poses one of the most significant and escalating challenges to modern urban systems, particularly in terms of its impact on transportation infrastructure. The increasing frequency and severity of extreme weather events have amplified the risks associated with pluvial flooding, leading to widespread socio-economic disruptions and substantial economic losses. Between 1990 and 2014, severe convective storms caused economic damages at an average annual growth rate of 9%, with urban areas being especially vulnerable due to the high concentration of population, infrastructure, and impermeable surfaces [1–3]. In Europe, catastrophic events such as the 2013 floods in Germany and the Czech Republic resulted in losses exceeding $16.5 billion, highlighting the growing urgency of effective urban flood management [1].

Urban road networks are particularly sensitive to flooding. Roads constitute a significant portion of impermeable urban surfaces, approximately 30% in North American cities and 8.5% in London are prone to rapid surface water accumulation during intense rainfall events [4,5]. As a result, flooding often reduces road capacity, either through direct physical damage or by making road sections impassable. These impacts lead to congestion, delays, and extended socio-economic consequences far beyond the immediate flood zone [6,7]. For instance, during the 2021 floods in Germany's Ahr Valley, nearly all bridges were

destroyed, causing critical bottlenecks and severely hindering emergency response and recovery operations [8].

In addition to direct physical and economic consequences, flooding significantly disrupts urban mobility. It delays emergency services such as ambulances and fire trucks, limits access to essential services can isolate entire neighbourhoods [9,10]. These problems are further exacerbated by cascading failures in interdependent infrastructure systems, such as power, water, and telecommunications, which are tightly coupled with transportation networks [10].

Climate change is expected to further compound these issues. According to the Intergovernmental Panel on Climate Change (IPCC), heavy precipitation events are projected to increase in both frequency and intensity throughout the 21st century [3]. Combined with aging infrastructure, urban sprawl, and insufficient drainage systems, this trend is expected to make pluvial flooding even more common and disruptive. The economic consequences can be staggering: for example, road closures during floods in the UK are estimated to cost around £100,000 per hour for each main road affected [11,12].

Despite advances in hydrological and transport modelling, significant knowledge gaps remain regarding the differentiated impacts of flooding on various road users and vehicle types. While many studies have focused on the effects on private vehicles, limited attention has been given to public transport, particularly bus networks, which are critical for low-income and transit-dependent populations [13,14]. Buses are especially vulnerable to flooding due to their reliance on fixed routes, frequent stops, and the need for accessibility at curbside locations. Disruptions to public transport can lead to disproportionate accessibility losses and exacerbate social inequalities [15].

There is a growing consensus in the literature that urban flood resilience must be addressed through integrated, system-level approaches. Resilience, in this context, refers to the ability of transport networks to absorb, adapt to, and recover from flood disruptions while maintaining essential functionality [16]. It encompasses not only the robustness of infrastructure but also system adaptability, redundancy, user behaviour, and the effectiveness of institutional response mechanisms [17].

Among the most promising strategies for improving resilience are mitigation measures, such as infrastructure reinforcements, early-warning systems, dynamic rerouting, and flood-aware trip planning. Such measures help mitigate the functional impacts of flooding and preserve connectivity across the transport network. Evaluating the effectiveness of these measures requires modelling not only the physical flood extent but also its operational consequences on traffic flow and accessibility [18,19].

To date, however, most studies have adopted static or macro-scale perspectives that fail to capture the dynamic and multimodal nature of urban mobility. There is limited integration of high-resolution hydrodynamic flood modelling with fine-grained traffic simulation platforms, which are capable of representing both individual vehicle behaviors and network-wide flow dynamics [13].

This thesis aims to fill that gap by developing an open-source integrated modelling framework that evaluates the indirect impacts of pluvial flooding on both private and public transport modes. The framework combines open-source high-resolution flood modelling with open-source traffic simulation tools, highlighting the accessibility, transparency, and reproducibility of the approach. Beyond assessing current vulnerabilities, it enables the evaluation of adaptation and mitigation measures, examining their effectiveness in reducing disruption costs and improving overall network resilience under different flood scenarios. While the framework will be applied to a specific UK urban region for demonstration, its open-source foundation makes the methodology broadly transferable and supportive of resilience planning in other flood-prone regions worldwide.

1.2. AIM AND OBJECTIVES

The primary aim of this research is to develop an open-source integrated modelling framework that evaluates the resilience of regional road transport networks under pluvial flood conditions. The framework combines CityCAT (for flood modelling) and SUMO (for traffic simulation), both of which are open-source platforms, ensuring transparency, reproducibility, and transferability of results.

This approach places particular emphasis on both private vehicles and public transport—especially buses, given their critical role in providing accessible and sustainable urban mobility. By integrating flood and traffic models at the vehicle level, the framework

enables a detailed assessment of how flood-induced disruptions propagate across multimodal transport systems.

Beyond assessing vulnerabilities, the framework is designed to quantify the indirect costs of disruptions (e.g., travel delays, trip cancellations, and associated economic losses) and to evaluate the effectiveness of adaptation and mitigation strategies in reducing such costs and improving overall network resilience. The ultimate objective is to provide a decision-support tool for transport authorities and policy makers, helping them prioritize resilience investments and design more robust, adaptive transport systems for the future.

1.2.1. Principal Objective

The principal objective of this thesis is to design, implement, and apply an open-source resilience assessment framework that couples dynamic flood modelling (via CityCAT) with traffic simulation (via SUMO). This framework allows for:

- Capturing the spatial and temporal evolution of flood impacts on transport networks,
- Analyzing disruptions at the vehicle level, with emphasis on public buses and their role in maintaining accessibility, and
- Estimating both performance indicators (e.g., trip completion ratio, vehicle delay) and economic costs of disruptions.

1.2.2. Secondary Objectives

To achieve the overall aim, the following specific objectives are defined:

- To review the state-of-the-art in modelling flood impacts on transport systems, with emphasis on resilience, vulnerability, and multimodal perspectives.
- To establish an integrated, open-source simulation framework by coupling CityCAT and SUMO, incorporating road closures and speed reductions as dynamic disruptions.
- To implement the framework in the Tyne and Wear Road network (UK), using real-world traffic counts and GTFS public transport data for calibration and validation.
- To analyse how pluvial flooding affects different modes—particularly private cars and public buses—in terms of accessibility, delays, and service disruptions.

- To evaluate the effectiveness of selected adaptation and mitigation strategies (e.g., rerouting, traffic detours, priority for public buses) in enhancing network resilience.
- To quantify the indirect costs of flood-induced disruptions and assess how resilience measures can reduce these costs over time.
- To provide insights for transport authorities and decision-makers, supporting evidence-based resilience planning in flood-prone urban regions.

1.3. RESEARCH QUESTIONS

This thesis addresses the following research questions:

- How do pluvial flood events affect the performance of multimodal regional transport networks in terms of accessibility, reliability, and functionality?
- What are the differing impacts of flooding on private vehicles versus public buses, and how do these manifest in trip completion, delays, and cancellations?
- How can an open-source coupled flood–traffic framework support evidence-based resilience assessment and decision-making?
- Which indicators and metrics are most suitable for quantifying both resilience and the indirect costs of flood disruptions?
- To what extent can targeted mitigation strategies reduce disruption costs and improve overall network resilience?
- How transferable is the proposed open-source framework for resilience planning in other flood-prone regions worldwide?

1.4. THESIS OUTLINE AND OVERVIEW

This thesis is organized into six chapters, each addressing a distinct component of the research. 1Chapter 1 provides an introduction to the topic, outlining the background, motivation, aim, research questions, and the overall structure of the work. Chapter 2 presents a comprehensive review of the literature related to flood impacts on transport systems and resilience assessment methodologies, identifying current gaps. Chapter 3 describes the methodological framework, including the integration of the CityCAT hydrodynamic flood model with the SUMO traffic simulator. Chapter 4 focuses on the application of this framework to the Tyne and Wear region, detailing the case study context, data sources implementation across different flood scenarios, and flooded traffic

indirect costs quantification. Chapter 5 presents resilience analysis and the evaluation of some mitigation measures to enhance network resilience. Finally, Chapter 6 concludes the thesis by summarizing key findings, discussing limitations, and offering recommendations for future research. The overall structure and workflow of the thesis are illustrated in Figure 1.1

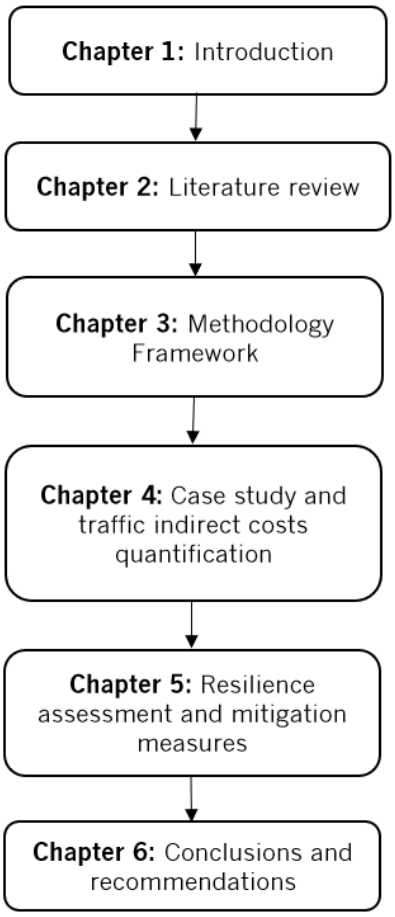


Figure 1.1. Thesis outline.

1.5. SUPPLEMENTARY SCIENTIFIC CONTRIBUTIONS

In addition to the main research activities presented in this thesis, the author has contributed to several scientific publications and technical reports, which have supported and enriched the scope of the work. These contributions have either directly informed the development of the methodological framework or provided complementary insights into flood-related transport resilience.

1.5.1. Journal Publications

(i) **Jafari Shahdani F**, Matos JC, Ribeiro P. A systematic literature review of the hybrid methodologies in assessing flood indirect impacts on transportation. Applied Sciences. 2023 Apr 30;13(9):5595. https://doi.org/10.3390/app13095595

This publication presents a structured review of studies that combine hydrological and transport models to assess flood impacts. It provided the theoretical foundation and justification for the integrated modelling approach used in this thesis.

(ii) **Shahdani, F.J.;** Santamaria-Ariza, M.; Sousa, H.S.; Coelho, M.; Matos, J.C. Assessing flood indirect impacts on road transport networks applying mesoscopic traffic modelling: The case study of Santarém, Portugal. Appl. Sci. 2022, 12, 3076. https://doi.org/10.3390/app12063076.

This work applied a mesoscopic traffic model to assess the impact of flooding on a regional road network. It served as an early proof-of-concept for the methodological approach later developed in this thesis.

1.5.2. Conference Publications

(iii) **Shahdani F.J.,** Son Dang, Matos, J.C. (2025). Resilience Assessment of Transportation Infrastructure in the Northwest Atlantic Corridor. In: ESREL SRA-E in Stavanger, Norway. 15-19 June 2025. doi: 10.3850/978-981-94-3281-3_ESREL-SRA-E2025-P6992-cd

This conference paper presented preliminary results of the resilience assessment performed using the integrated modelling framework. It contributed to the refinement of simulation scenarios and resilience metrics applied in the current thesis.

(iv) **Shahdani F.J**., Santamaria-Ariza, M., Coelho M., Sousa H.S., Matos J.C.. (2021). The indirect impact of flooding on the road transport network: A case study of Santarém region in Portugal. In: 30th European Safety and Reliability Conference (ESREL). Angers, France. 19-23 September 2021. pp. -. ISBN: 978-981-18-2016-8. https://doi.org/10.3850/978-981-18-2016-8_591-cd.

This earlier work explored traffic disruption caused by flooding in a Portuguese region. While conducted as a parallel study, it provided valuable experience in applying traffic models in flood conditions.

1.5.3. Technical reports

(i) **Jafari Shahdani F.**, Son Dang, Matos, J.C. (2025). Models and Tools Closing Gaps, SARIL Deliverable 3.2. Grant Agreement No. 101103978.

This report documents the development of tools for assessing disruptions in transport systems. The modelling framework used in this thesis benefited from the tools and insights developed in SARIL.

(ii) **Jafari F.**, Santamaria-Ariza, M., Arango E., Sousa H.S., Eidsvig U., Nadim F., Piciullo L., Stein- holt I.H., Klaeboe R., Ludvigsen J., Hadjidemetriou G., Matos, J.C., Morais M.. (2021). Dynamic Risk-based Predictive Models, SAFEWAY Deliverable 5.1. Grant Agreement No. 769255.

This deliverable introduced predictive modelling for risk and resilience in transport infrastructure. Although broader in scope, it influenced the approach taken to resilience evaluation in this thesis.

CHAPTER 2

STATE OF THE ART IN ASSESSING THE FLOODED ROAD NETWORKS' INDIRECT COSTS AND RESILIENCE

2.1. INTRODUCTION

The growing frequency and intensity of flood hazards pose critical challenges to road transportation networks worldwide. Recent studies emphasize the importance of assessing these networks' resilience to mitigate the socio-economic impacts of flood-induced disruptions. This chapter provides a comprehensive overview of state-of-the-art methodologies for evaluating the impacts of flooding on road networks, with a focus on hybrid approaches that integrate hydrological and traffic models. A systematic review of recent literature highlights advancements in modelling techniques, including the simulation of flood depths, road inundation, and their effects on transportation systems' functionality and structural integrity. Key findings from the reviewed studies underline the utility of hybrid methods in predicting indirect impacts, such as travel delays, reduced speed, and additional travel distance, while also identifying gaps in current research. By exploring evaluation metrics, disrupted scenarios, and resilience indicators, this chapter aims to establish a foundation for improving flood impact assessment frameworks, informing future studies and infrastructure planning strategies.

Resilience of road transportation networks is a critical aspect of modern infrastructure systems, ensuring the sustainable movement of goods, people, and essential services. Pluvial flooding, caused by intense and short-duration rainfall events, poses a growing threat to these networks. Unlike other types of flooding, such as riverine (fluvial) or coastal floods, pluvial flooding often occurs with little warning, amplifying its disruptive potential. These events can cause significant damage to transportation networks, leading to road closures, increased travel times, and cascading impacts on socio-economic activities. As the frequency and intensity of pluvial flooding are projected to increase due to climate change, enhancing the resilience of road networks to these disruptions has become an urgent priority.

Pluvial flooding impacts transportation networks both directly and indirectly. Direct impacts include physical damage to roads, bridges, and related infrastructure, while indirect effects manifest as disruptions to accessibility, congestion, and economic losses due to delays. For example, the 2011 flooding in Barcelona disrupted transportation services, caused road closures, and led to cascading failures in traffic light systems, ultimately affecting urban mobility and emergency responses [2]. These disruptions highlight the critical need for comprehensive assessments and mitigation strategies to enhance the resilience of road networks against pluvial flooding.

Research in this domain has advanced significantly, exploring diverse methodologies to assess flood impacts, develop resilience metrics, and propose strategies for mitigation and adaptation. Kadaverugu *et al.* [3] analysed flood modelling techniques, emphasizing the evolution from traditional hydrological approaches to real-time, crowd-sourced modelling methods. This evolution reflects advancements in data collection, computational power, and analytical frameworks, enabling more accurate assessments of pluvial flood impacts on transportation networks. Tachaudomdach *et al.* [4] conducted a systematic review of transportation infrastructure resilience to flooding, underscoring the importance of integrating these methods into broader urban planning initiatives.

Despite these advancements, gaps remain in the comprehensive assessment of road network resilience under pluvial flooding conditions. Many studies have focused on direct impacts, such as physical damage to infrastructure, while the indirect impacts—such as loss of accessibility, cascading system failures, and prolonged recovery times—remain

underexplored. Rebally *et al.* [5] identified hybrid methodologies as effective tools for capturing the spatial and temporal dynamics of flood events and their impacts on transportation networks. These hybrid approaches, which combine flood and traffic models, offer a promising avenue for understanding and mitigating the complex interactions between pluvial flooding and transportation networks.

The concept of resilience has been widely applied in various disciplines, including engineering, geography, and urban planning. In the context of road networks, resilience is defined as the ability to anticipate, absorb, adapt to, and recover from disruptive events. Bruneau *et al.* introduced the "4R" framework—robustness, redundancy, resourcefulness, and rapidity—which has become a cornerstone of resilience studies [6]. However, its application to pluvial flooding scenarios, particularly in urban environments, remains limited. Addressing these gaps requires a multi-disciplinary approach that integrates pluvial flood modelling, traffic simulation, and resilience assessment frameworks.

The rest of this chapter is developed as follows. Section 2.2 provides an overview of the different types of floods and applied hydrological models in assessing flood impacts on road networks. Section 2.3 analyses and discusses the traffic models used in these methods, highlighting their applications and limitations. Section 2.4 reviews the integration methods of flood and traffic models, identifying challenges and opportunities for more effective analysis. Section 2.5 discusses the flood impact on the bus transportation system. Section 2.6 explores improvement strategies for flooded road network resilience and examines the indicators adopted to evaluate resilience. Finally, Section 2.7 summarizes the key findings and highlights the concluding remarks, setting the stage for the subsequent chapters.

By synthesizing insights from recent literature, this chapter aims to provide a comprehensive overview of the state of the art in assessing pluvial flood impacts on road transportation networks. It explores the methodologies, evaluation models, and resilience improvement strategies developed over the past decade, identifying key research priorities for enhancing road network resilience in the face of pluvial flooding.

2.2. FLOOD TYPES AND HYDROLOGICAL MODELS

2.2.1. Flood types

The main types of floods include fluvial, pluvial, and coastal floods, each arising from different hydrometeorological and geomorphological conditions (as shown in Table 2.1). Understanding the differences in these flood types is crucial for assessing their specific impacts on road networks and developing effective resilience strategies.

Fluvial floods, also known as riverine floods, occur when excessive rainfall or snowmelt causes rivers to exceed their banks, inundating adjacent areas. These floods can erode embankments, undermine bridge foundations, and submerge road networks for extended periods, leading to severe disruptions in transportation services. Fluvial flooding often affects major commuter routes located along river valleys, increasing congestion and travel delays [7]. Coastal floods, on the other hand, result from storm surges, high tides, and sea-level rise, particularly affecting low-lying coastal urban areas. These floods can inundate key roadways, leading to significant accessibility loss and economic disruptions [8].

Table 2.1. Causes and impacts of different flood types.

Flood type	Causes	Impacts
Pluvial/ground	Extreme rainfall	Embankment and cutting: settlement, sliding; Pavement: inundation, deterioration
Fluvial/riverin	Ample river charge	Bridge: foundation scour, shear failure of foundation, inundated deck, washed-away deck; Embankment and cutting: settlement, sliding, foundation scour; Pavement: inundation, deterioration
Coastal	Storm surge, sea level rise, and waves	Bridge: foundation scour, shear failure of foundation, inundated deck, washed-away deck; Embankment and cutting: settlement, sliding; Pavement: inundation, deterioration

Pluvial flooding, which is the primary focus of this research, occurs due to intense rainfall overwhelming urban drainage systems, leading to surface water accumulation on road networks. Unlike fluvial and coastal floods, pluvial flooding is independent of river or sea conditions and can develop rapidly, often within minutes or hours of heavy rainfall events [11]. This type of flooding is particularly problematic in urban environments where impervious surfaces, such as roads and pavements, prevent water infiltration, exacerbating flood severity. The frequency of pluvial flooding has been increasing due to climate change and urban expansion, making it a critical concern for transportation resilience planning [9,12].

The economic and societal consequences of pluvial floods are substantial. Studies estimate that flood-induced road disruptions can cost up to £100,000 per hour for each affected main road [10]. Moreover, road networks play a critical role in emergency response; disruptions due to pluvial floods can severely hinder the mobility of first responders, increasing the risk to human life [13]. Road surfaces, which constitute a significant portion of urban landscapes, are particularly vulnerable to pluvial flooding. In London, for example, roads occupy approximately 8.5% of the urban area, whereas in North American cities, the proportion is as high as 30% [20,21]. These impervious surfaces contribute to rapid runoff accumulation, increasing flood severity and reducing road functionality [22]. Traffic congestion resulting from flooded roads can propagate through the network, causing widespread delays, increased emissions, and economic losses [23,24].

The Intergovernmental Panel on Climate Change (IPCC) has projected that heavy precipitation events are "very likely" to increase in frequency and intensity throughout the 21st century, further exacerbating the challenge of maintaining resilient transportation systems [9,12]. Consequently, accurate modelling of pluvial flood dynamics is essential for designing adaptive strategies to mitigate disruptions to road networks.

2.2.2. Hydrological models

Hydrological models are central to understanding and quantifying flood hazards and their impact on road infrastructure. These models provide crucial insights into flood depth, extent, duration, and dynamics—factors that directly influence transportation network functionality and resilience. Broadly, flood models used in transportation resilience assessments can be divided into two categories: static inundation models and dynamic flood models, depending on whether or not they account for the spatiotemporal progression of flood events.

2.2.2.1. Static Inundation Models

Static flood maps assume a fixed flood extent and depth over time and are typically based on historical data, synthetic return periods, or worst-case scenarios. These maps are useful for identifying potentially vulnerable segments of a network and serve as a foundational input for many flood risk assessments and preliminary infrastructure planning studies. Table 2.2 provides a comprehensive summary of widely used static flood maps, their

geographic focus, flood type, modelling methodology, and key findings from recent literature.

For example, the FIRMs developed in the United States (Suarez *et al.* [25]) were used to assess urban network disruptions under fluvial and coastal floods. In the UK, national datasets such as RoFRS, uFMfSW, and AStGWF (Hankin *et al.* [38]) support infrastructure planning and risk analysis under various flood types.

In Poland, Borowska-Stefańska *et al.* [26] applied spatial vulnerability modelling to prioritize critical infrastructure. Similarly, Ahmad *et al.* [27] used remote sensing to assess flood-related land cover change in Kashmir Valley. In the US, Kasmalkar *et al.* [25,28] linked coastal flood projections to traffic disruption modelling in the San Francisco Bay Area.

In Iowa, Alabbad *et al.* [29] linked flood exposure to accessibility loss for critical facilities. In Portugal, Shahdani *et al.* [19] demonstrated the application of mesoscopic traffic modelling to evaluate indirect delays during pluvial flooding in Santarém.

Table 2.2. Static inundation maps used in recent flooded road network resilience studies.

Flood map	Applied region	Flood type	Purpose / Objective	Method / Data used	Key findings	Reference
FIRMs	United States	Fluvial and coastal	Evaluate systemwide impacts of flooding on urban transportation	GIS overlay, travel time estimation, historical flood and traffic data	Flooding causes significant increases in travel time and accessibility loss	Suarez *et al.* [7]
RoFRS	England	Fluvial and coastal	Assess flood risks to the strategic road network	Hydraulic modelling and spatial risk analysis	Identifies key segments of the road network highly exposed to flood risk	Hankin *et al.* [30]
uFMfSW	England and Wales	Pluvial	Identify areas at risk of surface water flooding	Pluvial flood modelling using rainfall-runoff and topography	Pinpoints surface water flood hotspots, supporting risk-based planning	Hankin *et al.* [30]
AStGWF	England, Wales, and Scotland	Pluvial	Provide flood hazard information for planning and infrastructure design	Combining flood model outputs with infrastructure exposure data	Supports infrastructure resilience planning through national-scale mapping	Hankin *et al.* [30]
Poland's flood map	Poland	Fluvial and coastal	Evaluate road vulnerability to flooding and create national flood map	Hydrodynamic modelling, GIS-based vulnerability assessment	Highlights flood-prone areas and vulnerable road assets in Poland	Borowska-Stefańska *et al.* [26]
Kashmir flood map	Kashmir valley	Fluvial	Assess land use changes and flood extent in Dal Lake region	Satellite imagery and field validation, land cover classification	Flooding led to substantial land use transformation in key areas	Ahmad *et al.* [27]

ART flood map	San Francisco Bay Area	Coastal	Assess resilience of traffic systems under episodic coastal flooding	Coastal flood modelling integrated with traffic simulation (SUMO)	Identifies vulnerable traffic segments and impact thresholds from flooding	Kasmalkar *et al.* [25,28]
Iowa flood inundation map	Iowa	Fluvial and coastal	Analyze accessibility to critical amenities during flooding	Dynamic flood simulation and accessibility mapping	Demonstrates reduced accessibility to emergency services under flood conditions	Alabbad *et al.* [29]
Santarém flood map	Santarém	Fluvial	Evaluate flood-induced impacts on traffic dynamics using simulation	Pluvial flood model + mesoscopic traffic simulation (SUMO)	Simulates travel time delays and vehicle rerouting under flood scenarios	Shahdani *et al.* [19]

These studies demonstrate the relevance of static models for high-level planning, particularly when real-time data or computational resources are limited. However, they cannot capture the progression and timing of flood-induced impacts, leading to the growing use of dynamic hydrological models.

2.2.2.2. Dynamic Hydrological Models

Dynamic models simulate the evolution of flooding over time and space. They may involve rainfall-runoff processes [31], one-dimensional (1D) river channel flow [32], two-dimensional (2D) overland flow models [33], or coupled 1D/2D systems [34,35]. These models provide a more realistic understanding of flood propagation, recession, and their interactions with road infrastructure.

Among them, CityCAT (City Catchment Analysis Tool) stands out as a high-resolution, fully hydrodynamic model developed by Newcastle University which is publicly available upon request from the university. According to Glenis *et al.* [36], CityCAT simulates both surface runoff and drainage system response using a 2D finite volume method over a high-resolution grid, allowing the inclusion of building footprints, road geometry, and terrain elevation. The 1D component handles the flow within the urban drainage network, enabling the model to represent surcharge and surface-drain interactions.

Figure 2.1 illustrates how surface and subsurface interactions are handled in coupled 1D/2D models like CityCAT. The surface water flows are routed through the 2D

grid, while flow into and out of the underground drainage system is captured at inlet and outlet nodes, improving realism in urban flood modelling.

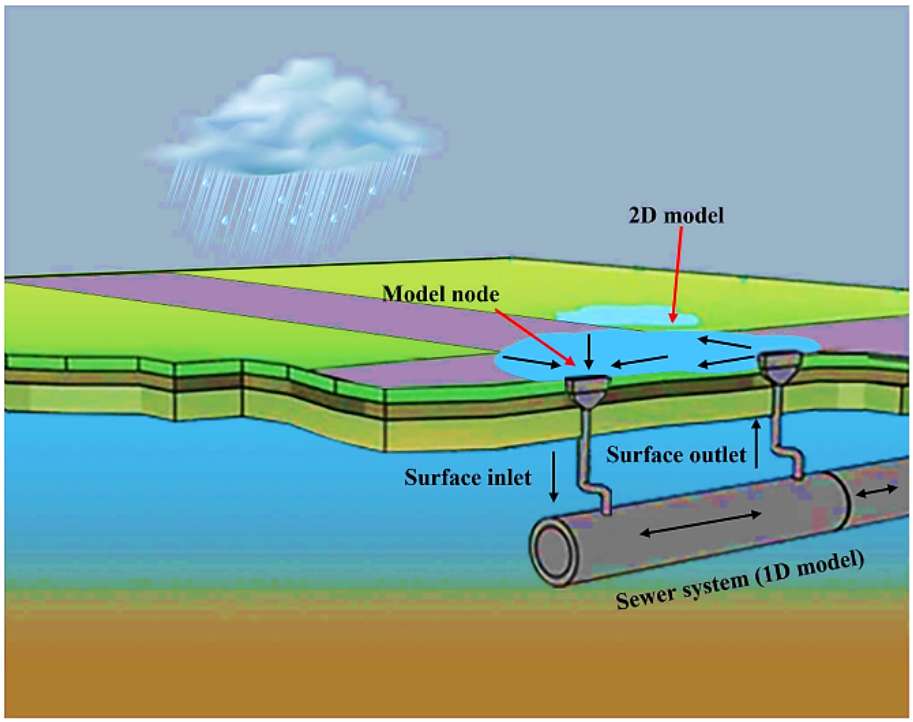


Figure 2.1. Interaction between 1D and 2D models [2].

CityCAT can simulate a wide range of synthetic or historic storm events, and account for urban green infrastructure and adaptation measures. While its output is highly detailed and validated in multiple studies, its computational load can be significant in large domains, making GPU acceleration or parallel computing important in practice.

In this thesis, CityCAT is used to simulate pluvial flooding in the Tyne and Wear region under synthetic return periods (1-in-10, 1-in-50, and 1-in-100 years). Its outputs, water depth maps at 20-minute intervals, are then used to influence vehicle speeds and network accessibility in traffic simulations using SUMO. Unlike studies relying on static flood overlays, this time-sensitive approach allows a realistic evaluation of how disruptions evolve during an event.

This dynamic flood simulation also enables a richer assessment of resilience and supports the development of adaptation strategies that consider both timing and severity of disruption. The integration of CityCAT with SUMO enables a hybrid flood-traffic simulation framework that addresses the limitations observed in static-only studies.

2.3. TRAFFIC MODELS

Transportation networks consist of interconnected assets that interact with natural environments. During flood hazards, individual components of these networks may fail, leading to significant disruptions in traffic flow. Assessing the impact of flooding on transportation systems is crucial for informing decision-makers and enabling effective mitigation strategies to minimize adverse consequences.

Recent studies have employed two widely used approaches for evaluating flood impacts on traffic including graph-based analysis and simulation techniques. These methodologies help analyze how transportation networks respond to flood hazards, particularly in terms of capacity reduction and potential road or bridge closures. By capturing these disruptions, these assessment methods provide valuable insights into the resilience of road networks, aiding in the development of strategies to enhance their robustness against future flood events.

2.3.1. Graph-based methods

The topological or graph-based approach is widely regarded as one of the most effective and commonly used methods for assessing the resilience of transportation networks, primarily due to its simplicity. In this method, a real-world transportation network is represented as a set of vertices connected by edges [37].

Formally, a graph G is defined as G = {V, E}, where V = {v_1, v_2, …, v_n} represents a subset of vertices corresponding to specific starting and ending points within the network. These vertices serve as origins and destinations for transportation users. Meanwhile, the subset E = {e_1, e_2, …, e_n} consists of road segments and bridges that establish connections between these vertices. The connectivity between any two vertices, i and j is captured within an adjacency matrix, providing a structured representation of the network's topology:

$$A_{ij} = \begin{cases} 0, & if\ there\ is\ no\ edge\ between\ vertices\ i\ and\ j \\ 1, & otherwise \end{cases} \quad (1)$$

where A = adjacency matrix (Figure 2.2). The topological approach has been extensively applied to evaluate the performance of transportation networks during hydrological disasters, particularly in identifying critical vertices and edges within the network

[34,38,39]. In these studies, road segments and bridges are represented as edges, while origins and destinations are depicted as vertices. When a transportation network is affected by flooding, the inundated road segments, bridges, and affected origins and destinations are removed from the network graph. By comparing the original and flooded network graphs, the impact of hydrological disasters on transportation network resilience can be visually assessed [40].

Using this approach, Barker *et al.* [41] evaluated the significance of network components by measuring both the negative effects of link disruptions on system resilience and the positive effects of link survivability. Furthermore, Anderson *et al.* [42] developed a method to efficiently detect isolated nodes within the network, where an origin is classified as isolated if it lacks a viable route to any destination.

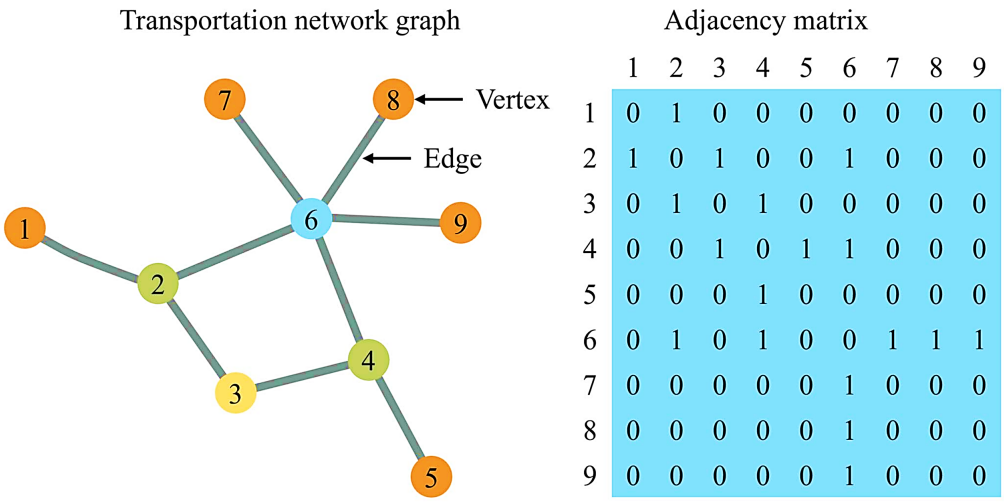


Figure 2.2. Transportation network graph and adjacency matrix.

In practical applications, bridges can be represented as vertices, given their critical function in linking areas separated by water bodies or major highways. For instance, Alabbad *et al.* [29] modeled bridges and essential emergency facilities as vertices to estimate the number of people who could access the nearest emergency service before and after a flood event. Similarly, some studies have considered road intersections as vertices to account for interactions between intersecting roads [43,44] Depending on the research objective, particularly in connectivity analysis between specific roads, roads themselves can be designated as vertices, while intersections are treated as edges [44].

The topological approach effectively captures the relationships among network components and helps assess network resilience characteristics. While it is relatively simple to implement and interpret, this method does not account for the degradation of edge capacity, which can exacerbate network vulnerability during extreme events. Furthermore, the information available in network graphs is often insufficient for estimating economic losses, particularly indirect costs such as travel delays. Additionally, the topological method does not distinguish between different vehicle types, such as passenger cars and heavy trucks, which may have varying speed limits and operational constraints within the network.

2.3.2. Simulation method

Simulation plays a crucial role in assessing the flood impacts on traffic, offering detailed and dynamic insights that surpass the capabilities of topological (graph-based) methods. Unlike purely structural representations, simulation approaches incorporate multiple aspects of the transportation system, such as link-level free-flow speeds, congestion dynamics, speed reductions under flooding, and the origin-destination (OD) travel demands of various user groups. These models are capable of identifying critical links, evaluating cascading failures, and analyzing adaptive behaviors like vehicle rerouting in response to road closures.

Simulations allow for the quantification of travel delays, traffic redistribution, bottleneck formation, and overall degradation of network functionality. As such, they provide a comprehensive framework to evaluate the functional performance of road systems under hydrological hazards, which is a key dimension of transportation resilience assessment. Furthermore, simulations can differentiate between scenarios where drivers are pre-informed about network disruptions (e.g., through early warning systems or real-time navigation aids) and those where drivers encounter flooded roads unexpectedly and adapt reactively.

Traffic simulation models are generally divided into three main categories based on the level of detail they provide and the scale at which they operate: macroscopic, mesoscopic, and microscopic models. These categories reflect the abstraction level used to

model traffic flows and user behaviors. Figure 2.3 presents an illustrative comparison of these three simulation levels, highlighting their main attributes and use cases.

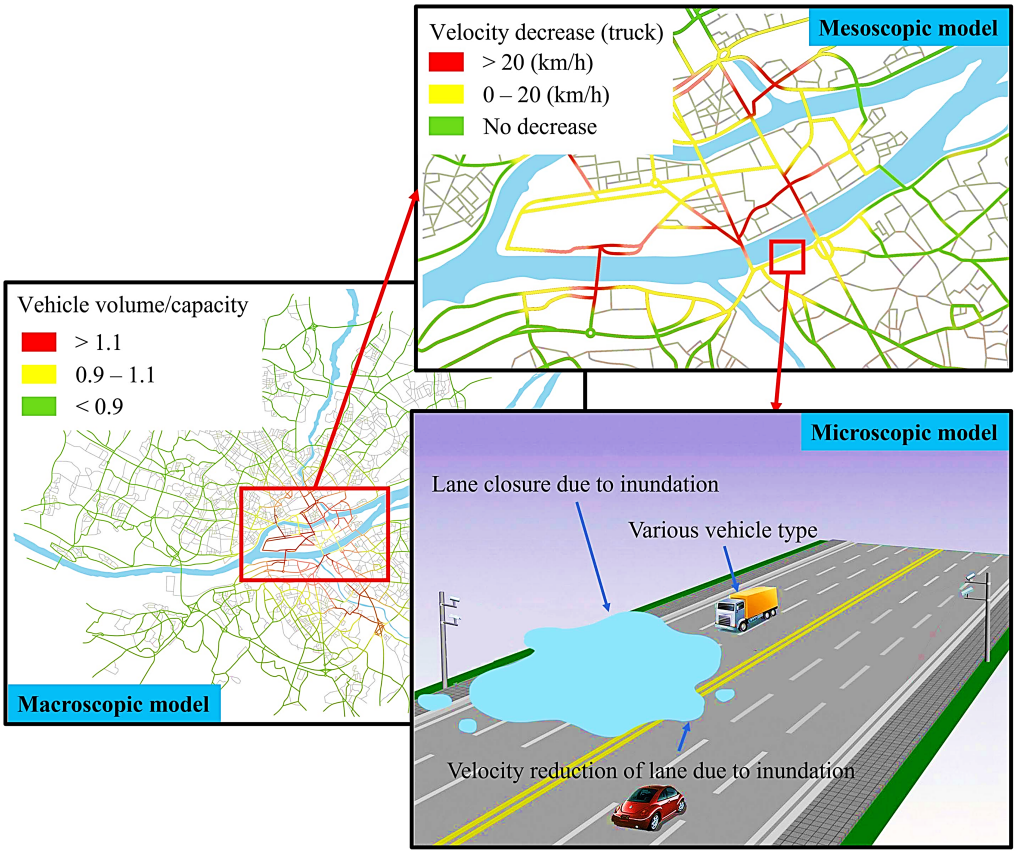


Figure 2.3. From macroscopic to mesoscopic and microscopic model.

Each modelling level serves different analytical needs, depending on the trade-offs between computational cost, spatial/temporal resolution, and behavioral detail. For instance, macroscopic models simulate traffic as continuous flows, making them suitable for large-scale evaluations with minimal computation, while microscopic models focus on individual vehicle behaviors, providing greater accuracy in smaller areas but at higher data and processing demands. To facilitate a clearer comparison, Table 2.3 provides an overview of key attributes and limitations of each simulation type.

Table 2.3. Key characteristics of simulation levels

Simulation Level	Resolution	Behavioral Detail	Data Requirements	Computational Cost	Common Tools
Macroscopic	Network-level (flow/density per link)	No individual driver behavior; uses aggregate flow	Low (basic network + average flows)	Low	VISUM, EMME, TransCAD
Mesoscopic	Vehicle-level (aggregated behavior)	Individual OD trips, simplified interactions	Moderate (traffic flows + link performance functions)	Medium	AIMSUN meso, DynusT, SUMO

Microscopic	Vehicle-level (individual behavior)	Detailed car-following and lane-changing behavior	High (vehicle types, routes, driver parameters)	High	SUMO, VISSIM, AIMSUN micro

The following subsections provide further elaboration on each model type, along with examples from the literature that have used them for flood impact assessment.

2.3.2.1. Macroscopic simulation

Macroscopic traffic models describe traffic flow using aggregated parameters such as density, flow, and average speed across road segments. This modelling level treats traffic similarly to fluid dynamics, where individual vehicle behavior is not captured. Parameters such as free-flow speed, speed-density relationships, and flow-capacity constraints are often used to simulate congestion and travel delays.

In flood impact analysis, macroscopic models are widely used to assess general impacts at large scale, such as regional or urban levels. For example, Chang *et al.* [45] analyzed traffic disruptions in Portland due to flooding by overlaying flood maps on road network data. Yin *et al.* [46] estimated travel delay durations in Shanghai under different flood return periods using a similar overlay technique. Singh *et al.* [47] applied macroscopic modelling to generate vulnerability maps in India, indicating speed reductions under various rainfall-induced flooding scenarios.

While macroscopic simulations are computationally efficient and suitable for high-level planning, they have several limitations. These models do not distinguish between different vehicle types or simulate individual behaviors such as lane changing, overtaking, or dynamic rerouting. Moreover, they often assume uniform impact on all lanes of a flooded road, which may not reflect real-world conditions where partial functionality remains.

2.3.2.2. Microscopic simulation

Microscopic traffic models simulate the behavior of individual vehicles and drivers in the network. Each vehicle is represented with specific attributes such as vehicle type, speed profile, and driver reaction time. These models incorporate detailed behavioral sub-models like car-following, lane-changing, and gap acceptance to replicate realistic traffic flow.

Microscopic simulations are particularly useful for flood impact studies requiring fine-scale spatial and temporal resolution. For instance, Shabou *et al.* [48] introduced the MobRISK model to estimate driver exposure to flash floods based on driver types and behaviors. Wang *et al.* [49] quantified the increase in travel times caused by floods across China's road network using a high-resolution vehicle-level simulation.

Simulation of Urban MObility (SUMO), an open-source microscopic traffic simulator, has been widely used in recent transport studies. Pyatkova *et al.* [50] developed a SUMO-based framework to evaluate economic impacts by simulating fuel consumption and speed variations. Knight *et al.* [51] assessed the role of green stormwater infrastructure using SUMO, analyzing how changes in flood extent affected average speeds and congestion levels. These detailed analyses enable a more accurate estimation of indirect impacts, such as increased emissions and vehicle operating costs.

Despite its advantages, microscopic modelling requires extensive data inputs and high computational power.

2.3.2.3. Mesoscopic simulation

Mesoscopic traffic models offer a middle ground between the high-level abstraction of macroscopic models and the detailed representation of microscopic simulations. In these models, vehicles are tracked individually but their behavior is governed by aggregate traffic flow principles. Mesoscopic simulations incorporate origin-destination data, departure time, and routing behavior while simplifying intra-link interactions.

Suarez *et al.* [7] applied a mesoscopic model to assess the impact of flooding on commuter and shopping trips in the Boston Metro Area. Their model used household-level data to determine which trips would be cancelled and which could be rerouted to alternative destinations. Shahdani *et al.* [19] employed a mesoscopic traffic model to simulate the effects of various flood disruption scenarios in Santarém, Portugal, capturing changes in route choices, travel times, and vehicle volumes. Evans *et al.* [2] analysed speed reductions in Barcelona under different flood intensities and developed exceedance probability curves to estimate economic losses. These applications demonstrate the efficiency and flexibility of mesoscopic simulations in capturing realistic traffic responses without incurring the full computational burden of microscopic modelling.

In simulation-based analyses, two main assumptions govern rerouting behaviour. Some studies assume complete driver awareness, where drivers adjust routes immediately upon detecting a flooded segment using real-time information or navigation systems [45,48,49]. Others adopt a more realistic approach, modelling limited driver awareness—where rerouting only occurs when drivers physically encounter the flooded road segment [19,52]. These distinctions significantly influence simulation outputs and are essential for accurate resilience assessment.

Overall, the simulation approach enables the comprehensive analysis of flood-induced disruptions and supports the development of mitigation strategies to enhance network robustness. By integrating flood depth, road geometry, and behavioural responses, simulation methods provide powerful tools for evaluating transportation system resilience under hydrological stress.

2.4. FLOOD AND TRAFFIC MODELS INTEGRATION

The integration of flood and traffic models plays a crucial role in understanding the dynamic interactions between hydrological events and urban mobility. This process helps quantify how pluvial flooding affects road network performance and informs the development of effective adaptation and mitigation strategies. Integration methods can be broadly categorized into two types: static and dynamic.

Static integration assumes flood conditions remain constant throughout the simulation. This binary approach (flooded vs. non-flooded) is suitable in cases where flood propagation is slow or irrelevant to traffic impacts. For example, studies such as Suarez *et al.* [7] and Alabbad *et al.* [29] apply static models to evaluate disrupted links and reconfigure shortest paths in simplified network graphs. While computationally efficient, static integration tends to underestimate the temporal variability of flood impacts and does not accurately reflect real-time driver behavior.

Dynamic integration, in contrast, incorporates the temporal evolution of flooding. By accounting for the propagation of floodwater over time, it allows for real-time adjustments to road accessibility and traffic circulation. Studies like Yin *et al.* [46], Wang *et al.* [49], and Kasmalkar *et al.* [25] have demonstrated how dynamic flood models—

especially when linked with traffic simulation platforms—can more realistically capture the cascading effects of flooding. This dynamic approach enhances the accuracy of resilience assessments, especially when evaluating rerouting, congestion formation, or travel delay progression.

A core aspect of this integration lies in how flood depth affects vehicle movement. A range of flood depth-disruption relationships has been developed in recent years to define speed reduction or road closures based on inundation levels. These are summarized in Table 2.4, which includes key disruption rules such as vehicle inaccessibility thresholds (Li *et al.* [53]), closures for emergency vehicles (Pérez-Morales *et al.* [54]) and widely used functions to relate inundation depth to maximum allowable speed (Pregnolato *et al.* [13,55]). For instance, Pregnolato *et al.* [13] proposed the following empirical function, referred to here as Equation. (2), to relate vehicle speed with flood depth:

$$V = 0.0009w^2 - 0.5529w + 86.9448 \quad (2)$$

Where V is the flooded link speed in km/h and w stands for the inundation depth in mm. This quadratic function was derived from safety literature, experimental studies, expert opinion, and real-world video analysis, and is commonly applied in simulation studies (e.g., [13,25,49,55]) to dynamically represent vehicle speed under different flood conditions.

Despite the predominance of flood depth in these models, additional hydrodynamic parameters, such as floodwater velocity and duration, can significantly alter traffic impacts. For instance, Dong *et al.* [40] showed that even modest floods with high velocity could trigger systemic collapse in road networks due to the compound effects of vehicle displacement, increased accident risk, and roadbed erosion.

Moreover, model integration is enhanced when a bidirectional feedback mechanism is introduced. In such systems, traffic behavior may influence water accumulation patterns (e.g., vehicle-induced water displacement) and vice versa. Although this is still an emerging area of research, it represents a frontier in fully coupling flood-traffic systems.

In practice, integration is often conducted using GIS platforms as an intermediary between hydrologic models (e.g., CityCAT) and traffic simulators (e.g., SUMO). These tools

allow for the spatial overlay of flood layers and road networks to dynamically update link attributes such as speed, closure status, or routing availability.

Table 2.5. Flood depth-disruption models.

Relationship	DESCRIPTION OF CRITERIA/APPLICATION	APPLIED REGION / CASE STUDY	References
Closure: flood depth > 0	Full closure of roads upon any water depth presence	Boston Metro Area, Iowa, USA	Suarez *et al.* [7], Alabbad *et al.* [29], Dong *et al.* [40], and Wang *et al.* [56]
Inaccessibility of vehicle: flood depth > 0.15 m	Minimum depth beyond which typical vehicles are unable to operate	Nanjing, China	Li *et al.* [53]
Closure: flood depth > 0.3 m	Standard threshold for road closure in urban hydrologic studies	Shanghai, China; Global urban settings	Pyatkova *et al.* [50] and Yin *et al.* [46]
Closure for emergency vehicles: flood depth > 0.5 m/flooded area > 5 m2	Special condition for emergency vehicle operation with area threshold	Spain	Pérez-Morales *et al.* [54]
Closure: flood depth >= 0.3 m; Speed reduction to 20 km/h: 0.1 m < flood depth < 0.3 m	Differentiated treatment for partial vs full flooding scenarios	Santarém, Portugal	Shahdani *et al.* [19]
Equation. (2)	Quantitative estimation of max safe speed based on flood depth	San Francisco Bay Area, UK (Newcastle)	Kasmalkar *et al.* [25], Pregnolato *et al.* [13,55], and Wang *et al.* [49]

To conclude, accurate flood-traffic integration requires consideration of not only static vs. dynamic frameworks but also the granularity of road data, driver behavior models, and physical flood characteristics. Models like CityCAT, which provide flood depth, when linked to simulation platforms like SUMO, can produce more realistic assessments of transport network resilience. This is particularly valuable for real-time decision-making and for the testing of mitigation measures under evolving climate risks.

2.5. FLOOD IMPACTS ON BUS TRANSPORT NETWORKS

Although the literature on flood-related disruptions in transportation systems has grown in recent years, studies specifically addressing the impacts of flooding on bus transit networks remain relatively limited. Much of the existing research has traditionally focused on rail systems, metro infrastructure, or general transport network performance, often overlooking the unique operational characteristics and vulnerabilities of surface bus networks. However, several recent contributions have attempted to bridge this gap by

analyzing the exposure, resilience, and recovery of bus-based systems during extreme weather events such as floods.

Alabbad and Demir [57] investigated the flood risk to public transit systems in Johnson and Linn counties, Iowa, with a focus on bus routes and accessibility. By integrating Geographic Information System (GIS) tools with General Transit Feed Specification (GTFS) data and overlaying simulated 500-year flood maps, they identified significant service disruptions. Their analysis revealed a loss of 526 bus stop visits during the morning peak period in Johnson County, and a notable decline in job accessibility—by 11.5% in Linn County and 7.2% in Johnson County. The results demonstrated that these disruptions disproportionately affected socioeconomically vulnerable groups, such as low-income individuals and households without access to private vehicles. The study highlighted the critical need for enhancing the flood resilience of bus infrastructure and recommended measures such as temporary bus service adjustments, adaptive routing strategies, and investment in flood-resilient infrastructure.

Zhu *et al.* [58] conducted a resilience assessment of a bus–metro hybrid network in Zhengzhou, China, emphasizing how intermodal interactions influence system robustness under flood conditions. They built a multi-layer complex network model that incorporated both physical infrastructure and service-level characteristics, and simulated flood-induced cascading failures. Their model considered flood risk indices derived from meteorological and topographic data, along with network centrality metrics, to identify vulnerable nodes. Importantly, they found that the failure of key metro nodes led to increased demand on the bus system, revealing the systemic dependencies between modes. Their simulations showed that targeted recovery strategies prioritizing high-betweenness nodes significantly accelerated functional restoration. This work underlined the importance of multi-modal coordination in resilience planning.

Ma *et al.* [59] further explored the dynamic behavior of a bus–metro complex bilayer network (CBN) under rainstorm conditions. Their approach involved a flow-based coupled map lattice (CML) model to simulate cascading failures resulting from overload and intermodal interactions. The study introduced a “vulnerability operator” combining changes in network structure (e.g., size of the largest connected component) and function (e.g., passenger volume). Notably, they identified a two-phase failure pattern triggered by

rainstorm intensity thresholds and showed that network degradation was more strongly driven by topological breakdown than by passenger loss. The authors also demonstrated that reducing node coupling strength (i.e., the interaction between metro stations and bus stops) could effectively decrease system vulnerability, offering valuable operational insights for emergency management.

A different approach was taken by Huang *et al.* [60], who developed a resilience analysis framework tailored to urban bus networks in Beijing. Their model combined the CRITIC–entropy weighting method for indicator selection, resilience cycle theory for modelling disturbance phases, and complex network theory for system evaluation. The framework provided a method for quantifying route-level resilience, by incorporating temporal and spatial dynamics of bus operations. Their findings emphasized that certain bus routes consistently exhibited higher resilience, which could be attributed to their topological position and redundancy. This method allows transportation agencies to identify weak spots in the network and prioritize them in resilience improvement efforts.

Mudigonda *et al.* [61] assessed the recovery of New Jersey's public transit systems—especially bus versus rail services—after Hurricane Sandy using a wide range of Big Data sources. Their findings showed that the bus system, relying on road infrastructure, recovered significantly faster than the rail network, which suffered from power outages and system-wide damage. They developed resilience performance metrics such as resilience triangles and route friability scores to evaluate vulnerability and recovery efficiency. These tools were suggested as practical aids for transit agencies in disaster preparedness, as they allow for the identification of critical routes and links and offer guidance for resilient operational planning.

Finally, Zhang and Ng [62] proposed a hypothesis-driven resilience framework for urban transit systems, including scenarios involving compound failures from both natural hazards (e.g., flooding) and targeted disruptions. Their model used the entropy weight method (EWM) and TOPSIS to identify critical nodes and optimal recovery sequences, demonstrated on the Mass Transit Railway (MTR) in Hong Kong. Although their primary case focused on rail systems, the proposed methodology is equally applicable to bus networks, particularly in evaluating cascading failures and planning for staged recovery after floods

Collectively, these studies contribute to a growing but still underdeveloped body of knowledge on flood impacts in bus transport systems. They emphasize the need for more data-driven, multi-modal, and equity-aware approaches to planning resilient public transport infrastructure. However, a key observation is that bus systems—despite operating on road infrastructure—are often overlooked in road network resilience analyses. This omission is particularly critical given that buses serve as a primary public transport mode in many urban and suburban contexts, especially for low-income populations.

In most existing resilience studies of road networks, the focus has been largely limited to private vehicles or freight flows, while the interaction between road infrastructure and public transport services such as buses has been insufficiently explored. In contrast, the current study incorporates both bus transit systems and general road network performance under flood conditions, aiming to develop a more comprehensive understanding of road network resilience. By explicitly accounting for bus operations and passenger mobility, this study contributes a novel perspective that integrates both infrastructure functionality and public service continuity, offering a more holistic assessment of transport system performance in the face of flood-induced disruptions.

2.6. FLOODED NETWORK RESILIENCE INDICATORS AND IMPROVEMENT METHODS

Assessing the resilience of transportation networks under flooding conditions requires a comprehensive understanding of both the direct and indirect effects of hydrological disruptions. To quantify resilience and improvement methods, researchers employ a variety of Key Performance Indicators (KPIs), each tailored to a specific aspect of network performance. The selection of appropriate indicators is crucial and is often based on factors such as data availability, spatial scale, and methodological frameworks. Moreover, indicators were grouped according to the well-established 4R resilience framework originally proposed by Bruneau *et al.* [6], categorizing them into Robustness, Redundancy, Resourcefulness, and Rapidity dimensions to enable structured and interpretable resilience assessment.

Among these, centrality-based indicators (e.g., degree, betweenness, and eigenvector centrality) are used to identify critical nodes and links that disproportionately

influence network connectivity and flow efficiency. These metrics help detect vulnerabilities where localized disruptions may cause system-wide failures. In the context of flooding, for example, high betweenness nodes may become choke points if flooded, amplifying overall travel delay [63–65].

Accessibility-based indicators evaluate how easily users can access essential services and destinations during or after a flood. Metrics like the average path length, accessibility index, or modified Hansen index quantify the spatial and functional fragmentation caused by inundation [37,39,66]. These are particularly important in urban areas, where population density and reliance on road-based access heighten the socio-economic impact of road closures.

Performance-based indicators are commonly used to assess the functional degradation of transport systems. These include measures of additional travel time, vehicle rerouting, reduced speeds, and uncompleted trips. They provide dynamic insights into network behavior under stress and are directly linked to user experience [7,28,67]. For instance, the proportion of rerouted vehicles can be used to estimate the level of adaptability of a network to sudden hazards [19,26].

Cost-based indicators capture both direct (e.g., infrastructure repairs) and indirect (e.g., productivity losses) economic impacts of flooding. Methods such as net present value (NPV) and cost-benefit ratio analyses are instrumental for evaluating the efficiency of resilience investments [13,32,55,68,69]. These help authorities justify and prioritize funding for specific interventions.

Composite indices like the Urban Flood Resilience Index (UFRI) and Trip Resilience offer multidimensional assessments by combining robustness, redundancy, recovery, and resourcefulness measures [53,70–72]. These frameworks are increasingly used to support holistic resilience evaluations, especially where simple metrics fall short.

Table 2.6. Indicators used in resilience assessments.

Category	Category based on 4R resilience framework	KPI	Definition	Remarks	References
Accessibility-based	Robustness/Resourcefulness	Average path length	Average shortest path length	Assess the significance of individual links and the effects of hydrological hazards	Testa *et al.* [39]
		Accessibility index	Inverse of shortest path lengths		Papilloud and Keiler [66]
		Accessibility score	County-level accessibility index accounting for distance and traffic volume		Sohn [37]
		Transport accessibility	Integrated function of weighted attractiveness and distance decay		Borowska-Stefańska *et al.* [26]
		Modified Hansen index	Adjusted accessibility index incorporating population and opportunities		Papilloud and Keiler [66]
		Population at the risk of isolation	Population's limited physical access to public facilities		Logan *et al.* [73]
Centrality-based	Redundancy/ Robustness	Size of critical nodes	Count of nodes directly connected to critical nodes via the shortest paths	Detect key nodes in extensive networks	Alabbad *et al.* [29] and Loreti *et al.* [34]
		Giant component size	Extent of the biggest interconnected node group		Wang *et al.* [56]
		Eigenvector centrality	Significance of a node based on its links to influential nodes.		Yadav *et al.* [64]
		Node/edge betweenness centrality	Count of shortest paths that traverse node/edge i		Kermanshah and Derrible [63] and Xing *et al.* [65]
		Weighted degree centrality	Integration of node connectivity and link significance		Xing *et al.* [65]
		Degree centrality	Count of nodes connected to node i		Kermanshah and Derrible [63]
Cost-based	Resourcefulness	Direct/indirect loss	Financial impact from repair costs and unmet travel demand	Useful for decision-makers to assess economic losses and enhance protection and retrofitting strategies	Hackl *et al.* [32] and Pregnolato *et al.* [13]
		Loss of service cost	Network performance loss due to non-operational components		Baroud *et al.* [68]
		Cost-benefit ratio	Proportion of mitigated economic loss to retrofitting expenses		Ishibashi *et al.* [69]
		Total network restoration costs	Total of all individual component repair expenses		Baroud *et al.* [68]
		Net present value of the benefits	Decrease in disruption-related expenses following mitigation measures		Pregnolato *et al.* [55]
Performance-based	Rapidity/Robustness	Vehicle travel distance	Longer travel distances caused by detours	Measure the effects of hydrological hazards on travel demand	Kasmalkar *et al.* [28], Suarez *et al.* [7], and Yang *et al.* [67]
		Vehicle travel time	Extended travel duration due to detours and slower vehicle speeds		Kasmalkar *et al.* [28], Suarez *et al.* [7], and Yang *et al.* [67]
		Vehicle travel speed	Decreased vehicle speed caused by flooding		Suarez *et al.* [7] and Borowska- Stefańska *et al.* [26]
		Proportion of vehicles that changed routes	Proportion of rerouted trips to total trips		Borowska-Stefańska *et al.* [26] and Shahdani *et al.* [19]
		Uncompleted journeys and blocked travel routes	Count of trips aborted due to flooded starting points or destinations		Kasmalkar *et al.* [28], Suarez *et al.* [7]
Other	-	UFRI	Metrics for durability, operational efficiency, and restoration ability	Measure different resilience aspects	Moura Rezende *et al.* [70] and Rezende *et al.* [71]
		IFHI	Vulnerability of bridges to flooding		Loli *et al.* [74]
		Flood resilience indicator	Metrics for redundancy, robustness, rapidity, and resourcefulness		Li *et al.* [53]
		Trip resilience	Metrics for robustness, redundancy, and recovery		Aghababaei *et al.* [72]

As summarised in Table 2.6, the majority of resilience indicators adopted in previous studies on flood-induced transport disruptions fall predominantly under the category of Robustness within the 4R resilience framework. Indicators such as accessibility metrics, centrality-based measures, and travel performance parameters primarily aim to capture the ability of the transport system to maintain functionality during disruptive events, rather than focusing on recovery speed, redundancy, or resource allocation.

While some indicators may overlap with other resilience dimensions—such as redundancy (e.g., alternative routes via network centrality) or resourcefulness (e.g., economic impact measures)—the emphasis remains largely on evaluating how well the system withstands disruption.

Therefore, this study places a particular focus on robustness, aligning both with the trends observed in the literature and the specific nature of flood-related disruptions, where maintaining access and system performance during inundation is of critical importance.

To fully understand and address the vulnerabilities in transport systems, resilience evaluation has been extended across the temporal phases of a disruption including Pre-event (mitigation), During-event (relief), and Post-event (restoration). These phases are discussed in the following subsections.

2.6.1. Pre-event phase: mitigation

The pre-event phase plays a pivotal role in enhancing the resilience of transportation systems by implementing preventive measures that reduce the potential impacts of flooding. Proactive mitigation strategies aim to either minimize the probability of network exposure to hazards or reduce the severity of disruption when exposure occurs. As illustrated in Figure 2.4, transportation systems that adopt mitigation measures demonstrate significantly improved performance during and after disruption, represented by a higher baseline level of functionality and a faster rate of recovery.

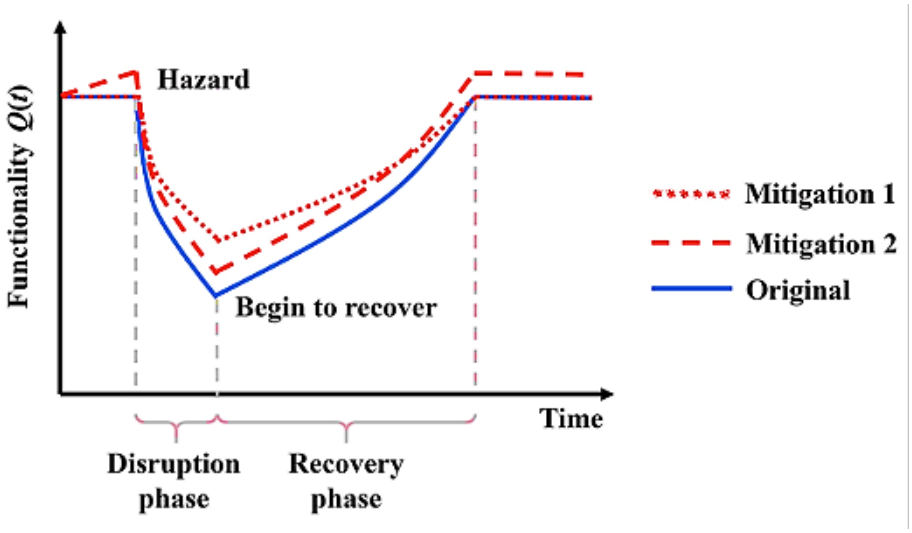


Figure 2.4. Comparing example of transportation network performance with and without mitigation strategies during disruption and recovery phases.

Mitigation strategies can be broadly categorized into structural, nature-based, and technological measures. Structural interventions include the construction of levees, flood walls, embankments, and elevated roadbeds that physically protect infrastructure from inundation. For instance, raised bridge decks can reduce the risk of water overtopping and structural damage, while shear keys and riprap protection reinforce stability under high hydraulic forces [75,76]. Nature-based solutions, such as green stormwater infrastructure (GSI), rain gardens, bioswales, and urban wetlands, are increasingly favored for their dual benefits in flood attenuation and environmental enhancement. Studies by Kasmalkar *et al.* [25] and Knight *et al.* [51] highlighted how GSI can reduce surface runoff and mitigate traffic disruption by lowering flood depths on critical urban corridors.

Another group of important measures involves capacity enhancements in urban drainage systems, including expansion of sewer pipes, installation of retention basins, and creation of flood diversion channels [77,78]. Such interventions improve a network's ability to accommodate excess rainfall, thereby reducing the incidence and extent of surface flooding that disrupts transport.

Beyond physical upgrades, digital technologies and early warning systems are emerging as critical tools for pre-event risk mitigation. Intelligent transportation systems (ITS), real-time sensors, and AI-based flood prediction tools enable dynamic risk monitoring and proactive management. As discussed by Mitoulis *et al.* [79] and Pregnolato *et al.* [80], these systems allow authorities to implement timely traffic control measures, reroute

vehicles in anticipation of flooding, and prevent unnecessary exposure to inundated segments.

Given the limited resources available for pre-disaster upgrades, especially in large networks, optimization models are used to prioritize investment. These models help identify critical segments whose protection yields the highest benefit-cost ratio. For instance, Starita *et al.* [81] introduced a model that selects road segments for protection based on minimizing expected shortest path costs under varying disruption scenarios. Similarly, Zhang and Alipour [76] proposed a two-stage optimization framework that integrates both retrofitting (pre-event) and repair (post-event) planning, ensuring cost-effective long-term resilience.

Complementary approaches to functional resilience have also emerged, such as the hazard-based duration modelling framework presented by Gonçalves *et al.* [82], which evaluates resilience based on the survival probability of trips completed within acceptable travel times across different socio-economic population groups. While such models offer valuable insights into travel-time-centered resilience at the individual user level, they are primarily oriented towards behavioral modelling rather than system-level functional performance under infrastructure disruptions, which is the primary focus of this study.

In sum, pre-event mitigation strategies serve as the foundation for transport resilience by minimizing hazard exposure, reducing network vulnerability, and enhancing the capacity to absorb and recover from disruptions. These interventions must be carefully planned and prioritized, balancing economic constraints with resilience goals.

2.6.2. During hazard: relief

The relief phase focuses on the real-time management of transportation networks during a flood event. The primary goals are to ensure the continued mobility of emergency services, support evacuation operations, and facilitate the distribution of essential supplies. This phase is particularly challenging due to uncertainties associated with flood propagation, varying user behavior, and incomplete information about road conditions.

A major challenge in this phase is that drivers are often unaware of flooded road segments until they encounter them, leading to unplanned detours, congestion, or even

abandonment of trips. Simulation studies such as Shahdani *et al.* [19] and Pregnolato *et al.* [13] show that the absence of real-time information can significantly delay rerouting and amplify disruption. To address this, SUMO-based traffic simulations can model multiple routing scenarios with varying levels of driver awareness, offering insights into potential traffic bottlenecks and route blockages during evolving flood conditions.

Evacuation planning is one of the most critical applications in this phase. Several optimization-based models have been proposed to enhance evacuation effectiveness by accounting for road capacity constraints, shelter capacities, and dynamic changes in accessibility. Li *et al.* [83] introduced a capacitated multi-commodity flow model that balances evacuation time and traffic load, while Goerigk *et al.* [84] developed a risk-aware model minimizing the number of shelters used and total risk exposure. In contrast, Kashyap *et al.* [85] explored the integration of Unmanned Aerial Vehicles (UAVs) for flood reconnaissance and route guidance. UAVs can collect real-time flood data, allowing traffic controllers to dynamically adjust evacuation routes.

Table 2.7. Models for resource transportation and evacuation routes.

Decision variables	Objective	Constraint	References
Resource transportation routes	Minimum transportation time	Road capacity	Kashyap *et al.* [85]
Resource transportation routes	Minimum transportation time	Road capacity, minimum time to assign resources, resource assignment, resource reallocation transition time	He *et al.* [86]
Evacuation routes	Minimize evacuation time	Road capacity, time horizon to leave, road inflow capacity	Bretschneider and Kimms [87]
Evacuation routes	Maximum traffic flow and minimum evacuation time	Road capacity, entry node rate, shelter capacity	Li *et al.* [83]
Evacuation routes	Minimum evacuation time, risk, and the number of used shelters	Road capacity, shelter capacity, and parking space	Goerigk *et al.* [84]

Another critical component of the relief phase is the delivery of emergency resources. This includes food, medical supplies, drinking water, and rescue equipment. Models like those developed by He *et al.* [86] consider factors such as resource allocation time, reallocation transition time, and real-time updates to minimize delays in supply distribution. The integration of decision-support systems, UAVs, and adaptive routing algorithms enhances the robustness of relief logistics under unpredictable flood conditions.

Lastly, studies such as Pérez-Morales *et al.* [54] emphasized the importance of emergency center placement. By strategically locating shelters and emergency operation centers, authorities can significantly reduce average response time and optimize resource deployment. These models account for spatial distribution of demand, facility capacities, and acceptable travel times for affected populations.

In summary, the relief phase relies on the seamless integration of simulation tools, optimization algorithms, and emerging technologies to ensure rapid response, efficient evacuation, and timely delivery of aid during flood emergencies.

2.6.3. Post-event phase: restoration

Once the immediate impacts of flooding subside, the focus of transportation authorities shifts to restoring the functionality of the disrupted network. Restoration is not only a technical challenge but also an economic and logistical one, as it involves allocating limited resources to numerous damaged assets. Effective restoration depends on prior resilience assessments, prioritization frameworks, and a well-defined action plan.

One widely used strategy is to prioritize the repair of critical road segments or bridges that maximize origin-destination (OD) demand reconnection. Lertworawanich [88] proposed a two-stage particle swarm optimization model that first restores key connectivity nodes and then optimizes overall network flow efficiency. Likewise, Zhao and Zhang [89] developed a multi-objective optimization approach to balance unmet travel demand, total travel time, and budget limitations.

An essential component of restoration planning is cost and duration estimation. While infrastructure repair costs can be estimated using historical cost databases [32,90], predicting restoration timelines is more complex. Mitoulis *et al.* [79] addressed this challenge by designing a bridge restoration model based on expert surveys. Their model incorporates task interdependencies, idle times, and sequencing to better reflect real-world constraints. Barker *et al.* [41] further enhanced restoration analysis through a proportional hazard model, which evaluates recovery probabilities over time.

Restoration is also an opportunity to improve infrastructure design. Instead of simply replicating the pre-flood conditions, authorities are encouraged to adopt the "build back better" approach. This includes updating road and bridge designs to meet modern

standards, increasing drainage capacity, or adapting structures to withstand future climate scenarios. However, restoration strategies must remain hazard-specific: for instance, floods typically damage bridge substructures, while earthquakes and fires affect different components. Applying inappropriate restoration practices from other hazard domains may reduce overall resilience [75,76,91].

Finally, it is important to note that restoration is not a one-time event but a phased process that must consider longer-term community recovery, ongoing risk reduction, and the socio-economic needs of the region. Close collaboration with experts, city planners, and asset managers is essential to ensure that the restored network meets both current and future transportation demands.

This study evaluates the effectiveness of some Pre-event (mitigation) measures in enhancing the resilience of the network.

2.7. KEY FINDINGS AND CONCLUSION

Over the past few decades, the increasing frequency and severity of natural hazards, particularly floods, have drawn significant attention to the concept of transportation network resilience. As roads serve as critical lifelines during both routine operations and emergency scenarios, understanding and enhancing their ability to resist, absorb, adapt to, and recover from disruptions is paramount. This chapter provided an in-depth review of state-of-the-art studies on the resilience of transportation networks under flood conditions, covering flood modelling approaches, traffic simulation methods, integrated modelling frameworks, and a comprehensive set of resilience indicators.

A key insight from this review is the importance of flood type differentiation, specifically fluvial, pluvial, and coastal floods, which exhibit distinct spatial and temporal characteristics and consequently affect road networks in different ways. Although several studies rely on static flood maps or average depth conditions, dynamic modelling of flood propagation using hydrodynamic models offers a more realistic assessment of evolving accessibility constraints. Notably, the CityCAT model is increasingly used to simulate surface water flooding in urban environments due to its ability to represent buildings, green infrastructure, and drainage networks. However, such advanced models remain underutilized in integrated flood-traffic assessments.

This chapter emphasized that two broad methodological paradigms dominate resilience evaluation: graph-based analyses and traffic simulation approaches. Graph-theoretic methods, rooted in network science, provide efficient ways to explore topological vulnerability by identifying critical links and nodes, evaluating connectivity, and computing centrality-based indicators. While these methods require less data and offer intuitive insights, they often overlook flow dynamics and behavioural responses to flooding. By contrast, traffic simulation models, especially microscopic and mesoscopic types, enable the explicit modelling of vehicle behaviors, congestion, rerouting, and delay patterns under flood scenarios. Macroscopic models, while suitable for broad regional analysis, tend to oversimplify vehicle movement and do not reflect dynamic traveller responses.

Among the most important contributions of this thesis is the combined use of CityCAT and SUMO, enabling a dynamic integration of hydrological and traffic simulations. This hybrid approach surpasses static flood-disruption assessments by capturing temporal changes in road accessibility and traffic behavior. SUMO's open-source framework allows for fine-grained modelling of both public and private transport modes an essential advancement, as most prior studies neglect the bus flows in disrupted road networks. This thesis, therefore, pioneers a more realistic simulation environment that reflects real-world multimodal urban mobility under extreme weather events.

The selection of resilience indicators is another critical dimension explored in this chapter. Indicators were initially categorized into accessibility-based, centrality-based, performance-based, cost-based, and composite indices, each offering a unique lens to examine network performance under disruption. However, to provide a more structured understanding aligned with established resilience theory, these indicators were also mapped to the 4R resilience framework.

As shown in Table 2.6, the majority of indicators—such as accessibility scores, centrality measures, and performance metrics like travel speed and trip completion—primarily fall under the category of robustness, as they assess the system's ability to withstand disruptions while maintaining essential functionality. While some indicators also relate to redundancy (e.g., alternative paths via network structure) or resourcefulness (e.g., economic losses and restoration costs), the emphasis across the literature remains strongly on robustness. One of the main reasons for this focus is the lack of available data on the

recovery phase. Measuring recovery speed (rapidity) or long-term adaptive responses often requires detailed post-event data, which is rarely accessible in transport disruption studies, especially in the context of floods. Therefore, most existing research—including this study—tends to prioritise robustness-related metrics that can be derived more readily from simulation or pre-disaster datasets.

Despite progress in the literature, this review also revealed several key research gaps and areas for improvement:

- Underutilization of mesoscopic models: Although mesoscopic simulations offer a balanced trade-off between computational cost and behavioural fidelity, their adoption remains limited.
- Neglect of multimodality in the road networks: Many existing studies evaluate either private vehicles or public transit in isolation. This overlooks the costs of disruptions in the road networks, leading to incomplete resilience assessments. The approach taken in this thesis (modelling both buses and cars within a shared network) is a step forward in addressing this limitation.
- Limited dynamic integration of flood-traffic models: Static assessments dominate the literature, even though flooding and traffic are inherently dynamic processes. By incorporating time-varying water depths from CityCAT into the traffic network and flow in SUMO, this thesis enables a more accurate representation of how disruptions unfold and affect travel decisions over time.

By addressing the above gaps, this research contributes a novel methodology for evaluating the resilience of transportation systems to pluvial flooding, rooted in dynamic simulations and multimodal integration. The findings provide actionable insights for infrastructure managers and urban planners.

CHAPTER 3

METHODOLOGICAL FRAMEWORK

3.1. INTRODUCTION

This chapter presents the integrated methodological framework developed to assess the functional resilience of urban traffic networks under flood disruptions. The proposed framework couples high-resolution flood modelling with dynamic traffic simulation and a systematic resilience assessment based on performance indicators specifically adapted to flood-induced disruptions.

The methodology begins with pluvial flood simulations generated by CityCAT, producing detailed flood depth maps over time and across multiple flood scenarios. These flood depth maps are integrated with the road network using a GIS-based processing step, where a continuous flood depth–speed reduction function is applied to estimate the capacity reduction of each road segment under flooded conditions. This continuous modelling approach allows capturing partial service degradations on affected roads, providing a more realistic representation compared to traditional binary road closure assumptions.

Subsequently, traffic simulations are carried out using the mesoscopic traffic simulation platform SUMO. Multiple simulation runs are conducted to model normal

(baseline) conditions, flooded network conditions, and scenarios where mitigation measures are applied. The simulation outputs enable the quantification of network-wide performance under varying flood intensities.

To quantify resilience, a dynamic threshold approach is adopted. Key performance indicators (KPIs) are defined based on traffic efficiency, including: (1) safety, (2) accessibility, (3) reliability, and (4) efficiency. For each flood scenario, a performance matrix is computed using these indicators. The performance levels are then compared against predefined dynamic thresholds to establish a compliance matrix, from which an overall resilience index is calculated. The complete workflow of the proposed framework is illustrated in Figure 3.1. The following sections provide a detailed step-by-step explanation of each component.

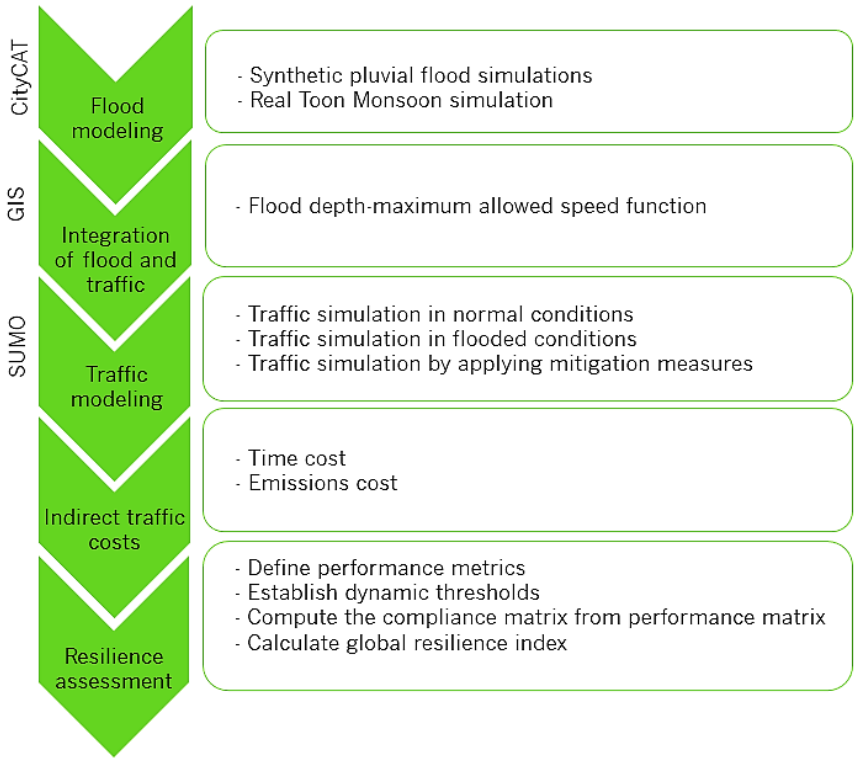


Figure 3.1. Methodological framework of this thesis.

3.2. FLOOD MODELLING

Accurate flood modelling forms a critical foundation for this study, as the outputs directly influence the subsequent traffic network performance and resilience assessment. In this research, the pluvial flood hazard is simulated using CityCAT, a fully distributed, physics-based hydrodynamic model specifically designed for urban environments (Iliadis *et al.* [92]). CityCAT has been selected due to its capability to capture both surface and

subsurface interactions, which are highly relevant for simulating flood scenarios in complex urban catchments.

3.2.1. CityCAT Model Overview

CityCAT integrates a coupled 1D/2D modelling approach, representing surface overland flow through two-dimensional shallow water equations, while modelling subsurface stormwater systems using a dynamic pipe flow module. One of its distinctive features is the explicit simulation of storm drain inlets and manholes, allowing a realistic representation of the hydraulic exchange between surface runoff and sewer drainage systems. Unlike many conventional flood models that rely on simplified assumptions for subsurface drainage, CityCAT incorporates detailed inlet and sewer network configurations, enhancing its suitability for dense urban environments where sewer surcharging often contributes significantly to flooding.

The surface domain is discretized through a high-resolution computational grid automatically generated from topographic data. In this study, a 5-meter grid resolution [93] was adopted to provide a fine-scale representation of flow paths, terrain features, and urban structures. Building footprints, green spaces, and permeable surfaces are incorporated into the computational mesh to accurately reflect urban land cover heterogeneity. Water infiltration in permeable surfaces is modelled using the Green-Ampt method [94], while impervious surfaces contribute to direct runoff.

For the subsurface drainage system, CityCAT employs the Mixed Flows in Pipes (MFP) model developed by Bourdarias, Ersoy, and Gerbi [95]. This improves upon the traditional Preissmann slot method by combining shallow water equations for free-surface flow with conservative formulations for pressurized conditions. Nevertheless, this component was not used in the model of the current study as the data on the sewers was not available and the simulation is 10 times slower.

3.2.2. Model Input Data

The input data required for CityCAT includes:

- High-resolution Digital Terrain Model (DTM) derived from Ordnance Survey data, providing detailed elevation data for surface flow routing.

- Hydrological boundaries representing rainfall intensities for various scenarios.
- Detailed urban land use layers, including building footprints, roads, green spaces, and impervious/permeable surfaces.

3.2.3. Flood Scenarios Design

Multiple flood scenarios were developed for the resilience assessment, allowing for a comprehensive evaluation of the traffic network's performance under a range of flood severities. The synthetic flood scenarios consist of:

- 1-in-10-year flood event (2-hour rainfall duration)
- 1-in-50-year flood event (2-hour rainfall duration)
- 1-in-100-year flood event (2-hour rainfall duration)
- Toon Monsoon flood event (2-hour rainfall event)

The presence of historical data in the Tyne and Wear region, collected during the flood on 28 June 2012 (Toon Monsoon Day), by the Traffic Accident Data Unit (TADU), enables some validation. This event had an estimated return period of 1 in 100 years, and an approximate duration of 2 hours leading to severe traffic congestion, which lasted more than six hours [96]. While longer rainfall durations (e.g., 4–6 hours) could theoretically generate greater cumulative rainfall and more prolonged disruption, the 2-hour storm events were prioritised in this study. This choice reflects both hydrological and traffic considerations. From a hydrological perspective, initial tests with different synthetic rainfall durations (e.g., 2-hour and 4-hour) showed that the 2-hour events produced the most severe flooding and disruption in Tyne and Wear. This outcome is consistent with hydrological reasoning: shorter storms deliver rainfall at a higher intensity, which tends to generate sharper flooding in small to medium-sized catchments, whereas longer storms produce greater total rainfall and are more critical for larger catchments. For Tyne and Wear, the 2-hour events resulted in the greatest flood impacts. From a transport perspective, these intense short events — especially when coinciding with peak demand periods — produced the steepest short-term decline in traffic network performance. Accordingly, the 2-hour scenarios were retained as representative of the most disruptive conditions for resilience analysis in this research.

Three synthetic design flood events were generated following the standard U.K. procedure from the Flood Estimation Handbook [97]. This scenario design approach offers a broad spectrum of flood hazard intensities, enhancing the robustness of the resilience assessment.

During model simulations, CityCAT employs an internal dynamic timestep, automatically adjusting depending on local water depths and flow conditions to maintain numerical stability, often reaching sub-minute or even sub-second time steps. The model outputs, however, were extracted at fixed 20-minute intervals to capture the temporal progression of inundation for subsequent integration with traffic modelling. This temporal resolution enables the consideration of evolving flood conditions and their interaction with traffic movements during each scenario.

3.2.4. Flood Model Outputs for Integration

Upon completing the hydrodynamic simulations, CityCAT outputs detailed flood depth raster representing the maximum inundation depths experienced during each simulation run. These spatial flood depth maps are produced at the same resolution as the computational grid (5 meters), ensuring alignment with road network geometry for subsequent analysis. The flood depth maps serve as the key input for the GIS-based integration process, where they are spatially overlaid onto the road network to assess flood exposure on individual road links.

3.3. INTEGRATION OF FLOOD AND TRAFFIC MODELS

A crucial step within the proposed framework is the integration of flood simulation outputs with the road traffic network to estimate the operational capacity of the network under flooded conditions. This integration process enables translating the hydrodynamic outputs from CityCAT into link-specific traffic disruption levels, thereby providing an essential input for the subsequent traffic simulation phase.

Traditional approaches often classify flooded road segments using binary states, either fully operational or entirely closed, depending on predefined flood depth thresholds. While such binary classifications simplify flood-traffic interactions, they fail to represent the gradual degradation in road functionality as floodwater depth increases. In contrast, this study adopts a continuous flood depth–speed reduction approach, allowing for more

nuanced modelling of flood impacts on road capacity by assigning a unique reduced speed for each road segment as a function of the inundation depth.

To implement this approach as illustrated in Figure 3.2, a GIS-based integration tool was developed using Python, overlaying the flood depth raster produced by CityCAT onto the traffic network layer. For each road link, the corresponding floodwater depth was extracted and assigned to that segment. The relationship between flood depth and the maximum allowed speed was then applied to calculate the speed reduction specific to each link.

The relationship used in this study to translate flood depth into speed reduction is based on the function proposed by Pregnolato *et al.* [80], which offers a scientifically validated and widely cited method for representing flood-induced traffic disruption (Figure 3.3). This relationship is derived from empirical data, expert consultations, and previous experimental studies and provides a realistic approximation of how traffic speed diminishes with increasing flood depth for pluvial flood scenarios in urban areas. The function was provided in Equation (2) in chapter 2.

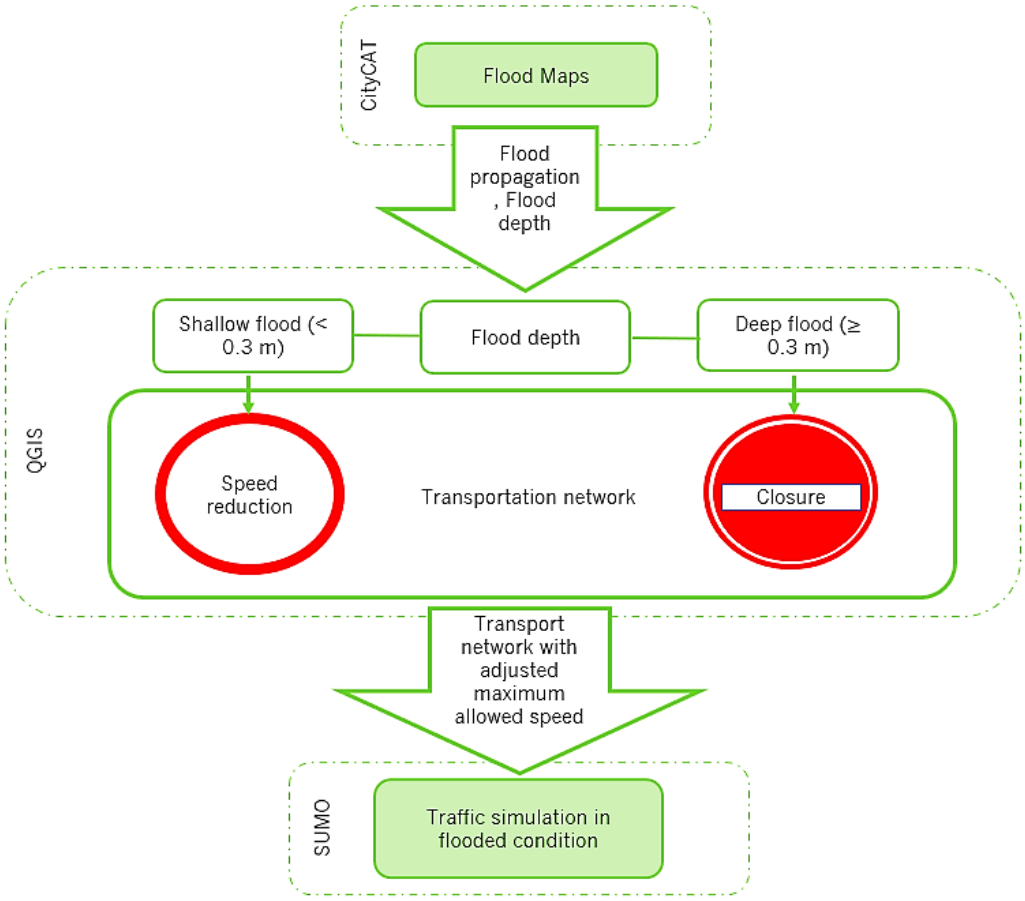


Figure 3.2. Integration tool to translate the flood model outputs into the sumo readable files.

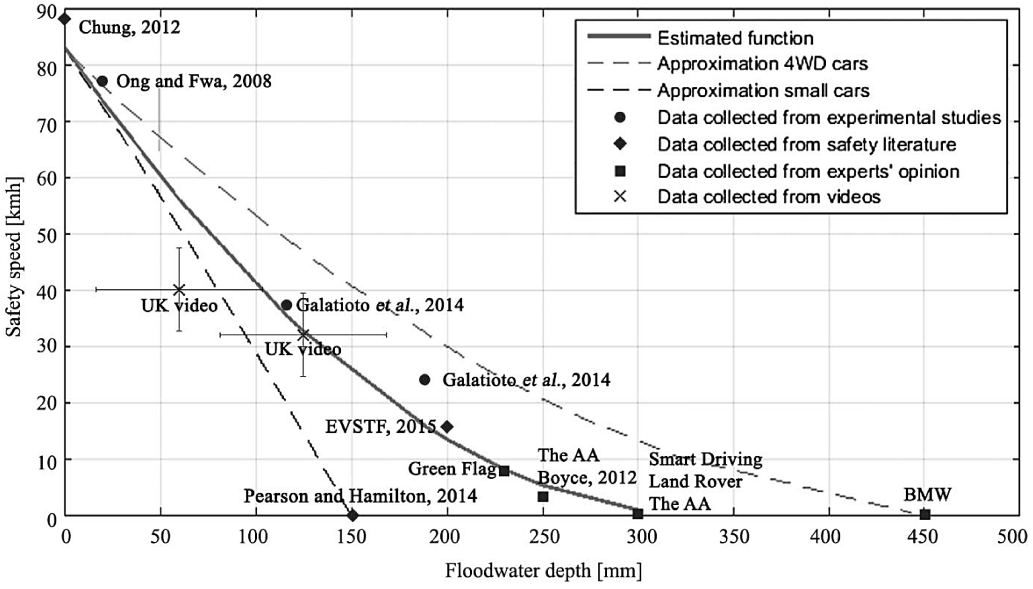


Figure 3.3. Relationship between floodwater depth and the maximum allowed speed for each link, [80].

3.3.1. Consideration of Vehicle Types and Multimodal Interactions

An important element of this integration is the explicit inclusion of both passenger cars and buses within the flood-traffic modelling framework. In most previous studies, buses were often overlooked, despite their critical role in transport networks. Based on discussions with transportation experts and supported by the author's own field experience, the maximum flood depth at which buses remain operational was determined to be approximately 300 mm (0.3 m), consistent with the threshold applied to passenger cars. Beyond this depth, water begins entering bus doors, rendering further movement impractical and unsafe.

It was further observed that, under wet but passable conditions, buses tend to maintain their normal operational speed due to their larger wheel diameters and overall stability compared to smaller vehicles. However, their performance remains ultimately constrained by general traffic flow conditions, as increasing flood depths cause congestion primarily driven by immobilized passenger cars. As flooding reaches approximately 300 mm, both vehicle classes are essentially halted due to direct mechanical limitations.

Consequently, in this study, the same speed-depth function derived from Pregnolato *et al.* [80] was applied uniformly to both buses and passenger cars. This assumption ensures consistency within the integration tool, which operates by adjusting maximum allowed speeds on a per-link basis rather than simulating individual vehicle mechanics. The uniform application of this function to all vehicle classes provides a pragmatic method for estimating link-level capacity reductions under flood conditions.

Overall, this integrated flood-traffic disruption methodology allows for detailed and realistic quantification of pluvial flood impacts on multimodal road transport networks. The resulting link-specific speed reduction profiles serve as a direct input to the traffic simulation stage of the framework, where the dynamic interactions between vehicle flows under flood-induced capacity constraints are simulated and analysed.

3.4. TRAFFIC MODELLING

Following the integration of flood depth data into the traffic network, the next stage of the framework involves simulating the resulting impacts of flood-induced disruptions on traffic flows. For this purpose, the open-source traffic simulation software SUMO (Simulation of

Urban MObility) was employed. SUMO provides a flexible and robust platform for modelling detailed traffic behavior under both normal and disrupted conditions.

3.4.1. SUMO Overview

SUMO is a highly adaptable traffic simulation tool developed by the German Aerospace Center (DLR), widely recognized for its capability to simulate real-world traffic dynamics across various transportation modes [98]. While SUMO was initially developed for microscopic simulation of individual vehicle movements, it also offers mesoscopic simulation, which enables greater computational efficiency while still capturing essential traffic flow dynamics. This flexibility makes SUMO well-suited for simulating urban transport networks of varying sizes under complex disruption scenarios such as flooding.

Key SUMO features relevant to this study include:

- Mesoscopic simulation of multimodal traffic, including passenger cars and buses.
- Dynamic Traffic Assignment (DTA) to model rerouting under evolving network conditions.
- Traffic demand modelling based on real-world traffic counts.
- Integration with GIS-based road networks, including OSM-derived network data.
- Scenario-specific input files, such as variable speed sign (VSS) files for speed reductions and reroute files for dynamic detours.

SUMO provides a wide range of features for traffic flow simulation and supports modelling of individual route choices in response to network disruptions such as flooding. Its mesoscopic modelling capabilities enable it to simulate traffic flow changes and vehicle rerouting behavior, which are essential for analyzing traffic responses.

A key strength of SUMO lies in its sophisticated rerouting functionality, which is essential for examining traffic dynamics during disruptions like pluvial floods. The model can apply road closures and speed limits at specific times and automatically redirects affected vehicles to alternative routes. This is achieved using Dynamic User Assignment (DUA), where the simulation calculates travel times and assigns routes accordingly to reduce overall travel time. SUMO's rerouting process is responsive to real-time changes in network conditions, making it particularly effective for investigating the interaction

between urban flooding and traffic systems. Through this, SUMO helps assess indirect economic effects, including increased delays and emissions, thereby supporting the development of more resilient urban mobility systems.

In this research, SUMO was used to simulate traffic conditions for three primary cases:

- Baseline (normal) network conditions,
- Flooded network conditions, and
- Flooded network with mitigation measures applied.

3.4.2. Model Input Data

The traffic simulation model developed in this study relies on a comprehensive set of input data sources that collectively define the structure, demand, and multimodal composition of the urban transportation system under investigation. The main components of the input data include road network data, traffic demand data, and public transport data.

3.4.2.1. Road Network Data

The spatial configuration of the road network was extracted from the OpenStreetMap (OSM) platform, an open-source, collaboratively maintained geospatial database widely used in transportation research [98] in ESRI Shapefile format. The extracted network includes detailed geometric and topological information, such as link identifiers (OSM IDs), nodes, street classifications (e.g., highway, primary, secondary), number of lanes per link, allowed vehicle types, speed limits, and directional flows. The imported OSM data was carefully processed and filtered in JOSM3 to ensure a successful transformation and then converted into SUMO-compatible network files using SUMO's netconvert tool, ensuring topological integrity and simulation-readiness of the network model.

3.4.2.2. Traffic Demand Data: Extraction from TrafficCounts

Unlike conventional simulation approaches that rely on synthetic or estimated origin-destination (OD) matrices, this study utilizes empirical traffic counts as the basis for defining travel demand. The TrafficCounts database provides observed vehicle counts collected through an array of traffic monitoring stations distributed across the study area. These observation points record traffic volumes on selected road links at specified time intervals, providing a valuable data source that directly reflects actual traffic usage.

To translate these observed link counts into full route-based traffic demand suitable for dynamic simulation, the “Routes from Observation Points” methodology provided by SUMO was applied (SUMO documentation [99]. This approach reconstructs plausible trip flows that explain the observed counts through an iterative estimation process. The procedure operates as follows:

I. The observed link counts from TrafficCounts are assigned to corresponding links in the SUMO network model.
II. SUMO then generates an initial set of possible routes (using shortest-path and random sampling algorithms) that traverse the network between plausible origins and destinations.
III. Through iterative adjustment, route flows are modified such that the simulated link-level volumes produced by these routes gradually converge toward the observed counts.
IV. The final route set represents a calibrated demand model where simulated traffic volumes across the network closely match real-world observations from TrafficCounts.

This observation-driven approach ensures that the baseline traffic demand reflects the actual network usage patterns as recorded in practice, without requiring synthetic OD estimation or behavioral trip modelling assumptions. Moreover, this method accounts for spatial and temporal variation in traffic volumes, capturing both peak and off-peak demand conditions observed in the region.

3.4.2.3. Public Transport Data: GTFS-Based Bus Network Representation

In addition to private vehicle demand, public transport operations were explicitly included in the simulation model to capture multimodality under both normal and disrupted conditions. Public transport data was obtained from GTFS (General Transit Feed Specification) feeds [100] which provide standardized datasets describing scheduled public transport services in a machine-readable format widely used across global transit agencies.

The GTFS dataset consists of multiple text-based files organized into tables, which collectively define routes, trips, schedules, and stop locations. The key GTFS components utilized in this study include:

Table 3.1. GTFS dataset files.

GTFS File	Description
routes.txt	Defines public transport routes (IDs, names, modes)
trips.txt	Specifies individual trip schedules associated with routes
stop_times.txt	Lists exact arrival and departure times at each stop
stops.txt	Provides spatial coordinates of all stops
calendar.txt	Defines the service days and operational calendar
agency.txt	Contains agency-level metadata
shapes.txt	Describes precise route geometries for visualization

GTFS data was converted into SUMO-compatible public transport schedules using SUMO's built-in GTFS import tool (SUMO documentation [101]. This conversion process automatically translates the full schedule of bus routes, stop locations, vehicle trips, and timetables into corresponding SUMO simulation elements.

The combination of GTFS-based bus services and observation-based private vehicle demand provides a realistic, multimodal traffic model that captures both personal and public transport dynamics within the simulation framework.

3.4.3. Route Assignment

The assignment of vehicle routes within the traffic simulation was performed using "SUMO's Automatic Routing" functionality, which dynamically determines vehicle routes during simulation execution based on real-time network conditions (SUMO documentation [102]. Unlike static route assignment methods that predefine all routes prior to simulation, automatic routing operates in an online, adaptive manner, allowing vehicles to update their routes as the simulation progresses and network conditions evolve.

Upon vehicle departure, SUMO initially assigns a route using the current network state, applying the Dijkstra shortest-path algorithm [103] to calculate the most efficient path based on the available network topology and link travel costs at that moment. The Dijkstra algorithm evaluates the shortest cumulative travel time from the vehicle's origin to its destination, selecting the route with the minimum total travel time across all feasible paths.

As the simulation proceeds, network conditions may change dynamically due to congestion build-up, flood-induced road closures, or speed reductions applied via additional files from the flood integration module. To ensure that route decisions remain

responsive to these evolving conditions, SUMO's automatic routing framework periodically reevaluates and updates vehicle routes before insertion during the simulation.

Under congested conditions, they can enter any lane at the road edge that is not blocked by traffic. If all lanes are occupied, they must wait until space becomes available, resulting in departure delays. Additionally, the model ensures that each vehicle completes its trip by reaching the intended destination. No vehicle will attempt to return to its origin before either completing its journey or before the simulation time ends.

3.4.4. Flood Impact Implementation

The flood-induced disruptions were integrated into the traffic simulation model using the outputs of the hydrodynamic flood modelling performed in CityCAT, processed through the GIS-based integration tool. Two primary mechanisms were employed to represent the flood impacts within SUMO:

- Complete Road Closures (Reroute Files)

  Road segments that were fully inundated beyond passable thresholds (0.3 m) were marked as entirely closed for vehicular traffic. These closures were encoded using SUMO's reroute files, which specify the list of closed edges and automatically prohibit vehicle entry onto these segments during simulation. As a result, vehicles encountering these closed links would dynamically adjust their routes, avoiding impassable roads based on the real-time automatic routing mechanism described earlier.
- Speed Reductions (Variable Speed Sign Files)

  For road links where flooding caused partial but not complete impairment of functionality, Variable Speed Sign (VSS) files were generated to dynamically modify speed limits over time. The GIS integration tool spatially overlaid flood depth raster onto the network at 20-minute intervals and translated these depth values into speed reductions based on the established flood depth–speed relationship. Each VSS file contained a sequence of step commands indicating when specific speed reductions would take effect for each link throughout the simulation period.

  This combined approach enabled the simulation framework to account for both the spatial and temporal dimensions of flood impacts on road network capacity,

yielding a highly detailed and realistic assessment of traffic system performance under pluvial flood scenarios.

3.4.5. Simulation Outputs

Upon completion of each simulation scenario, SUMO generated comprehensive output datasets capturing a range of performance indicators that can be used to assess the broader systemic impacts of flooding on transportation efficiency and the consequent indirect traffic costs.

The complete set of simulation results serves as the quantitative foundation for the indirect traffic costs calculation and resilience assessment presented in the following sections, where traffic costs and resilience metrics are analyzed and compared across normal, flooded, and mitigation scenarios.

3.5. INDIRECT COSTS OF DISRUPTION

Flood-related impacts on road traffic are typically divided into direct and indirect costs [104]. Direct costs refer to physical damage to infrastructure, such as damage to roads or bridges. Indirect costs, in contrast, encompass wider economic effects—these include losses caused by traffic disruptions, reduced productivity, and environmental consequences. This study concentrates specifically on indirect impacts, excluding physical infrastructure damage. By activating the traffic simulation under flood conditions, differences between the baseline and flood scenarios were assessed. These differences help reveal the effects of flooding on road network performance over time. The associated indirect costs, including travel delays and increased emissions, are then quantified.

3.5.1. Time Cost and Network-Wide Delay

One of the principal indirect consequences of flooding in transport networks is the increase in travel times compared to normal conditions. This additional travel time can be monetized and used as an indicator of the broader socio-economic disruption caused by such events. In this study, the indirect cost of flooding is assessed using two complementary concepts: the person-hours delay (PHD) across the network and the associated time cost, estimated via the Value of Time (VoT).

The person-hours delay represents the aggregate additional time that all travelers spend on the network under flooded conditions compared to a baseline scenario. It is calculated as the difference between the total person-hours of travel in each case, expressed as:

$$PHD = A_b - A_d \quad (3)$$

Where A_d denotes the total person-hours of travel in the disrupted (flooded) scenario and A_b is the corresponding value in the baseline (non-flooded) condition. Both are computed by summing the product of the number of trips between each origin-destination (OD) pair and the average travel time for those trips in the respective scenario.

To translate the delay into an economic cost, the Value of Time (VoT) is applied. VoT represents the monetary worth of travel time and is widely used in transport appraisal. In this study, the 2023 market price for commuting time is adopted, which is £10.11 per person per hour, as reported by the UK Department for Transport [105]. The time cost is then calculated as:

$$C_{time} = PHD \times VoT \quad (4)$$

where C_{time} represents the total time-related cost (£), PHD represents the total person-hours of delay (person·hours), and VoT is the value of time (£/person/hour).

3.5.2. Emission Cost

This study evaluates the environmental cost of traffic-related emissions by focusing on three key pollutants: carbon dioxide (CO_2), carbon monoxide (Co), and nitrogen oxides (NO_x). Furthermore, based on field observation and regional policies, it is assumed that urban buses operating in the Tyne and Wear region are fully electric and thus produce no direct tailpipe emissions. Consequently, only emissions from private passenger vehicles are considered in this cost estimation.

The total emission cost is calculated as:

$$C_e = \sum_{i=\{CO_2, CO, NO_x\}} Q_{i,O} \times S_i \quad (5)$$

Where C_e is the cost due to pollutant emissions; $Q_{i,O}$ denotes the total mass of pollutant i emitted by private vehicles during the flooded scenario (in kg), based on SUMO output.

S_i represents the unit damage cost for pollutant i sourced from 2023 UK valuations. The adopted damage costs are: $S_{CO_2} = 0.241$ £/kg, $S_{CO} = 0.0018$ £/kg, and $S_{NO_x} = 8.148$ £/kg [106]. This method calculates the total emission cost directly from actual emission outputs.

3.6. RESILIENCE ASSESSMENT

The increasing frequency and intensity of natural hazards, such as floods and wildfires, underscore the importance of developing robust resilience assessment frameworks for transportation networks. Resilience, as applied to transportation networks, broadly refers to the system's ability to maintain or rapidly recover acceptable levels of service when exposed to disruptive events. While multiple definitions of resilience exist in the literature, this study adopts a functional resilience perspective, emphasizing the system's ability to sustain operational performance during disruptive conditions and infrastructure recovery processes.

The resilience assessment framework which is shown in Figure 3.4 developed in this study is primarily adapted from the methodology proposed by Arango *et al.* [107], who introduced a novel approach for functional resilience evaluation based on dynamic performance thresholds. Their framework applies a multi-indicator threshold-based evaluation where several key performance indicators (KPIs) are compared against predefined acceptability thresholds to quantify system degradation under disruptive scenarios. Although originally developed in the context of wildfire disruptions, this methodology offers a versatile and transferable structure that is well suited to pluvial flood scenarios as investigated in the present study.

In this research, since the flood hazard modeled herein is time-dependent, with flood intensity evolving over the simulation period, the resilience assessment framework has been adapted to reflect a dynamic representation of functional resilience. Rather than relying on a static, single-value metric, the framework quantifies resilience continuously over time by evaluating the temporal performance of the transportation network during the disruption. This dynamic approach enables the assessment of how the system sustains its functionality at each time step, considering fluctuations in network capacity and travel demand.

Under this framework, multiple flood scenarios are simulated using the integrated CityCAT-SUMO modelling platform. For each synthetic flood scenario (hazard intensity),

quantitative performance metrics are extracted from the traffic simulation outputs and generate a performance matrix. Then comparing this matrix against predefined acceptable thresholds, a compliance matrix will be generated by identifying whether each performance indicator satisfies its corresponding acceptability threshold under each scenario. Finally, an aggregate resilience index is computed, providing a global quantification of the network's functional resilience across all simulated flood scenarios at each time step.

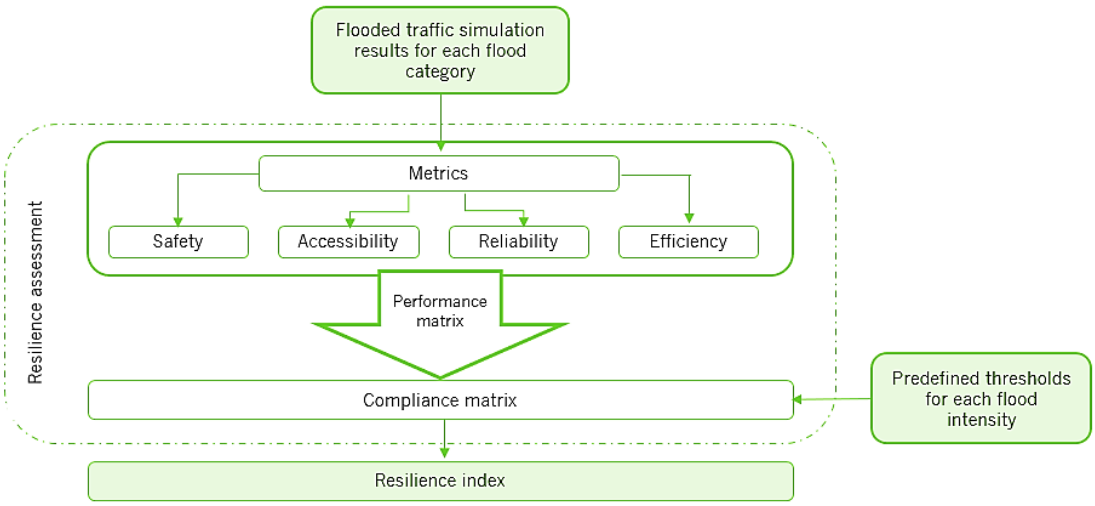


Figure 3.5. Resilience assessment methodology for a flooded network at each time step for each vehicle class.

The rationale for this approach is based on several key considerations. First, the characteristics of potential hazards are inherently uncertain, making it essential to maintain the core functions of the transportation network regardless of the disruption's intensity or duration. Second, the primary function of a traffic network is to support the movement of people and goods. This functionality can be evaluated across three levels: safety at the core, accessibility and reliability at an intermediate level, and efficiency at the outer level. In this study, network functionality is defined primarily in terms of human mobility. The selected metrics reflect widely accepted indicators in the resilience literature and were chosen to fulfill two essential criteria: (i) the avoidance of redundancy—each metric captures distinct aspects of functionality without overlapping definitions; and (ii) internal consistency—disruptions at the core level (e.g., road safety from flooding) consistently propagate to higher levels, affecting accessibility, reliability, and ultimately system performance. For instance, if an origin-destination (OD) pair becomes disconnected,

accessibility is lost, reliability drops to zero, and network performance is severely degraded. This hierarchical relationship is illustrated in Figure 3.6.

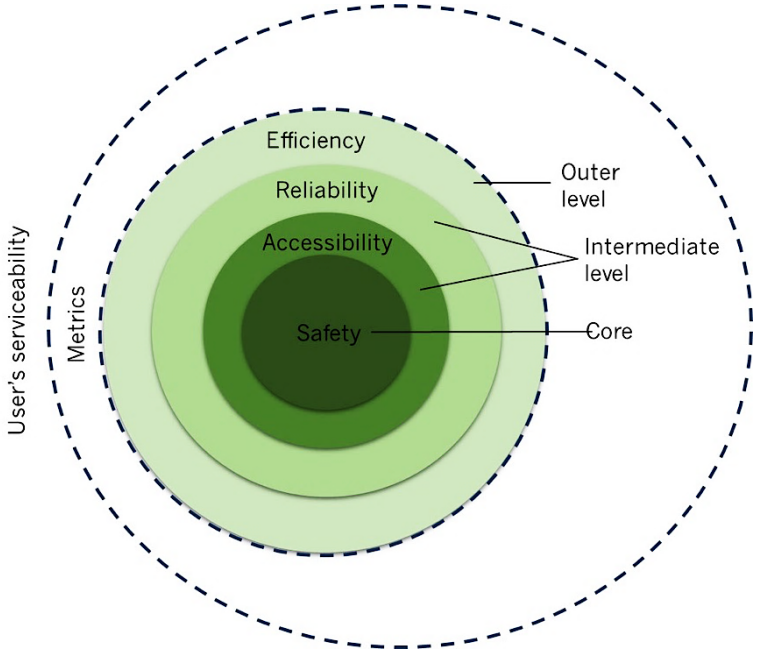


Figure 3.6. Metric's level based on user's serviceability for resilience assessment

This structure implies that during a disruptive event, regardless of hazard intensity, the primary goal is to keep user safe from the inundation. As the severity of the hazard increases, priorities shift in less severe cases, all metrics—safety, accessibility, reliability, and efficiency—may be addressed; in extreme cases where mitigation is unfeasible, the focus should be solely on enabling safe evacuation, even if reliability and efficiency deteriorate. Thus, the desired level of resilience, particularly in terms of robustness, depends on the hazard's intensity.

Finally, a single scenario is insufficient to fully capture the performance of the traffic network. Multiple scenarios are needed to gain a comprehensive understanding of network behavior under varying conditions.

3.6.1. Flood Return Period Classification

In this study, synthetic design floods representing three return periods (1-in-10, 1-in-50, and 1-in-100 years) were generated from 2-hour rainfall events, and the simulations were extended to 9 hours to capture flooding that persisted beyond the rainfall period**.** Rainfall intensities are derived from UK hydrological studies, consistent with previous applications in transport-flood interaction research such as Pregnolato *et al.* [55]. Table **3.2** summarizes the hazard levels, where the 1-in-10 event is considered a normal flood, and the 1-in-50 and 1-in-100 events are considered extreme floods with increasing severity. This classification allows for consistent comparison of transport network resilience under varying levels of rainfall-induced hazard.

Table 3.2. Flood Return Period Classification based on Pregnolato *et al.* [55] according to the Low (L), Median (M), and High (H) rainfall intensities (return period)

Return period	Rainfall intensity (mm/h)	Description	Flood category
1-in-10 years	20	High-probability, lower-intensity event with limited disruption potential.	L
1-in-50 years	30	Less frequent, moderate-intensity event likely to cause moderate disruption.	M
1-in-100 years	45	Rare, high-intensity event expected to cause severe disruption to transport.	H

3.6.2. Definition of Performance Metrics

The resilience assessment framework relies on the quantification of multiple performance metrics that collectively reflect the functional state of the transportation system under flood-induced disruptions. These metrics are derived directly from the traffic simulation outputs generated for each flood scenario and are selected to capture key aspects of network functionality relevant to mobility impacts. Four complementary performance metrics are defined in this study:

3.6.2.1. Safety

The concept of safety is grounded in the idea that road users should be protected from hazardous conditions, particularly during flooding, to maintain both safety and effective emergency access. This indicator is assessed by comparing a road segment (link)'s flood depth (w) to 0.3m. Specifically, the flood depth must not exceed the safety threshold determined for the flooded scenario. To quantify this, the threshold for road closures was

set at 0.3m, in line with studies on flood-related road closures in previous research. This value represents the safe operating flood depth of a specific road link i during a randomly occurring flood event of category c. The w value reflects the flood depth and serves as the basis for calculating the safety index, as shown in Equation (6).

$$Safety_{i,c} = \begin{cases} 0\ (unsafe) & if\ w_{i,c} \geq 0.3m \\ 1\ (safe) & if\ w_{i,c} < 0.3m \end{cases}, \quad \forall i \in N, \forall c \in C \tag{6}$$

In this context, c represents the flood category being evaluated, selected from the broader set of flood scenarios. For each road segment in the network set N, the flood depth on link i (w_{in}) is compared to the threshold for road closures 0.3 m. To assess safety at the network level, the proportion of road segments deemed safe—those meeting the threshold—is calculated relative to the total number of roads in the network for each flood category, as defined in Equation (7).

$$Safety_c = \frac{1}{N} \sum_{i \in N} Safety_{i,c}, \quad \forall c \in C \tag{7}$$

where N refers to the total number of links.

3.6.2.2. Accessibility

The accessibility metric evaluates the ability of users to travel across the network and helps identify any areas that have become isolated. A route r is defined as a series of links connecting an origin–destination (OD) pair, denoted as pq. When multiple route options exist for an OD pair, the network demonstrates redundancy. A network is considered fully accessible if every OD pair has at least one functioning route. The accessibility of a specific OD pair pq is calculated as shown in Equation (8).

$$Accessibility_{pq,c} = \begin{cases} 0\ (unaccessible) & if\ R_{pq,c} = \varnothing \\ 1\ (accessible) & if\ R_{pq,c} \neq \varnothing \end{cases}, \quad pq \in PQ, \forall c \in C \tag{8}$$

Here, $R_{pq,c}$ denotes the set of viable routes connecting the origin–destination (OD) pair pq under flood category c. If a link does not meet the exposure condition—that is, when $w_{i,c,h} \geq 0.3\ m$ it is considered unusable, and any routes containing that link are deemed inactive. In the higher flood category, reflecting higher rainfall intensity, more links are likely to become unsafe, leading to a reduction in overall network accessibility. Network-

level accessibility, Equation (8), is then measured by the proportion of operational routes remaining compared to the total number of routes available before the flood event.

$$Accessibility_c = \frac{\sum_{pq \in PQ} Accessibility_{pq,c}}{\sum_{pq \in PQ} R_{pq,0}}, \quad \forall c \in C \tag{9}$$

3.6.2.3. Reliability

Reliability in transportation refers to the confidence and consistency of travel conditions [108], with a particular emphasis on travel time reliability. In this study, we adopt the definition from Nogal *et al.* [109], which describes travel time reliability as the likelihood that road users can reach their destinations within a predetermined time frame under existing traffic conditions. Accordingly, travel time reliability is assessed for all origin–destination (OD) pairs and for each flood category. The reliability of a specific OD pair is determined by the ratio of the shortest travel time among available routes under normal conditions $Re_{pq,0}$ to the shortest travel time under the flood scenario being analysed, as shown in Equation (10).

$$Reliability_{pq,c} = \frac{\min\left\{t_r ; r \in R_{pq,0}\right\}}{\min\left\{t_r ; r \in R_{pq,c}\right\}}, \quad \forall pq \in PQ, \forall c \in C \tag{10}$$

It is important to note that the shortest route under normal traffic conditions may not remain the shortest during a flood event. This is because flood can either render the optimal route impassable or trigger traffic diversions that lead to increased congestion. Since travellers often have multiple route options between an origin and a destination, it is more meaningful to compare the minimum travel time across all available routes for each OD pair, rather than evaluating individual routes one by one.

A reliability ratio closer to 1 indicates that the OD travel time remains stable and close to optimal, while values approaching 0 suggest reduced reliability for the user. If none of the routes for a given OD pair are operational (i.e., $Accessibility_{pq,c} = 0$), the travel time is considered infinite, resulting in $Reliability_{pq,c} = 0$. At the network level, overall reliability, Equation. (11), is computed as the average reliability across all origin–destination pairs.

$$Reliability_c = \frac{1}{|PQ|} \sum_{pq \in PQ} Reliability_{pq,c}, \quad \forall c \in C \tag{11}$$

Where $|PQ|$ denotes the number of OD pairs.

3.6.2.4. Efficiency

Efficiency reflects the network's ability to deliver service based on its capacity to accommodate demand and facilitate mobility. To evaluate this, the efficiency of each OD pair is determined using both the travel distance and the number of users associated with that pair. It is assumed that the shortest available route between two points offers the best travel experience, as it enables quicker trips. Therefore, the closer the actual travel distance is to the minimum possible (geometric or straight-line) distance, the higher the efficiency of that connection.

However, distance alone is not sufficient—user presence is also essential. A route, even if optimal in distance, contributes nothing to efficiency if it has no users. When multiple routes are available for a given OD pair, the overall efficiency is calculated as the weighted average of each route's efficiency, based on the share of users selecting them. To evaluate efficiency under a specific flood scenario, Equation (12) is used.

$$Efficiency_{pq,c} = \frac{1}{|R_{pq,c}|} \frac{d_{pq}^{f}}{\sum_{r \in R_{pq,c}} X_r} \sum_{r \in R_{pq,c}} \frac{X_r}{d_r}, \quad \forall pq \in PQ, \forall c \in C \tag{12}$$

In this context, $|R_{pq,c}|$ represents the number of available routes for a specific OD pair under a given flood category and is used to compute the average efficiency for that OD. For each available route, the ratio between the geometric (straight-line) distance, d_{pq}^{f}, and the actual route length, dr, is calculated. This ratio is then weighted by the proportion of users traveling on each route, expressed as $\sum_{r \in R_{pq,c}} \frac{X_r}{\sum_{r \in R_{pq,c}} X_r} \frac{d_{pq}^{f}}{dr}$. As a result, an efficiency score is computed for each route as $\frac{X_r}{\sum_{r \in R_{pq,c}} X_r}$. Rearranging these terms yields the formulation presented in Equation (13). An efficiency index closer to 1 indicates that the OD pair functions efficiently, whereas values approaching 0 reflect poor efficiency. At the network level, efficiency is assessed by taking the average of the efficiency scores across all OD pairs.

$$Efficiency_{c} = \frac{1}{|PQ|} \sum_{pq \in PQ} Efficiency_{pq,c}, \quad \forall c \in C \tag{14}$$

The metrics were formulated to ensure logical consistency and continuity among them. Accessibility is closely linked to safety, as a well-accessible traffic network with multiple evacuation options increases the likelihood that users can evacuate safely. Conversely, in a poorly accessible network, disruptions to key routes may isolate entire areas, making evacuation impossible and increasing the risk of fatalities during a flood—this relationship is represented by Equation (8).

Once accessibility is lost—meaning an OD pair becomes disconnected—travel time reliability for that pair can no longer be ensured, as reflected in Equation (10). Moreover, if an OD pair has no available routes, its efficiency is considered zero, in accordance with Equation (12).

3.6.3. Threshold Definition and Compliance Matrix

The resilience assessment framework employed in this study relies on comparing the performance of the transportation network under disruption against predefined acceptability thresholds for each performance indicator. This approach allows for quantifying not only the absolute degradation in system performance but also determining whether the system remains functionally acceptable under different flood scenarios.

3.6.3.1. Threshold Definition

For each of the four performance indicators previously defined, a corresponding threshold for each flood category is established to represent the maximum acceptable degradation level for system functionality. These thresholds are adapted from Arango *et al.* [107], The selected thresholds reflect realistic expectations of network tolerance under flood conditions. The following thresholds are defined for each performance metric in Table 3.3.

Table 3.3. Performance metrics thresholds adopted from Arango *et al.* [107] for Low (L), Median (M), and High (H) rainfall intensities (return period).

Performance Metric	**Flood category**		
	L	**M**	**H**
Safety	1	1	1
Accessibility	1	0.5	0.2
Reliability	1	0.6	0.2
Efficiency	1	0.4	0.1

It is worth mentioning that the exact threshold values should be validated through expert consultation or sensitivity analysis in future extensions of this work. The thresholds

presented here serve as reasonable baseline parameters for demonstrating the application of the framework.

3.6.3.2. Compliance Matrix Generation

Once thresholds are defined, simulation results for each flood scenario are evaluated against these threshold values. For each performance metric and scenario, a binary compliance indicator is assigned as follows:

$$C_{i,j} = \begin{cases} 0 & if\ PM_{i,j} \le \theta_i \\ 1 & otherwise \end{cases} \quad (15)$$

Where $C_{i,j}$ is the compliance status for performance metric i under scenario j, $PM_{i,j}$ is the observed performance value for metric i in scenario j, and θ_i is the threshold for metric i.

This process transforms the performance matrix into a compliance matrix, which indicates for each metric and each scenario whether system performance remains acceptable (compliant) or has degraded beyond acceptable limits (non-compliant).

The compliance matrix serves as the basis for the final resilience index calculation, which integrates multiple performance indicators and scenarios into a unified quantitative resilience score, as described in the following section.

3.6.4. Resilience Index Calculation

Following the generation of the compliance matrix, the final step in the resilience assessment framework consists of aggregating the compliance results across all performance indicators and flood scenarios into a single quantitative resilience index. This index reflects the ability of the transportation system to maintain acceptable functionality under a set of flood-induced disruptions. The Resilience Index (RI) is calculated as:

$$RI = \sum_{i=1}^{M}\sum_{j=1}^{S} \frac{1}{M \times S} C_{i,j} \quad (16)$$

Where M denote the total number of performance metrics considered, S denote the total number of flood scenarios simulated, and $C_{i,j}$ denote the binary compliance indicator for performance metric i in scenario j, as previously defined. The total number of compliance instances across all indicators and scenarios is therefore $M \times S$.

This index produces a normalized value between 0 and 1, where RI = 1 indicates full resilience, i.e., the system remains within acceptable performance levels for all indicators across all scenarios, and RI = 0 indicates complete failure to meet any acceptable performance standard. However, the interpretation of this value must consider the system-specific context which means RI ≥ 0.85 suggests strong resilience, where the network maintains acceptable functionality under nearly all tested flood scenarios. 0.6 ≤ RI < 0.85 reflects moderate resilience, with some performance degradation observed in several scenarios, indicating potential weaknesses in the system that warrant targeted adaptation measures. RI < 0.6 signals low resilience, suggesting that the system consistently fails to meet performance thresholds under most disruption scenarios, and thus requires urgent mitigation planning or infrastructure reinforcement.

These threshold values are not universal and may be adjusted based on local policy objectives, acceptable service levels, or comparative benchmarks. In this study, they serve as a qualitative guide to facilitate the interpretation of numerical outputs.

The resilience index calculated through this method offers several advantages:

- It accounts for both the severity and diversity of disruptions (through the inclusion of multiple flood scenarios).
- It integrates multiple dimensions of system performance (through the use of several distinct performance indicators).
- It produces a transparent, easy-to-interpret score that can be directly compared across systems, regions, or adaptation strategies.

Importantly, this formulation emphasizes multi-dimensional functional resilience, as opposed to focusing solely on a single performance aspect (e.g., delay, accessibility, or emissions). The equal weighting applied to each indicator and scenario reflects the assumption that each performance dimension contributes equally to the overall resilience of the system.

3.6.5. Overall Resilience Calculation of the network

After computing the time-varying resilience of the network for each vehicle class (e.g., cars and buses) at each time step, an overall network resilience value can be derived by incorporating traffic flow as a weighting factor. Specifically, for any given time step t, the

total network resilience, Re_t, is calculated as the weighted average of the resilience of individual vehicle classes based on their respective traffic flows at that hour. This approach captures the contribution of each vehicle class to the network's functionality during the disruption. Once the temporal series of Re_t values has been established, it becomes possible to compute the recovery rate of the system using suitable metrics. The corresponding formulations are presented below.

$$Re_t = \frac{\sum_{v \in V} f_{v,t} . Re_{v,t}}{\sum_{v \in V} f_{v,t}} \quad (17)$$

To quantify how fast the network recovers after the disruption, the recovery rate can be defined as the slope of resilience over the recovery period. Assuming resilience starts recovering at time $t0$ and reaches its maximum (or a stable value) at time $t1$.

$$Recovery\ Rate = \frac{R_{t1} - R_{t0}}{t1 - t0} \quad (18)$$

And in order to quantify how fast the network loses its efficiency, the decline rate is defined as below:

$$Decline\ Rate = \frac{R_{before} - R_{lowest}}{t_{lowest} - t_{start}} \quad (19)$$

Where, R_{before} is resilience of the network before the start of disruption, R_{lowest} is the lowest value of the resilience of the network over time, t_{lowest} is the time at which the resilience is at its minimum value, and t_{start} is the beginning time of disruption.

CHAPTER 4

TRAFFIC INDIRECT COSTS QUANTIFICATION IN TYNE AND WEAR REGION

4.1. INTRODUCTION

This chapter presents the development and application of the suggested integrated framework to quantify the indirect costs of flood-induced disruptions on the road transport network in the Tyne and Wear region, UK. The region was selected due to its dense urban structure, complex multimodal transport system, and historical vulnerability to pluvial flooding—particularly exemplified by the "Toon Monsoon" event of June 2012. Using real and synthetic flood data, the study investigates how different flooding scenarios affect network performance, travel behaviour, and the economic implications of reduced transport functionality.

To achieve this, a multi-step methodology was implemented, involving hydrodynamic flood modelling (via CityCAT), integration of flood outputs into a traffic simulation environment (SUMO), and the quantification of delays, rerouting, and emissions. Notably, the study considers both private vehicles and public buses, the latter of which are often neglected in flood resilience assessments. Real-world GTFS data were used to reconstruct a simplified but representative bus network over the main roads of the region.

The analysis focuses on both operational indicators (e.g., running vehicles, trip duration, route length) and monetized impacts (i.e., delay costs and emission costs). Moreover, the study includes a sensitivity analysis using synthetic flood events with 1-in-10 and 1-in-50-year return periods in addition to the 1-in-100 scenario, to evaluate the robustness of network vulnerability under varying flood severities. The chapter concludes with validation of the simulation framework using real observed traffic and flood data, and correlation analysis to understand the spatial interplay between flood depth and traffic disruption.

4.2. CASE STUDY OVERVIEW: TYNE AND WEAR REGION, UK

The Tyne and Wear region, located in the Northeast of England, serves as the case study for this research due to its high population density, urban structure, complex transport network, and vulnerability to extreme weather events, particularly pluvial flooding.

Tyne and Wear is a metropolitan county comprising five local authority areas: Newcastle upon Tyne, Sunderland, Gateshead, North Tyneside, and South Tyneside. The total area is approximately 540 km², with a population of about 1.14 million residents as of 2022, making it one of the most densely populated urban regions in the UK [110].

The region is supported by a highly integrated and hierarchical road network, including strategic motorways, trunk roads, and local roads that facilitate both regional and national connectivity. Tyne and Wear's Road infrastructure plays a critical role in supporting daily commuting, freight movement, and access to key economic centres such as Newcastle and Sunderland [111].

The local bus network in Tyne and Wear is extensive and forms the backbone of public transportation across the region. Managed by Nexus, the buses cover over 500 routes, linking urban and rural areas and providing essential services for residents, students, and workers. Bus services are particularly critical for connecting low-income communities and reducing dependency on private cars [112].

The Tyne and Wear region in the United Kingdom was selected as the case study due to its historical susceptibility to pluvial flooding and the availability of comprehensive hydrological and traffic data, Figure 4.1. The day that the "Toon Monsoon" event happened in Tyne and Wear region serves as a critical benchmark for verification, calibrating and

validating the proposed framework for evaluating the indirect impacts of flooded road transport networks.

Tyne and Wear is characterized by its dense road network and highly urbanized areas, which are predominantly impervious and particularly vulnerable to surface water flooding. While these challenges are specific to the region, they make it a suitable prototype for studying pluvial flooding in other parts of the United Kingdom or developed countries [113]. A notable example of the region's vulnerability occurred on June 28, 2012, during the event locally known as the "Toon Monsoon" or "Thunder Thursday". This convective storm started around 15:00 and delivered approximately 50 mm of rainfall in around two hours, flooding a part of the main road links and causing severe traffic congestion that persisted for more than six hours [96].

Although direct damage to the road infrastructure and vehicle breakdowns occurred only in areas with deep floodwater, the event highlighted the cascading effects of the flooding on transportation. Additionally, hourly traffic flows on major road links are continuously recorded by TADU through automatic traffic counters, with the data stored in the Traffic Information Database (TRADS) [114]. This wealth of data provides a strong foundation for assessing and improving the resilience of the region's road network.

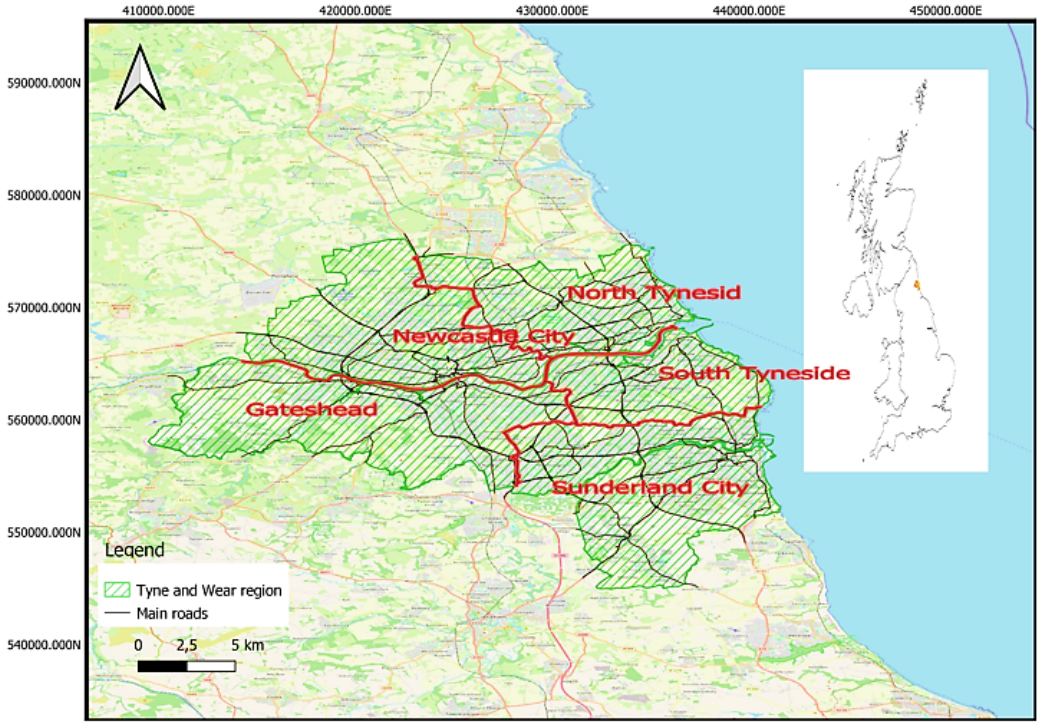


Figure 4.1. Location of the Tyne and Wear region, UK. Coordinate Reference System: EPSG:27700 - OSGB36 / British National Grid

Figure 4.2. presents the main road network of the Tyne and Wear region, sourced from OSM and dated December 28, 2023. This dataset was obtained from Ref. [115], which maintains and distributes regularly updated comprehensive copies of the OSM database.

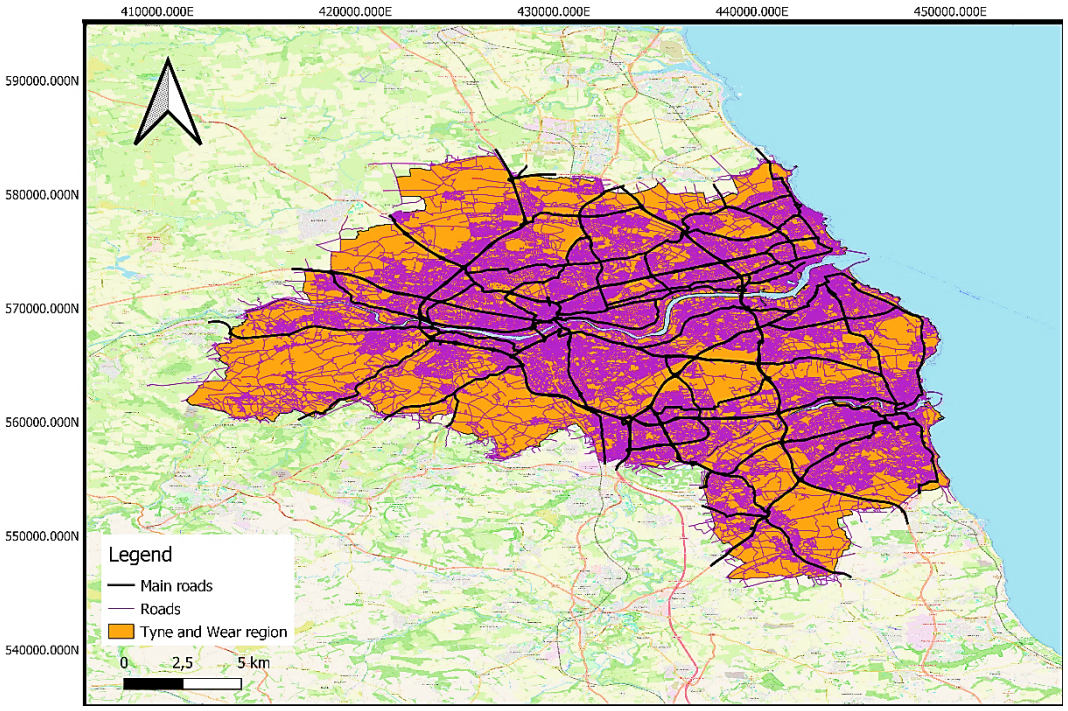


Figure 4.2. Main roads which consist 5.7% of the whole road network in the Tyne and Wear region, UK. Coordinate Reference System: EPSG:4326 – WGS 84/ World Geodetic System 1984.

As shown in Figure 4.2, the full road network in the Tyne and Wear region comprises 83,537 links across all road types. However, when focusing solely on the main roads—motorways, trunk roads, primary roads, and secondary roads—the network is reduced to 4,743 links. Due to the computational demands of processing such a large network, this study limits its scope to these main roads for the development of the proposed framework.

This decision is further supported by observations from the June 28, 2012 flood event, as reported by Pregnolato *et al.* [55]. During that event, major roads were severely affected, leading to a rapid overflow of traffic onto minor residential roads, which were quickly overwhelmed and failed to provide viable alternative routes. Furthermore, many road users lacked sufficient knowledge of local streets and tended to rely on the familiar main road network.

From a transport planning perspective, this approach aligns with a hierarchical classification of the road network, where arterial roads and major distributors constitute

the core structural network. These roads are the most critical for maintaining regional mobility and are thus prioritized in this analysis. While the exclusion of minor roads reduces local-level detail, it enables a more focused, mesoscopic evaluation of network resilience—particularly under disruptive events such as flooding. Consequently, this analysis targets the segments most essential to overall network performance.

One of the main objectives of this thesis is to include public bus transport in the analysis of flood-related impacts—an aspect often overlooked in previous studies. To accomplish this, bus routes and stops were mapped using General Transit Feed Specification (GTFS) data [116] (Figure 4.3a). However, because the road network used in this study excludes minor streets, many original bus routes and stops could not be directly integrated.

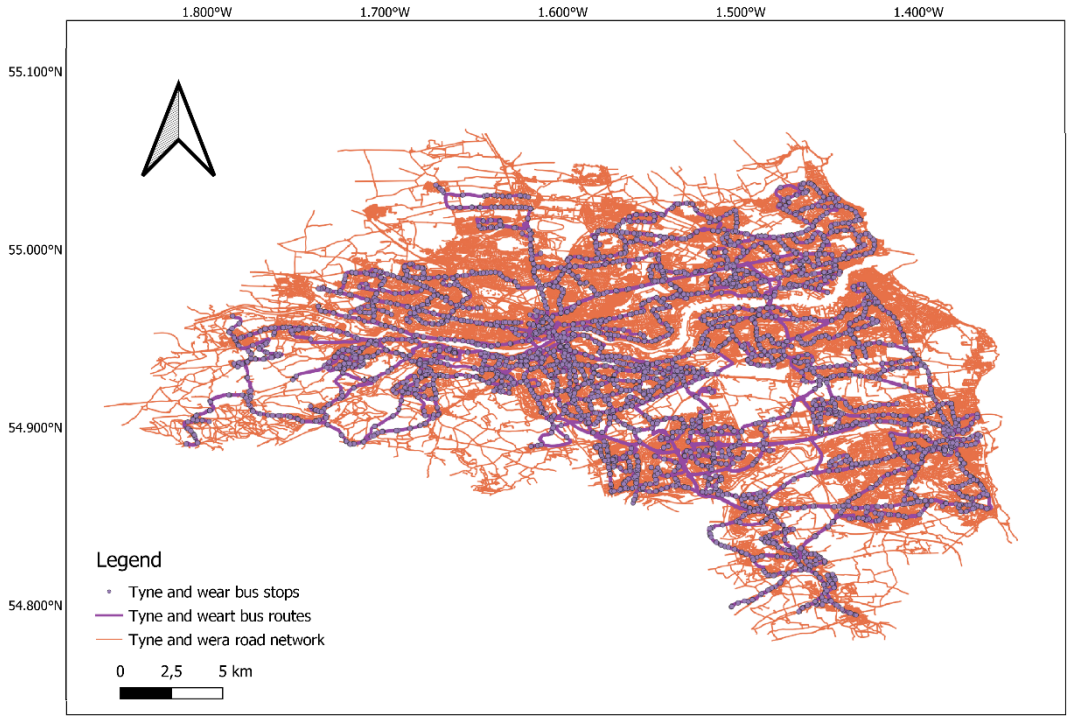
To address this, the public transport network was manually reconstructed to maintain realism as much as possible and ensure compatibility with the simplified road network. Specifically, bus routes with more than 50% spatial overlap with the analysed network were retained. This resulted in the inclusion of 182 out of 501 routes (approximately 36%), and 1,584 out of 3,889 original bus stops (about 41%) (Figure 4.3b). Removed stops were substituted with the nearest accessible stops on the network. Bus routes were then re-generated based on the connectivity and accessibility of the road model, and their schedules were adjusted accordingly to reflect realistic operational conditions under the new configuration.

This methodology ensures that the adapted bus network still represents a substantial share of public transport services in the region, particularly those operating along high-volume, strategic corridors. The final cleaned and reconstructed network—including bus stops and routes—is illustrated in Figure 4.3c.

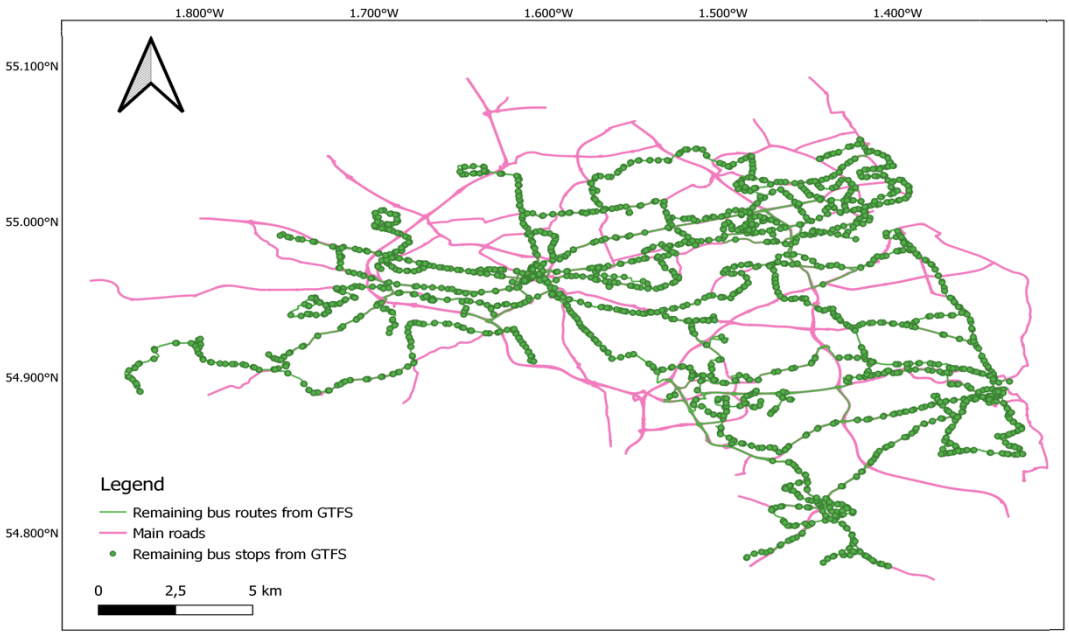
Finally, the road and public transport network was converted into XML format compatible with the SUMO platform, using its netconvert tool [117]. This conversion process enables integration into the traffic simulation model.

As it is shown in Figure 4.4 to prepare the network for simulation, a structured workflow was developed to ensure the consistency and usability of both the road and public transport networks. The process began by importing the complete road network

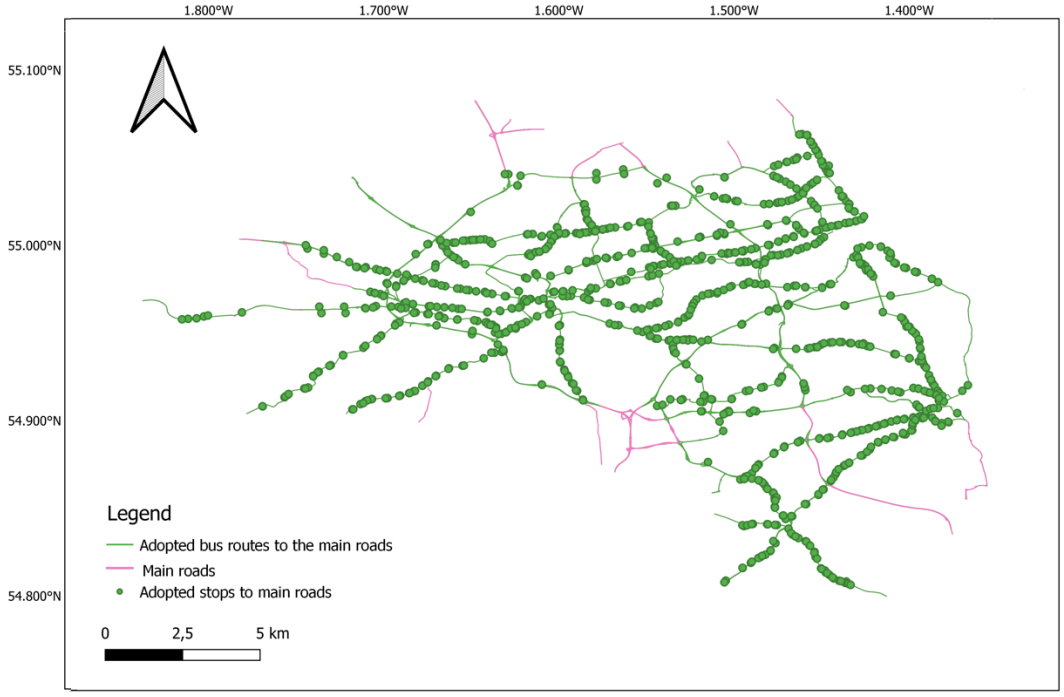
data (i.e., shapefiles) and filtering it to retain only the main roads—motorways, trunk, primary, and secondary roads—which are most relevant for regional traffic analysis and resilience assessment. The OSM data provided road geometry, classifications (e.g., motorway, primary), maximum speed limits, and number of lanes.



(a)



(b)



(c)

Figure 4.3. Process of preparing the road and bus network in this study for the Tyne and Wear region, UK. (a) The full real network of this region including all the roads, bus stops and routes; (b) Main roads network and bus routes with more than 50% spatial overlap with the analysed network; (c) The final cleaned and reconstructed bus network including bus stops and routes in the main roads network of this study. Coordinate Reference System: EPSG:4326 – WGS 84/ World Geodetic System 1984.

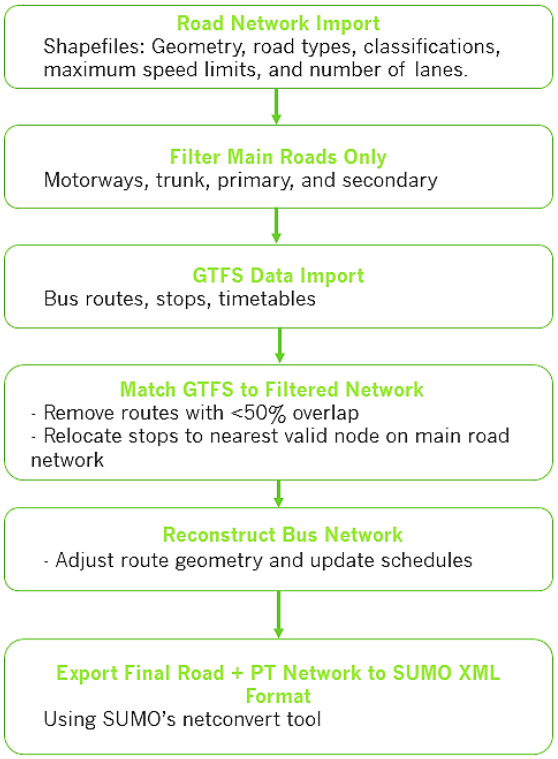


Figure 4.4. Network processing workflow for the main roads in Tyne and Wear region, UK.

In parallel, GTFS data containing bus routes, stops, and schedules was imported. Only those bus routes with significant overlap (≥50%) with the retained road network were selected. Bus stops located on excluded minor roads were mapped to their nearest accessible stop on the main network. The bus routes were then reconstructed based on connectivity within the simplified road model, and timetables were adjusted accordingly. The real bus counts on 28th June 2023 from the Traffic and Accident Data Unit (TADU) [118] were used to calibrate the bus timetables to make the edited bus network as compatible as possible.

Therefore, traffic demand in this study includes passenger vehicles and buses over the course of one day. Traffic counts are a common type of traffic data collected either through automated devices such as induction loops and radar detectors or through manual counting. These counts are recorded over a specific period and may cover multiple time intervals. Additionally, traffic counts can be categorized by vehicle type. In this research, traffic counts were required for two specific days: 28th June 2023-as a normal working day with no recorded hazard disruption to traffic-and the day of the Toon monsoon event (28th June 2012). The Toon monsoon event day was picked to validate the proposed framework in this study. Since classification data was unavailable for 2012 and vehicle types were categorized based on vehicle length, those shorter than 5.2 meters were classified as passenger cars. Therefore, validation could be done only for passenger vehicles.

As shown in Figure 4.5, there were 435 automatic traffic counters on main roads in the region in 2012, increasing to 511 by 2023. The actual traffic data was sourced from the Traffic and Accident Data Unit (TADU) [118], which provides volume counts, speed data, and vehicle type classifications for all motor vehicle monitoring sites in the Tyne and Wear region.

It is important to note that not all roads in the region were considered in this study. Applying total traffic counts across the network would result in an unrealistic traffic distribution. To ensure a more accurate representation, it was necessary to adjust the traffic counts accordingly. Data from a subdirectory of the gov.uk website [119] provides traffic distribution percentages by road type for the Tyne and Wear region. According to these records, main roads accounted for 60% of the total traffic in both 2012 and 2023. Therefore, in this study, only 60% of the recorded traffic counts were used in the analysis.

Finally, according to the explained editions, the running passenger vehicles and buses over time in the main roads network in the Tyne and Wear region in this study are shown in Figure 4.6.

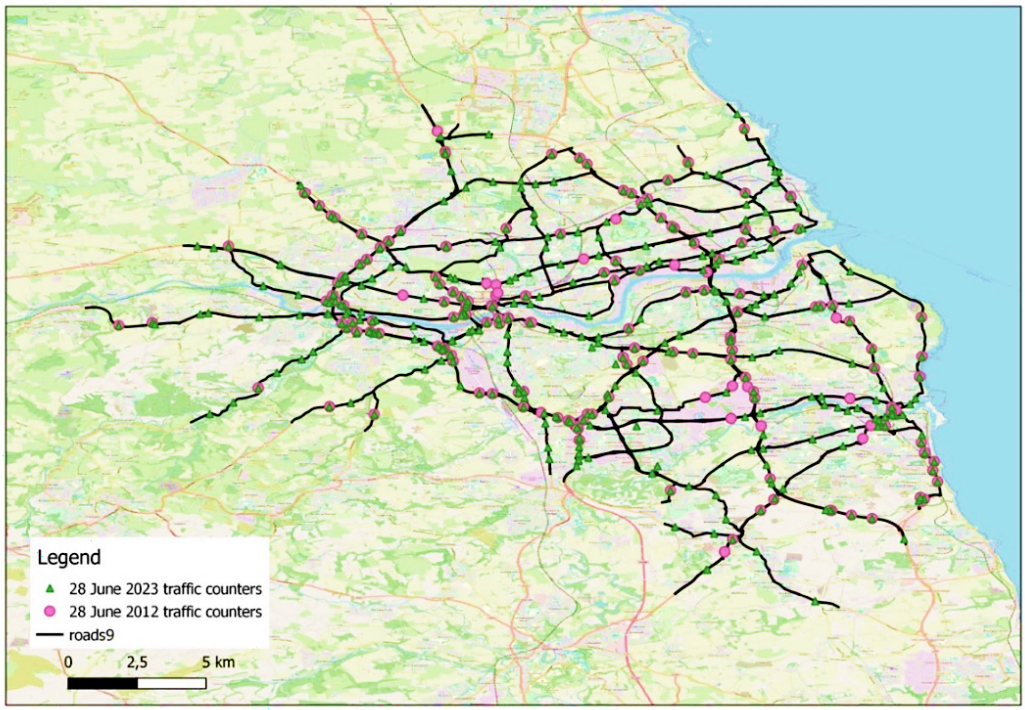


Figure 4.5. Traffic counters on main roads in 2012 and 2023 in Tyne and Wear region, UK.

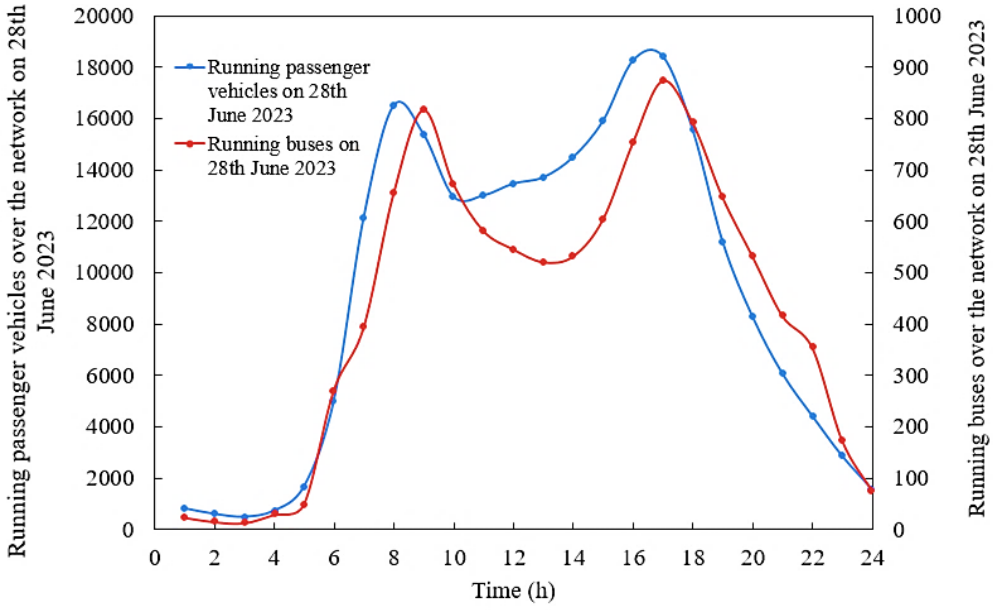


Figure 4.6. Running vehicles over time in the main roads network of Tyne and Wear region, Uk on 28th June 2023.

Regarding the adjusted bus schedules for the day 28th June 2023, bus flows are defined within the bus routes file, trying to keep the same distribution as the real recorded bus counts over the network. This file specifies the start and end times of bus trips, along with the frequency of departures for each route.

Apart from the traffic counters distribution, it is essential to consider the spatial distribution of rainfall monitoring stations within the study area. As shown in Figure 4.7, five rainfall stations are located across the Tyne and Wear region, all of which recorded data during the June 28, 2012, flood event.

Rainfall data from these stations were obtained from [120] and were used to characterize the temporal and spatial variability of the event. These datasets serve as a crucial input for running the hydrodynamic flood model for the event to validate the integrated dynamic modelling framework proposed in this study.

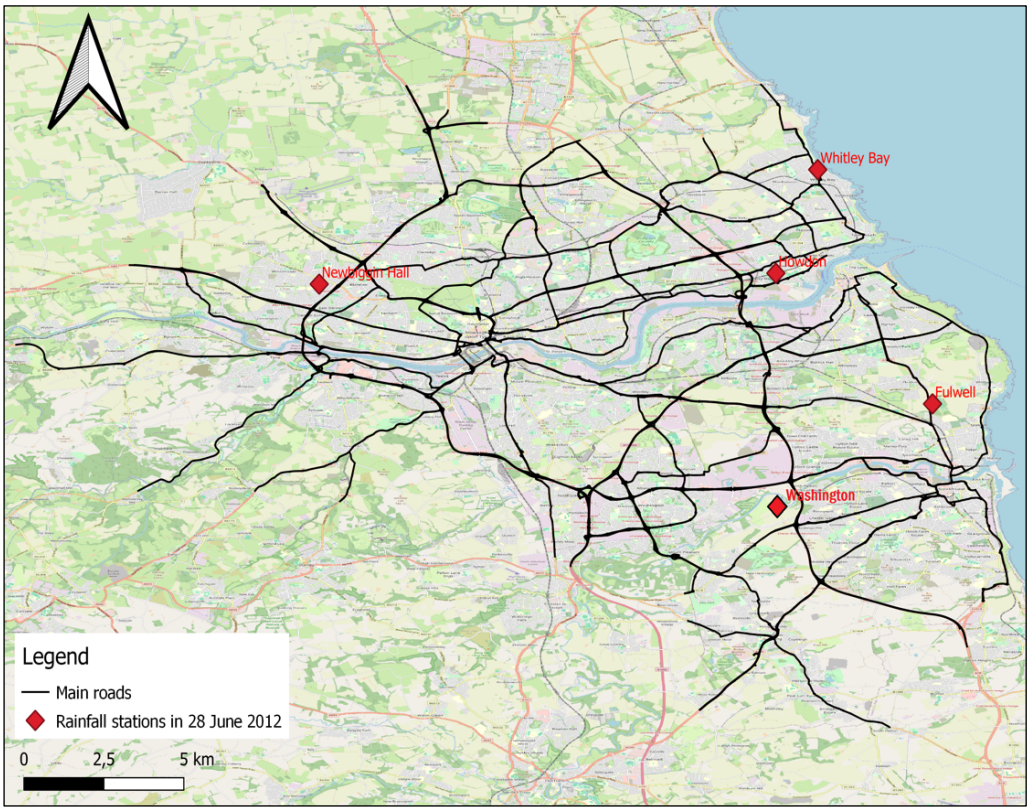
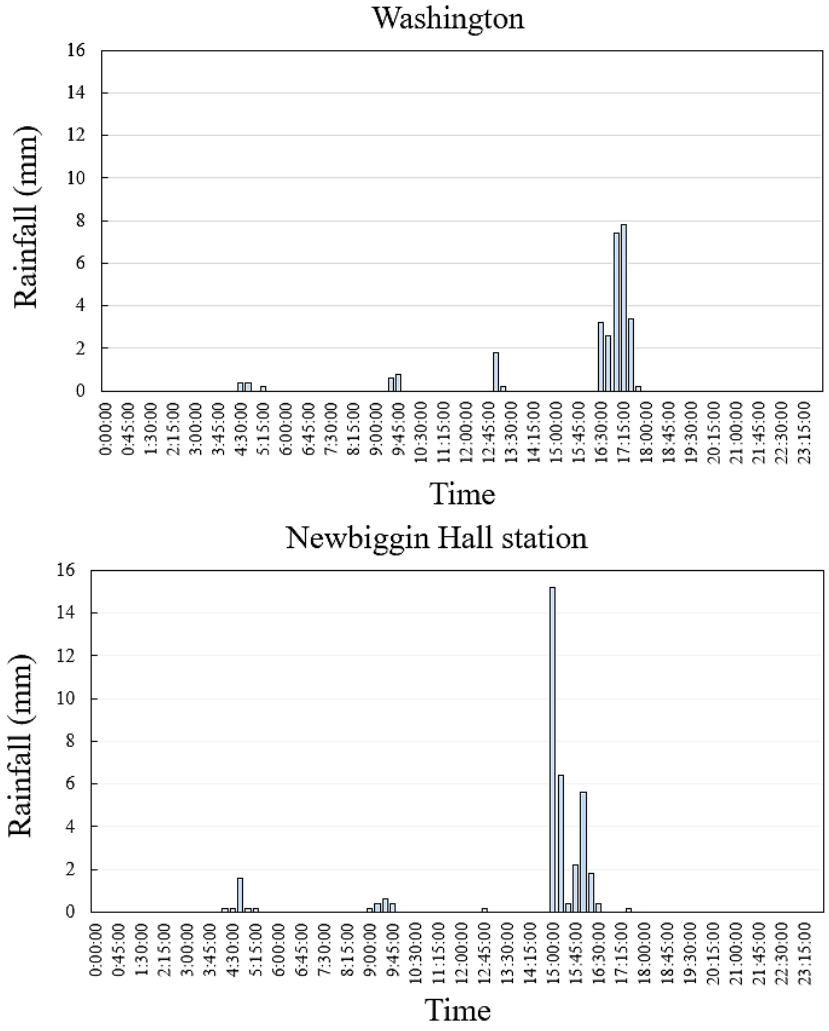


Figure 4.7. Selected rainfall station's location.

Figure 4.8 presents the rainfall profiles observed at these stations on the Toon Monsoon day, downloaded from [120]. Each subplot in Figure 4.8 corresponds to a specific station: Howdon, Fulwell, Whitley Bay Marine, Washington and Newbiggin Hall. In Howdon station, rainfall data show intermittent precipitation throughout the day, with notable peaks

between approximately 15:00 and 17:00, reaching a maximum intensity of around 8 mm within a 15-minute interval. In Fulwell station, rainfall was relatively low, with multiple minor peaks, all below 1.6 mm. In Whitley Bay Marine station, a significant peak is observed in the late afternoon, with rainfall intensity reaching approximately 12 mm within a 15-minute interval, indicating a highly localized extreme rainfall event. In Newbiggin Hall Station, a substantial rainfall event occurred around 15:00, with a peak of approximately 16 mm recorded within a single 15-minute interval. In Washington station, the rainfall data exhibit intermittent precipitation throughout the day, with a pronounced peak in intensity observed between 16:00 and 17:00. During this period, the maximum recorded rainfall reached approximately 8 mm within a 15-minute interval.



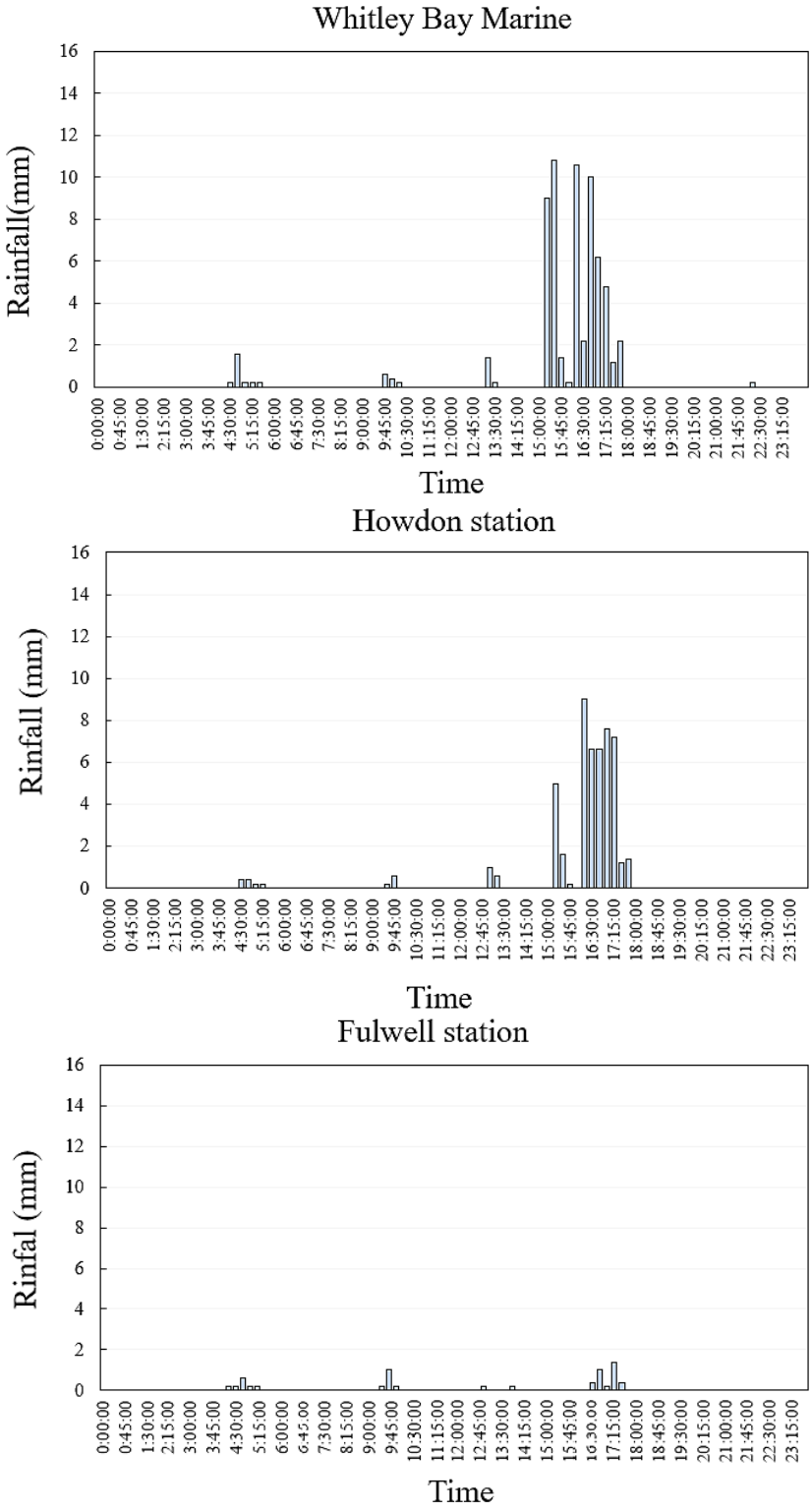
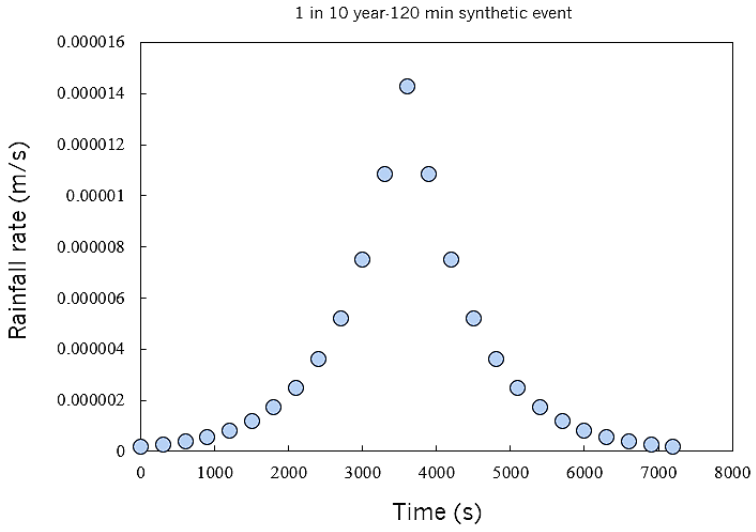


Figure 4.8. 15-minute recorded rainfall in five stations during the Toon Monsoon.

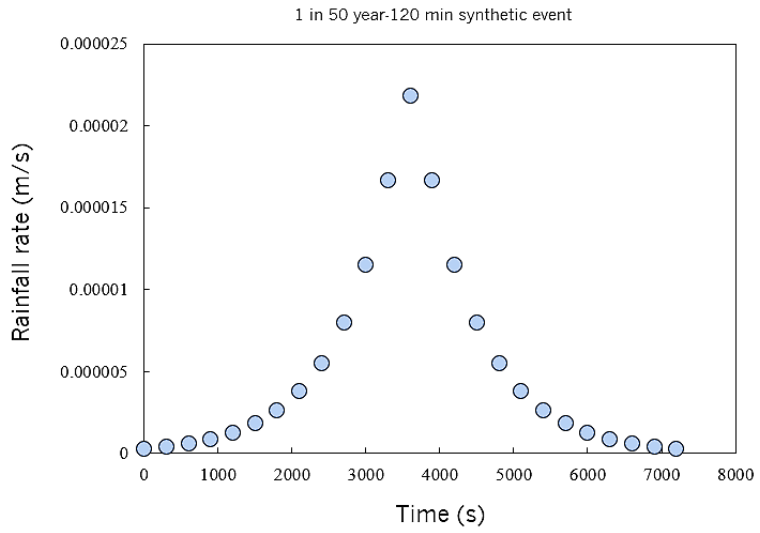
These 15-minute interval records highlight the spatial and temporal variability of rainfall during the Toon Monsoon event, with some stations experiencing brief but intense rainfall bursts while others recorded lower, more distributed precipitation throughout the day. To simulate the pluvial flood event using CityCAT, it is crucial to define the spatial distribution

of rainfall. For this purpose, the Thiessen polygon method by CityCAT was applied to establish the spatial rainfall pattern [121].

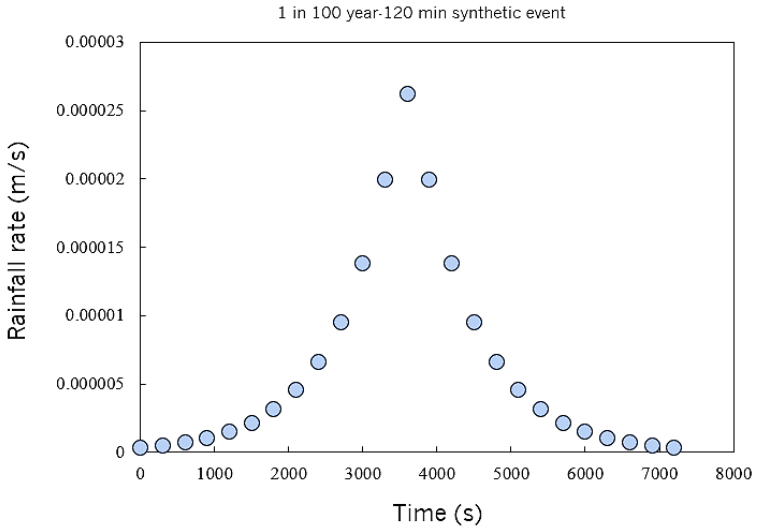
As evident from these diagrams, the Toon Monsoon event started at the evening traffic peak hours, between 15:00 and 17:00. To assess the indirect costs of traffic and the resilience of the transport network, three synthetic flood events—each with a duration of 9 hours, matching that of the Toon Monsoon—were generated. These synthetic flood events were generated following the standard U.K. procedure from the Flood Estimation Handbook [122]. Figure 4.9 shows the rainfall pattern for each synthetic flood scenario.



(a)



(b)



(c)

Figure 4.9. Rainfall profile applied for each synthetic scenario. a) 1 in 10 year-2 hours synthetic rainfall; b) 1 in 50 year-2 hours synthetic rainfall; c) 1 in 100 year-2 hours synthetic rainfall.

These return periods represent extreme precipitation scenarios that occur once in 10, 50, and 100-years. The first plot represents a 1 in 10-year 2-hour synthetic rainfall event. The residual rain rate peaks around the midpoint of the event, showing a sharp increase followed by a decline. The second plot illustrates a 1 in 50-year 2-hour synthetic event, which follows a similar pattern but with a higher peak residual rain rate. This indicates a more intense precipitation event occurring over the same duration. The final plot corresponds to a 1 in 100-year 2-hour synthetic event, exhibiting the highest peak residual rain rate among the three cases. This suggests an extreme precipitation event with a very low probability but significant intensity.

In this study, a two-hour rainfall event was assumed to result in 9 hours of flooding on the network. This assumption is based on observations from the Toon Monsoon event, where floodwater and surface water impacts were reported to persist for the following days after the initial rainfall. Therefore, since the traffic simulation period in this research covers a full day, it was assumed that the flood duration—from the start of the rainfall to the end of the day—would capture the main impacts. The flood models were developed and simulated accordingly.

For each of these scenarios, the speed reduction, according to the depth of floodwater over time, is calculated for each link using the integration tool.

4.3. SCENARIO SETUP

To explore the indirect flood costs on the road transport network, a set of traffic simulation scenarios were created (Table 4.1) based on normal and flooded traffic conditions. The analysis of indirect costs of flood in this research is based on the 1-in-100 year 2-hours synthetic rainfall occurring at the evening peak hours that led to a 9-hours flooding.

Table 4.1. Scenarios setting

Scenario	Traffic data	Flood data
Baseline	28 June 2023	-
Synthetic flood 1	28 June 2023	9 hours synthetic flood 1-in-100 year
Synthetic flood 2	28 June 2023	9 hours synthetic flood 1-in-50 year
Synthetic flood 3	28 June 2023	9 hours synthetic flood 1-in-10 year
Real Toon Monsoon	28 June 2012	9 hours real pluvial flood

Since the Toon Monsoon event corresponds to a flood with a 100-year return period, the analysis of the indirect costs of flooding focuses exclusively on this event. The two additional synthetic flood scenarios will be utilized to conduct sensitivity analysis and assess the resilience of the network. The Toon Monsoon event was also simulated to verify and validate the performance of the framework.

4.4. FLOOD IMPACTS ON ROAD INFRASTRUCTURE

The hydrological model simulated a 1-in-100-year flood event predominantly affecting the Newcastle, Sunderland, and South Tyneside local authority areas within the Tyne and Wear region (Figure 4.10). To capture the dynamic progression of the flood in the traffic simulation, a nine-hour flooding period was modelled following a two-hour 1-in-100-year rainfall event.

This flooding duration was divided into twenty-seven epochs, each lasting twenty minutes. During each epoch, water depth on every road segment was calculated, using a 0.3-metre threshold to distinguish between shallow and deep flooding. Roads with shallow water were assigned speed reductions, while those with deep water were considered impassable and closed to traffic (Figure 4.11).

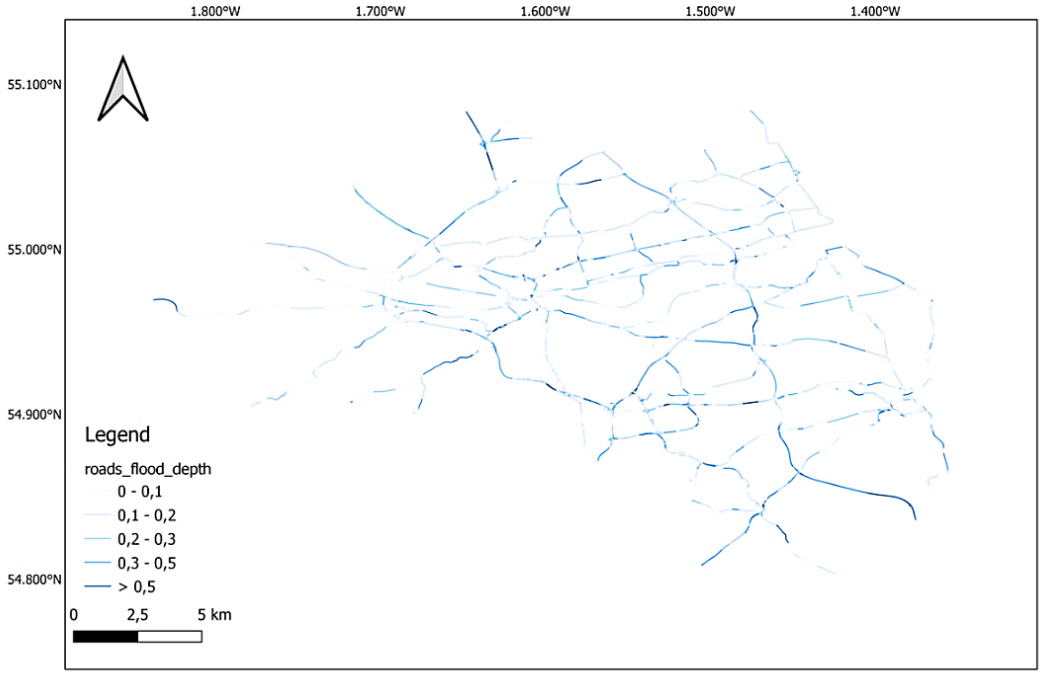


Figure 4.10. Peak water depth on roads in Tyne and Wear region during the 1-in-100-year synthetic flood event simulated in CityCAT

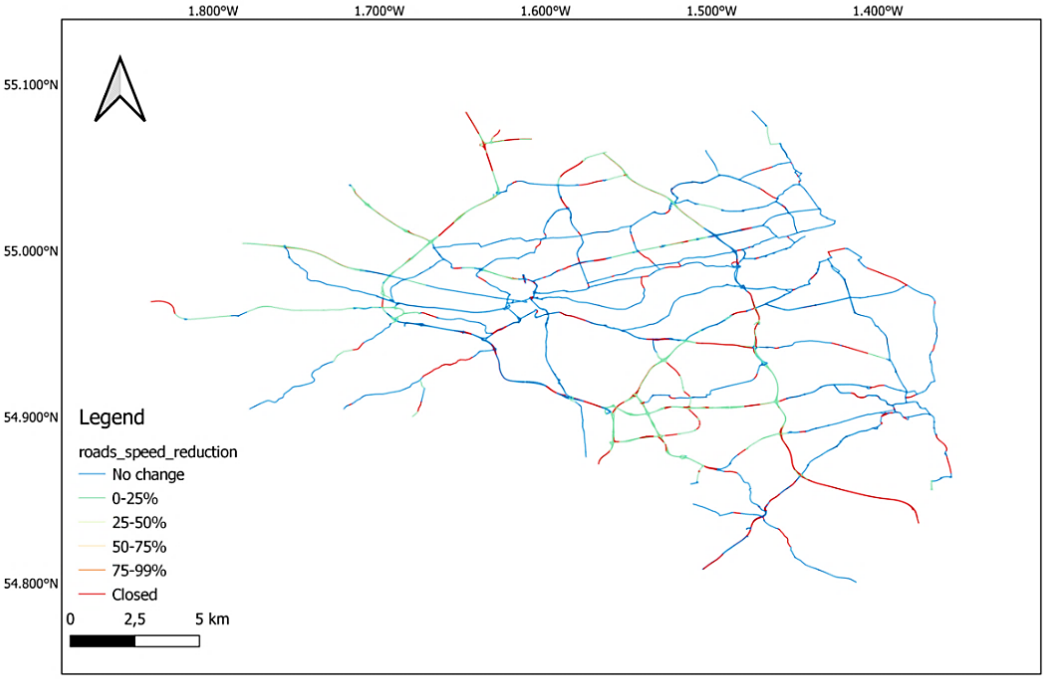


Figure 4.11. Maximum Speed reduction on roads in Tyne and Wear region during the 1-in-100-year synthetic flood event simulated in CityCAT

Figure 4.12 illustrates the evolution of road closures and speed reductions throughout the flooding period for the 1-in-100-year synthetic flood scenario. Two key dimensions are represented: the absolute length (in kilometers) of affected roads and their relative share as a percentage of the total network length.

In the early stages of the flood (around 15:20), both the number and percentage of affected roads begin to increase sharply. The length of roads with reduced speed rises rapidly, reaching its peak at approximately 17:20, where over 160 km of the network experience speed restrictions—equivalent to around 68% of the total road length. Similarly, road closures also intensify during this period, with the length of fully closed roads peaking at nearly 75 km, or about 30% of the network.

After reaching their respective peaks, both types of disruption show a gradual decline. The reduction in affected road length begins steadily after 17:40 and continues until the end of the simulated day. By 23:40, the closed roads length has decreased to approximately 30 km (~12%), while speed-reduced segments remain significant but diminished, dropping to about 100 km (~40%). This pattern reflects the dynamic nature of floodwater propagation and drainage in the network.

Notably, the percentage of reduced-speed roads consistently remains more than twice the percentage of closed roads, indicating that in most cases, flooding impacts road functionality without causing complete closure. This distinction is important, as speed-reduced segments, although still usable, contribute to congestion, increased travel times, and network-wide performance degradation.

Overall, the figure highlights the temporal intensity and gradual recovery of flood impacts on the road network. The significant portion of the network affected during peak hours demonstrates the system’s vulnerability under extreme flood conditions.

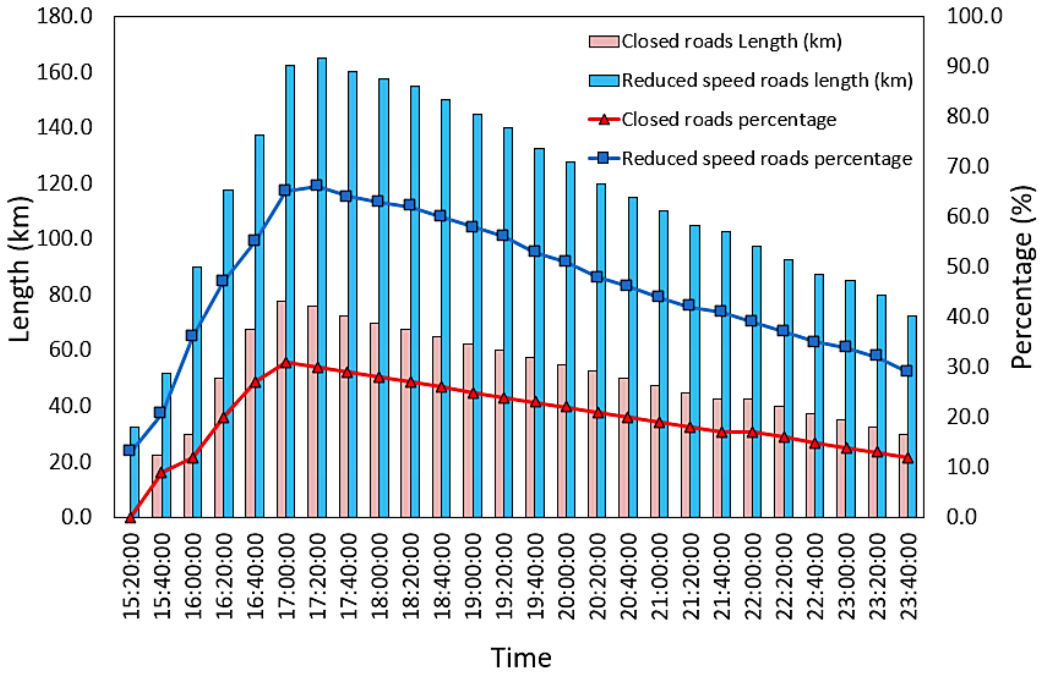


Figure 4.12. Road length and percentage of closed or speed-reduced roads over the flooding time for 1-in-100-year synthetic flood scenario

The average speed for each road segment was calculated over the full 24-hour simulation period. Figure 4.13 illustrates the distribution of average speed changes across all road links during the 1-in-100-year synthetic flood scenario. The majority of road segments experienced a speed reduction, with the highest proportion of links falling in the (-10%, 0) and (-50%, -30%) intervals. However, it is important to note that not all links experienced a decrease in speed.

A small but significant proportion of links maintained their original speeds (0% change), and some even showed speed increases (up to 25%). This can be attributed to traffic rerouting during the flood event. As certain road segments became inundated or congested, vehicles were redirected to alternative routes. In some of these alternate links, the traffic volume decreased relative to normal conditions, potentially due to network reconfiguration or driver behavior. Consequently, average speeds in these segments increased rather than decreased, highlighting the complex and uneven impact of flooding on the road network.

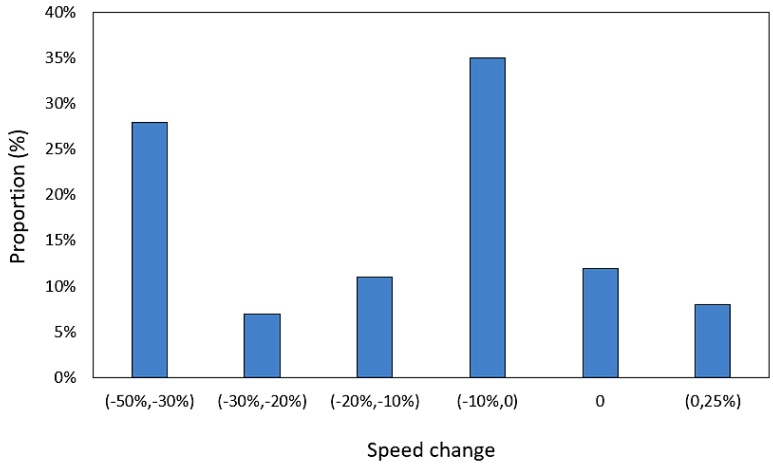


Figure 4.13. Speed change percentage distribution of the 1-in-100-year synthetic flood scenario

4.5. FLOOD IMPACT ON TRIPS

Figure 4.14 illustrates the impact of the 1-in-100-year synthetic flood scenario on vehicle activity within the network. Panel (a) presents the number of running vehicles (passenger cars and buses) over the 24-hour simulation period, while panel (b) shows the number of rerouted car trips by departure time.

As observed in panel (a), the number of running passenger cars under flood conditions initially follows a similar daily pattern to the normal scenario. However, from around 15:00 onward—coinciding with the onset of flooding—there is a sharp divergence. The number of cars present in the network increases substantially compared to the normal condition, peaking between 17:00 and 20:00. This is attributed to the effects of flooding on network performance: road closures and speed reductions lead to increased congestion and prolonged travel times, causing vehicles to remain on the network longer than usual.

A similar pattern is observed for buses: although the number of active buses is generally lower in absolute terms, the flood scenario results in noticeably more buses remaining in the network for longer periods, especially during the evening peak. This is not because more bus trips are introduced, but rather because many buses become delayed or stuck in congestion due to flooded or closed road segments.

It is important to note that in this simulation, buses were assumed to strictly follow their predefined timetables and routes, with no ability to reroute or adapt to road closures. Additionally, no cancellations of scheduled bus services were modelled. This modelling assumption was used to maintain simplicity in initial analysis, and its realism will be

revisited in subsequent sections using external data sources such as official reports and news articles related to similar flood events (e.g., the Toon Monsoon).

Panel (b) shows that rerouting only applies to passenger cars, with the number of rerouted trips spiking sharply after 16:00, aligning with the escalation of network disruptions. The peak occurs around 18:00, when over 13,000 car trips per hour were dynamically rerouted to avoid blocked or impaired routes. In contrast, no rerouting was implemented for buses, which explains their absence in this figure. This modelling constraint highlights the asymmetry between private vehicles and public transport in terms of adaptive capacity during flooding.

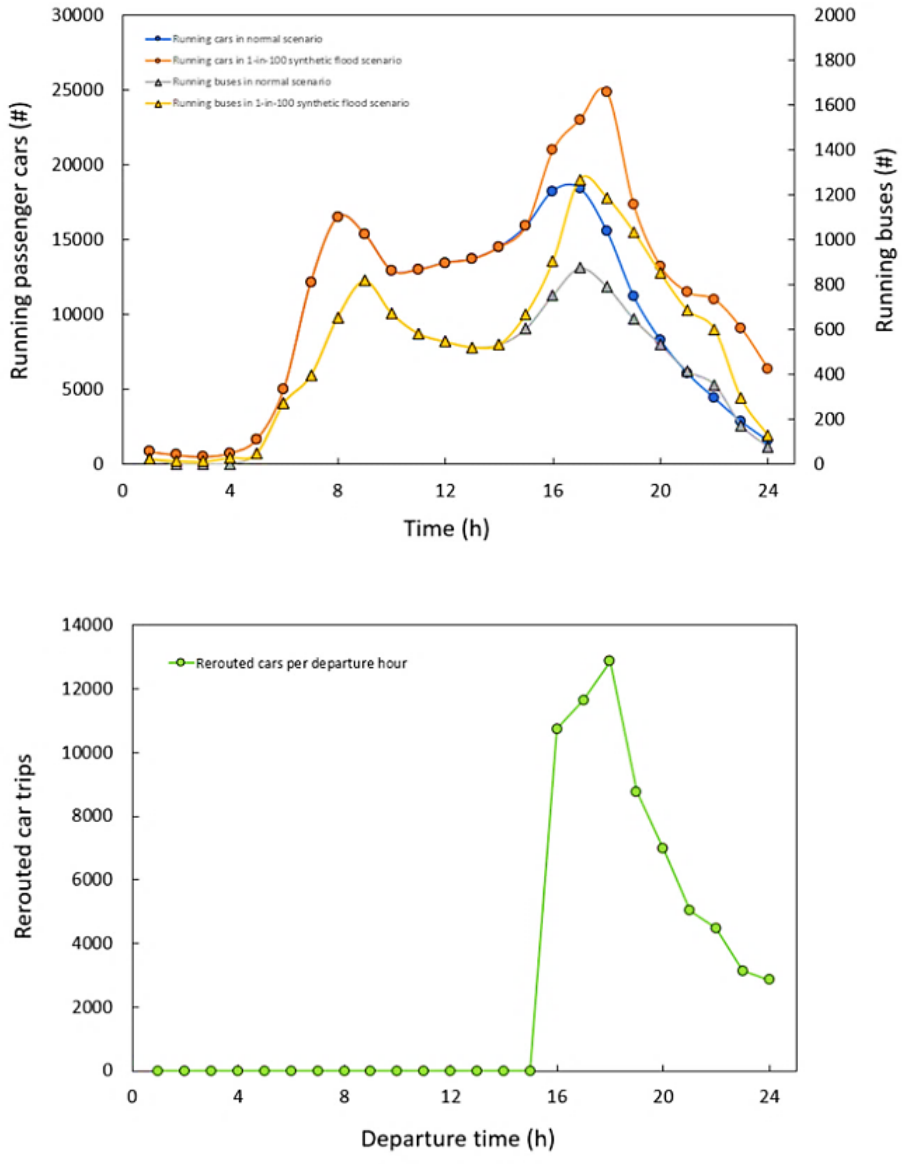


Figure 4.14. Simulation state over time and trip information of 1-in-100 flood scenario. (a) Number of the running vehicles (cars and buses) in the network over time. (b) Number of the rerouted cars over time.

In summary, Figure 4.14 reveals how flooding significantly increases the number of vehicles (both cars and buses) active in the network, not because more trips are generated, but because trips take longer to complete due to congestion, delays, and lack of routing flexibility. The inability of buses to reroute or cancel services further contributes to their extended presence in the network, underscoring a key limitation in public transport resilience under static routing assumptions.

Figure 4.15 presents the aggregated characteristics of trips by departure hour under the 1-in-100-year flood scenario. Panel (a) shows the total trip duration (in hours) and panel (b) shows the total route length (in kilometers) for both passenger cars and buses, compared between normal and flooded conditions.

In panel (a), under normal conditions, the total duration of car trips exhibits a bimodal distribution, peaking around the morning rush hour (08:00) and again in the late afternoon (17:00–18:00). However, under flood conditions, a significant increase in total car travel time is observed from 16:00 onwards, reaching a maximum around 18:00–19:00. This sharp rise is directly linked to the coincidence of flood-induced disruptions such as road closures and speed reductions, and traffic congestion during rush hours. The increased duration does not reflect a higher number of trips, but rather that trips remain active in the network for longer periods due to impaired flow conditions.

Interestingly, buses also experience an increase in total duration during peak hours under the flooded scenario, despite having no rerouting flexibility. This increase is not due to additional services but results from the fact that buses become delayed or immobilized in traffic congestion, particularly when their routes intersect flooded or closed road segments. Since buses were assumed to maintain their predefined schedules and routes in the simulation (with no cancellations), those already deployed continue operating—even if the operational efficiency is reduced under such disruptive conditions.

Panel (b) compares the total route length (in kilometers) per departure hour for both cars and buses under normal and flooded scenarios. Each bar represents the cumulative kilometers travelled by all vehicles departing at a given hour.

For cars, the red bars (flooded condition) show consistently higher or equal route lengths than the blue bars (normal condition) during peak hours (especially 07:00–09:00

and 16:00–19:00). This reflects rerouting behavior in response to road closures or slowdowns. Due to network disruption, cars must take longer alternative paths to reach their destinations, increasing the aggregate distance travelled.

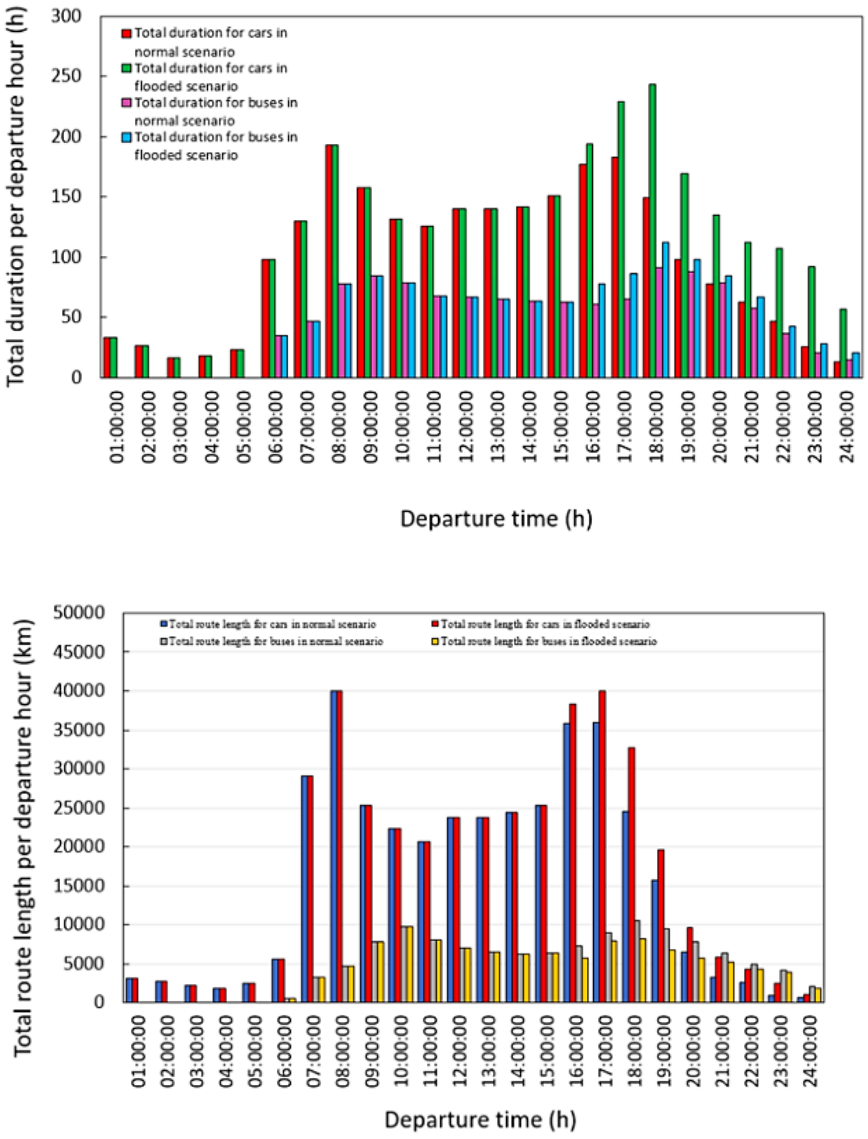


Figure 4.15. (a) Total trip duration and (b) total trip route length per departure hour for 1-in-100 flood scenario.

For buses, however, the yellow bars (flooded condition) indicate shorter total route lengths compared to the grey bars (normal condition), especially between 07:00 and 20:00, despite the number of departures being the same in both scenarios (as no cancellations were simulated). This reduction is not due to early terminations or vehicles getting stuck, but rather a result of slower movement and limited progress through the network during disrupted conditions. In flooded scenarios, buses advance more slowly and may not reach

the same extent of network coverage within the same simulation time window. Consequently, the total cumulative distance they travel is reduced.

Importantly, as flood severity diminishes in later hours (after 20:00), the gap between normal and flooded conditions gradually narrows. This reflects the recovery of the network, where fewer roads remain closed or speed-reduced, allowing buses to resume near-normal route coverage. By late evening (22:00–24:00), the total distance travelled by buses converges toward that of the normal scenario.

Overall, this analysis confirms that network-wide flooding disproportionately affects the effective travel distance of fixed-route services, such as buses. Unlike cars that benefit from dynamic rerouting, buses with predefined schedules and paths are constrained in their adaptability. These insights underscore the need for incorporating flexibility or real-time operational updates into public transport systems when dealing with large-scale disruptions.

4.6. TRAFFIC INDIRECT COSTS

Given that the simulated transport network includes both private vehicles and buses, it is necessary to account for the different average occupancies of these modes in the calculation of person-hours. For this purpose, each private vehicle is assumed to carry an average of 1.6 persons, based on the National Travel Survey for England [105], while each bus is assumed to carry 25 passengers, reflecting average urban occupancy levels [123]. Accordingly, vehicle-hours of delay obtained from simulation outputs are converted into person-hours by multiplying by these occupancy rates, ensuring that the higher impact of delayed public transport services is properly reflected in the network-wide delay metric.

Table 4.2., Indirect traffic cost of 1-in-100 synthetic scenario in the main roads of Tyne and Wear region, UK.

Parameter	Base scenario		1-in-100 scenario	
	Cars	Bus	Cars	Bus
PHD (h)	-	-	21,796	8,781
C_{time} (£)	0	0	220,358	88,776
C_e (£)	79,468	0	130,853	0
Total cost (£)	79,468		439,987	
Relative increase (%)	-		454%	

Under the 1-in-100 synthetic flood scenario in the Tyne and Wear region, the estimated indirect traffic costs significantly increase compared to the base scenario. As shown in Table 4.2, the baseline condition results in a total cost of £79,468, exclusively associated with car traffic, as no disruption or delay is assumed. In contrast, the 1-in-100 scenario yields a total indirect cost of £360,519, corresponding to a 354% increase. This cost comprises £130,853 from car traffic and £229,666 from bus delays.

While these figures already suggest a major economic impact, it is important to interpret them within the modelling assumptions. Notably, the number of vehicle-hours of delay (PHD) for cars is 21,796 and for buses is 8,781. When adjusted for occupancy levels (1.6 persons per car, 25 persons per bus), the corresponding time costs become significantly higher for buses (£88,776) compared to cars (£220,358), even though fewer bus vehicle-hours were delayed. This outcome reflects the amplified effect of delayed public transport due to higher occupancy per vehicle. The emission cost component was assumed to be £79,468 for cars under baseline conditions and £130,853 under the disrupted condition, with no added external costs for buses, consistent with the assumption that all buses in the region are fully electric.

However, several simplifying assumptions were made in this analysis and should be acknowledged. First, modal shift behavior was not considered. In the model, for example if a bus trip is delayed due to road disruption, all passengers associated with that service are assumed to remain with the bus mode.

Secondly, it was assumed that all buses in the region are electric and do not contribute to emissions costs. While this reflects the regional trend towards electrification — supported by observational evidence — a fraction of the bus fleet may still rely on combustion engines. This assumption might slightly underestimate the environmental costs associated with disruption-related delays in public transport.

The analysis demonstrated that even under the assumption of a fully electrified bus fleet—where emissions-related externalities were disregarded—flood-induced indirect costs remained substantial. These finding highlights that simply overlooking buses in road network analyses, as often seen in the literature, risks producing incomplete and potentially misleading insights. On the contrary, our results show that buses play a

significant role in shaping both disruption impacts and resilience outcomes. Therefore, future assessments of urban road transport systems should explicitly incorporate public bus operations when estimating flood-related costs and designing mitigation strategies. By doing so, decision-makers can achieve more realistic evaluations and adopt more effective measures to enhance network resilience.

4.7. INTEGRATION TOOL VERIFICATION AND RESULTS VALIDATION

To verify the overall tool developed in this research, it is necessary to first validate each of its key components individually and then assess the integration of the entire framework. The main components of the tool include: (i) the hydrodynamic flood model (CityCAT), (ii) the integration equation used to map flood outputs to traffic disruptions, and (iii) the traffic simulation model (SUMO). Each of these components has been previously validated and widely used in the literature. CityCAT, for instance, has been applied in multiple studies across the UK, demonstrating its capacity to simulate urban flooding with reliable results. Notably, it was employed by Pregnolato *et. al.* [80] to model flood scenarios in Newcastle Upon Tyne, UK, where the simulation outcomes closely matched observed flood extents. Similarly, the integration equation used in this research has been previously proposed and validated in studies such as Pregnolato et. al. [55], where it was used to translate flood severity into disruptions to traffic networks. As for SUMO, it has been extensively used for simulation of traffic networks and has demonstrated robustness and reliability in both normal and disrupted traffic conditions (e.g., [124]).

In addition to being theoretically validated through the literature, these simulation tools, both for flood and traffic modelling, and their integration framework were empirically assessed by comparing their outputs with real-world data, as discussed in the following section.

4.7.1. Verification and validation of CityCAT and SUMO outputs

To validate the CityCAT simulation results, the model was run using recorded data from the Toon Monsoon event. The simulation inputs included rainfall time series for five meteorological stations—namely Howdon, Fulwell, Whitley Bay Marine, Washington and Newbiggin Hall—previously introduced in the case study section. In addition, rainfall polygon zones were defined to spatially distribute the rainfall data, and layers of buildings

and green areas were also incorporated into the model. Using these inputs, the CityCAT model was executed to reproduce the flooding conditions observed during the event.

The model outputs were then qualitatively validated through comparison with photographs and video recordings taken during the Toon Monsoon. The results showed a strong agreement with real-world observations. For example, as shown in Figure 4.16a and b, roads A184 and A1058 were fully closed to traffic and experienced reduced speeds, respectively, due to flood depths exceeding and remaining below 0.3 meters. The simulation captured these impacts with high accuracy, as illustrated in Figure 4.16c.

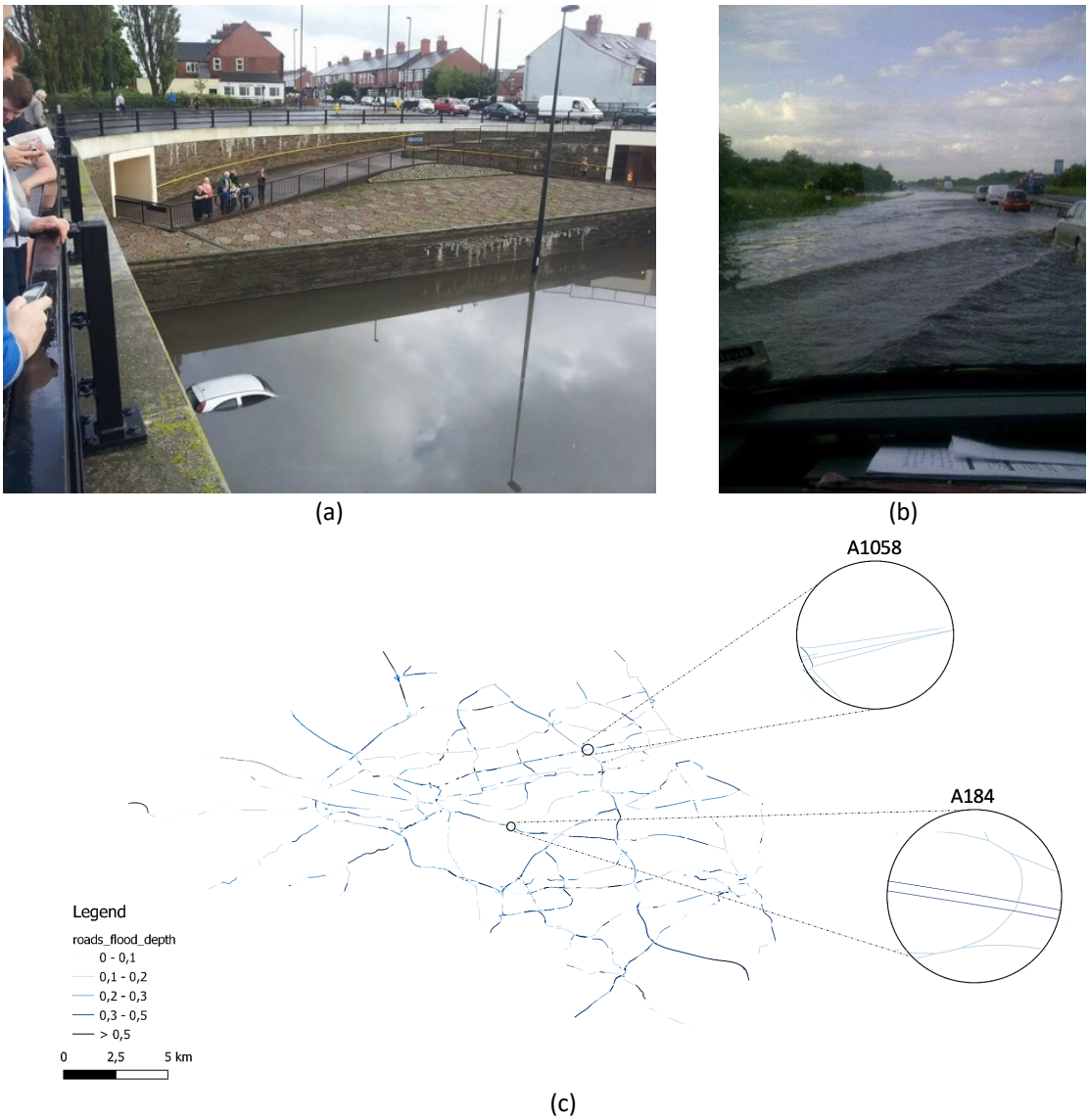
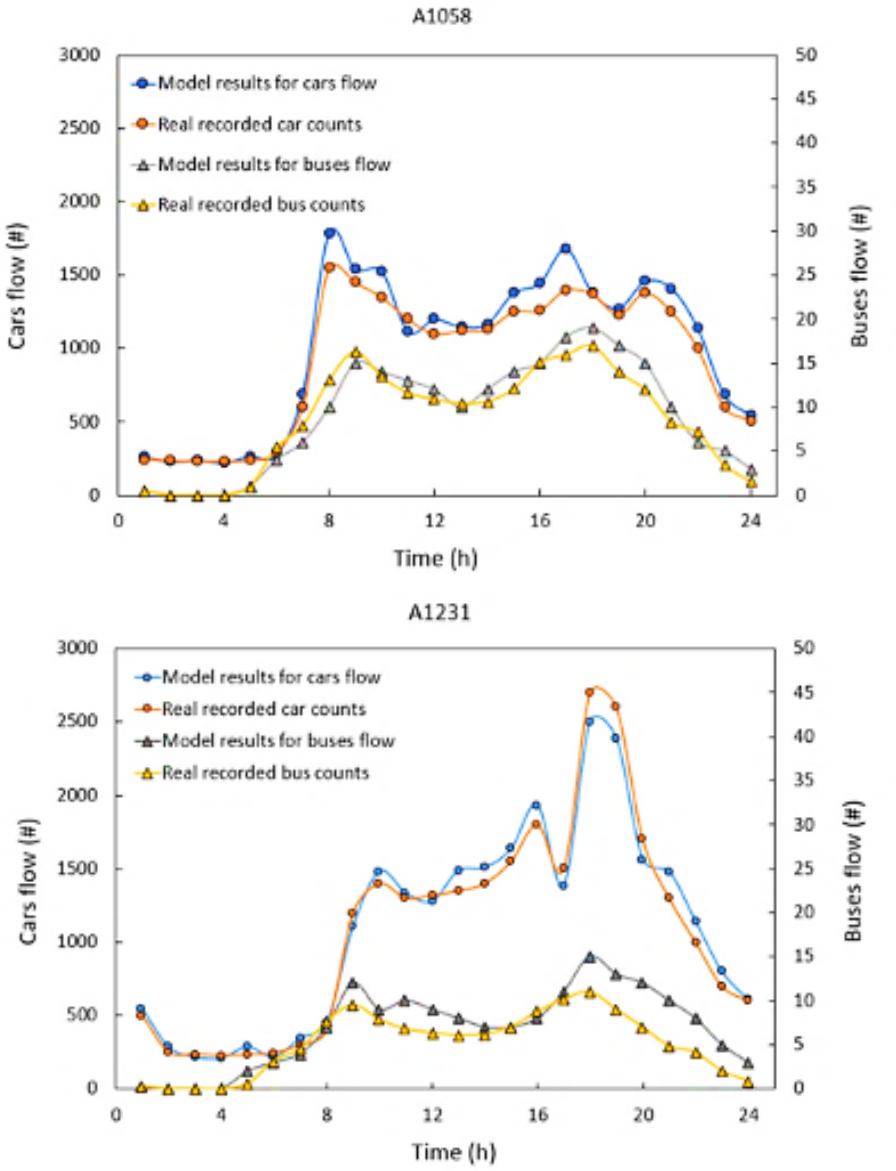


Figure 4.16. Matching the closed and reduced speed roads from simulation and the real recorded data; a) A184 road which is closed due to the deep height of inundation; b) A1058 road with speed reduction (Pictures from [125]); c) Maximum flood depth captured from CityCAT simulation

To verify the accuracy of the routing process in our traffic model, the simulation results generated using SUMO were compared with observed traffic data from a typical weekday, specifically 28 July 2023. At several monitoring locations, the simulated traffic flows were cross-validated against real-world traffic counts obtained from traffic cameras. As shown in Figure 4.17, the comparison includes both buses and passenger vehicles. The model exhibits a high level of accuracy in estimating traffic volumes across different vehicle types, confirming the reliability of the routing mechanism and the validity of the overall traffic simulation.



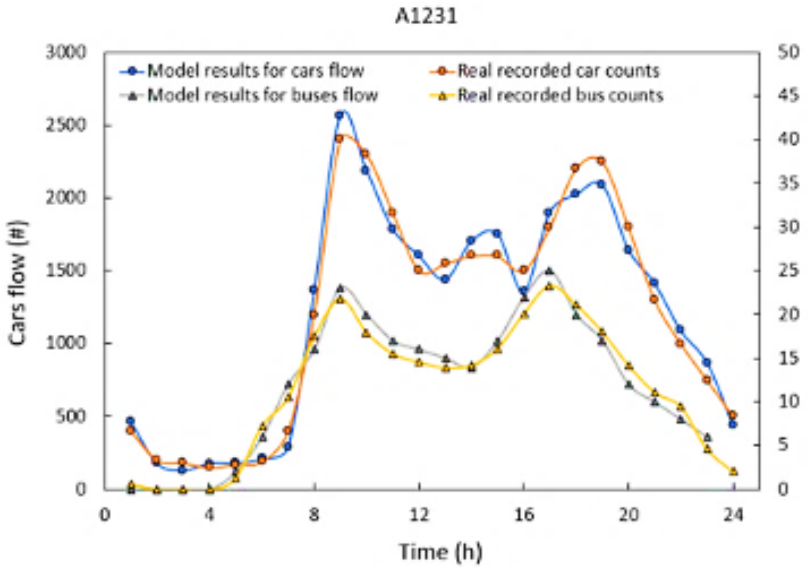


Figure 4.17. Comparison between the traffic flow on 28 June 2023 from traffic modelling (blue/ gray), and the real traffic flow from Tyne and Wear TADU (red/ yellow) (cars/buses per hour).

4.7.2. Validation of the integration tool

Validating transport models during disruptive events is difficult due to the rarity of extreme weather, which results in limited available data. Nevertheless, historical records gathered by the Traffic and Accident Data Unit (TADU) during previous flood events in Tyne and Wear region offer an opportunity for partial validation. To validate the integrated tool as a whole, the well-documented Toon Monsoon flood event using CityCAT was simulated. The resulting flood outputs were processed through the integration equation to determine the disrupted links and subsequently fed into SUMO to simulate traffic conditions under the flood scenario. The model output was then compared with real-world observations of traffic conditions during the Toon Monsoon event in June 2012.

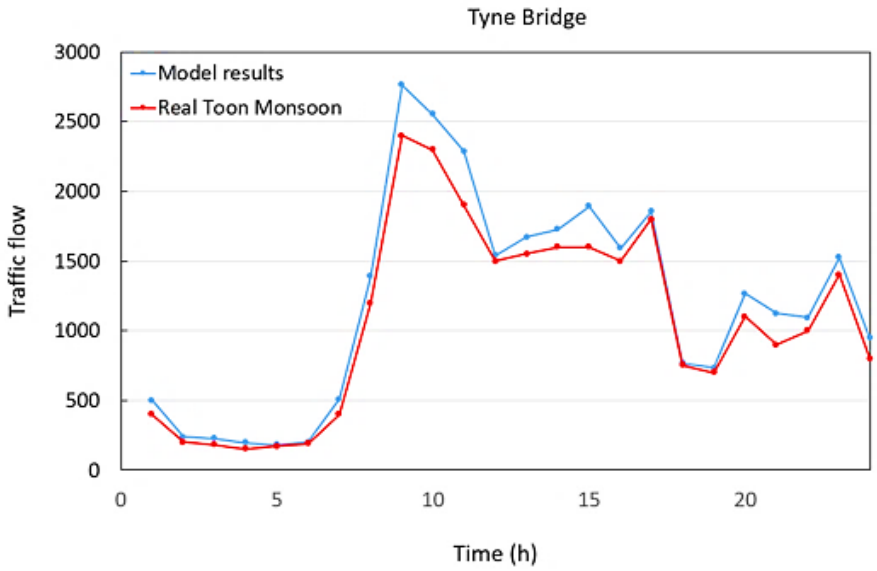
Hourly traffic flows on main road links are recorded by the Tyne and Wear Road Traffic and Accident Data Unit (TADU) by automatic traffic counters (ATCs) and stored in the traffic information database (TRADS). The simulated traffic flows under the flood condition were compared with this real observed traffic data for the same date. An example of recorded data, obtained through automatic traffic counters during the flood on June 28, 2012, is compared to the estimated traffic flow of the flooded traffic model in Figure 4.18.

As shown in Figure 4.18, the simulated results closely align with the real-world data. While there is a slight overestimation in the simulation, this can be reasonably attributed

to population and vehicle growth between 2012 and the reference year used for traffic demand generation (2023). The GEH statistic was computed for each site on an hourly basis. The formula to calculate the GEH is as Equation (20):

$$GEH = \sqrt{\frac{2(M-C)^2}{M+C}} \tag{20}$$

Where M is the model outcome and C is the recorded traffic count. The hourly variation of GEH statistic values across three representative sites: A1058, A1231, and the Tyne Bridge, throughout 24 hours were calculated. The GEH calculation provides a detailed comparison between the simulated and observed traffic flows, highlighting how model accuracy fluctuates during different times of the day. To assess overall accuracy at each site, the daily average GEH was calculated as follows: A1058: 3.43, A1231: 3.75, and Tyne Bridge: 3.72. All average GEH values are well below 5, indicating a strong level of agreement between the simulated and observed traffic flows across all locations. These results confirm the general validity of the traffic simulation model when flood-induced disruptions are integrated into the network.



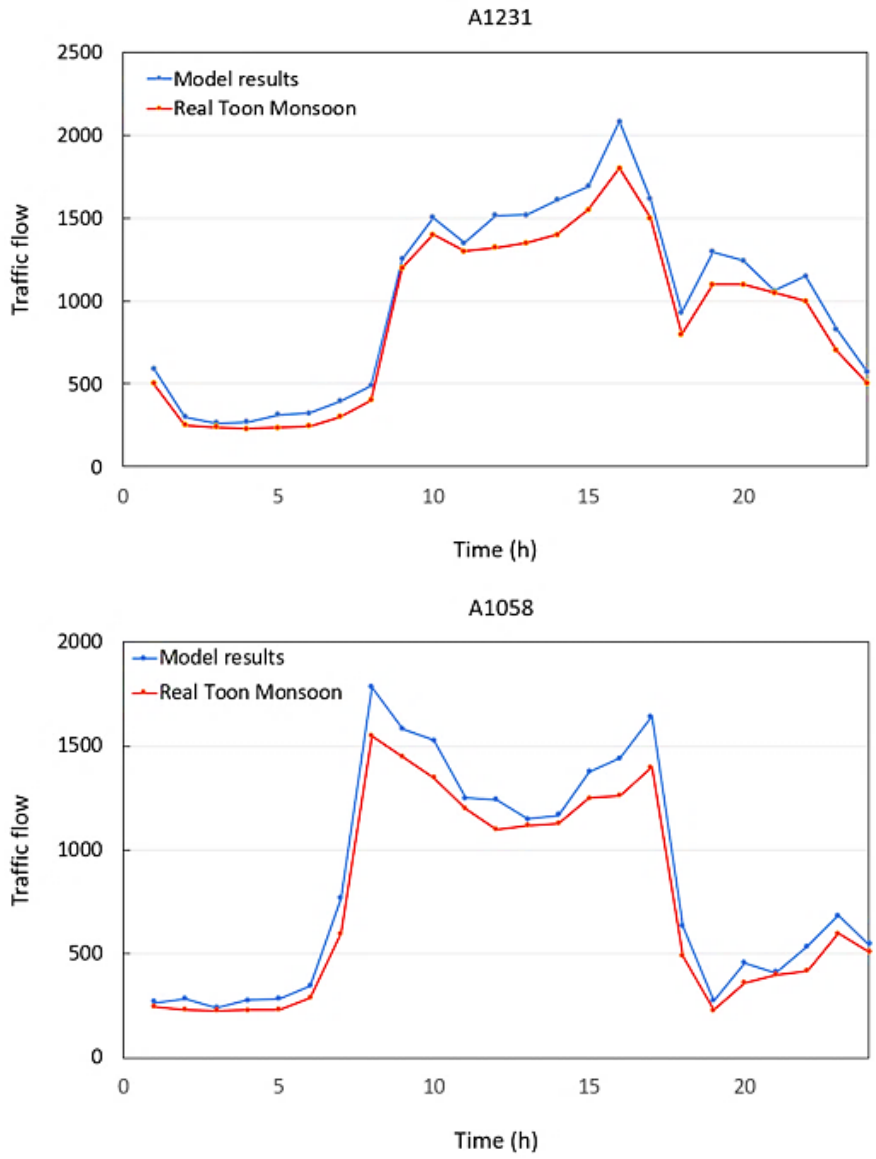


Figure 4.18. Comparison between the disrupted flow of the Toon Monsoon event on 28 June 2023 from traffic modelling (blue), and the real recorded traffic flow from Tyne and Wear TADU (red) (cars per hour).

4.7.3. Spatial correlation analysis

Regarding the cars traffic flow, the analysis of spatial correlation between increased traffic costs and flood depth changes rate reveals no statistically significant relationship in the 1-in-100-year flood scenario, based on both Pearson and Spearman correlation measures (Table 4.3). This implies that roads experiencing the greatest rises in traffic-related costs are not always those most directly affected by flooding. This finding underscores the importance of integrated modelling approaches, as it shows that the indirect consequences of extreme weather events may not spatially coincide with the physical hazards themselves.

Furthermore, although the Pearson test found no significant link between changes in traffic volume and traffic cost, the Spearman rank correlation revealed a consistent and significant positive relationship. This suggests a non-linear but monotonic association, indicating that traffic costs are influenced jointly by flooding and traffic volume variations, in a manner that is not purely linear.

Regarding bus traffic flow, the spatial correlation analysis reveals a moderate negative relationship between the flood depth change rate and traffic cost change, as indicated by the Pearson and Spearman correlation coefficients (Table 4.3). This reflects the modelling assumption that buses, like cars, remain active in the network even under flood conditions. If the flood depth exceeds the 0.3-meter threshold, the corresponding road segment becomes inaccessible, leading to delays. Buses continue to operate according to their scheduled departures, and disruptions manifest primarily through increased travel time.

Table 4.3. Correlation analysis results

Change Rate	**Test**	**Traffic cost change rate of road links (1-in-100 synthetic flood scenario)**	
		Cars	**Bus**
Flood depth change rate	Pearson correlation (2-tailed sigma)	-0.6436 (0.1136)	-0.7261 (0.0352)
	Spearman correlation (2-tailed sigma)	-0.6132 (0.2036)	-0.7415 (0.0213*)
Traffic volume change rate	Pearson correlation (2-tailed sigma)	0.5736 (0.3436)	0.6145 (0.0411)
	Spearman correlation (2-tailed sigma)	0.7576 (0.0004**)	0.7321 (0.0007**)

*Correlation is significant at the 0.05 level (2-tailed)
**Correlation is significant at the 0.01 level (2-tailed)

This approach allows for a more realistic simulation of network-wide dynamics, especially for public transport systems that are expected to maintain service continuity under adverse conditions. Moreover, the relationship between traffic volume change and cost increase is strong and significant for both vehicle types. The observed monotonic correlation, particularly evident in the Spearman coefficients, confirms that variations in network load and congestion levels are closely associated with changes in travel cost. Overall, the results indicate that the flood impacts on buses are substantial but behave in a continuous and predictable manner.

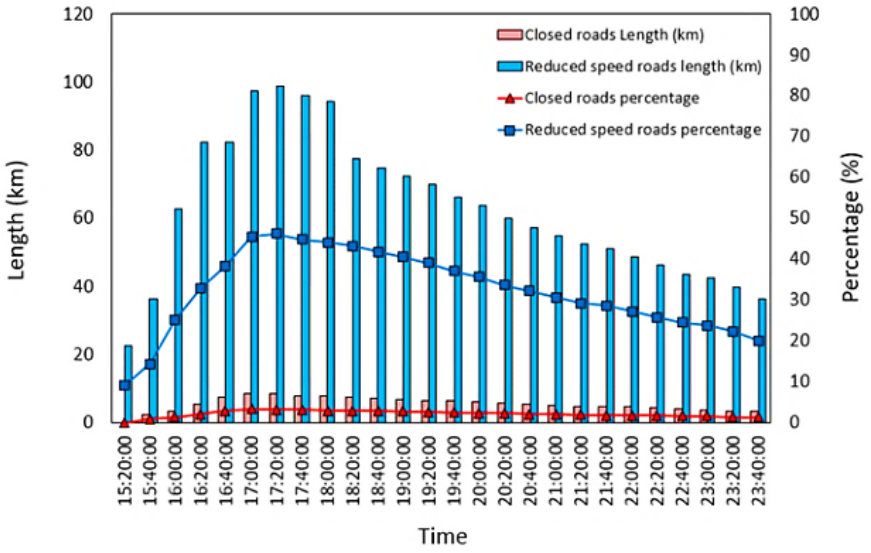
4.7.4. Sensitivity to the rainfall intensity

To examine the robustness of the observed flood impacts on transport network performance, a sensitivity analysis was conducted by simulating two additional synthetic flood scenarios with lower return periods—namely, 1-in-50-year and 1-in-10-year events—alongside the original 1-in-100-year scenario. The aim was to verify whether the same disruption patterns previously observed in the 1-in-100-year flood—such as road closures, speed reductions, and trip delays—are also evident under less extreme but more frequent flooding conditions. Figure 4.19 and Table 4.4 present the results of this analysis.

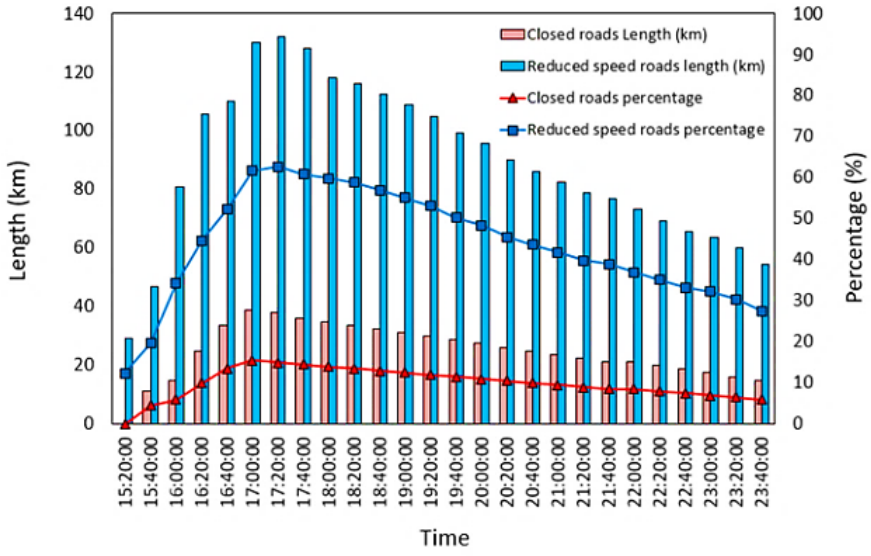
Subplots (a) and (b) illustrate the evolution of the total length and percentage of closed roads and reduced-speed roads throughout the flood period for the 1-in-10 and 1-in-50-year scenarios, respectively. Although the total affected road length is lower compared to the 1-in-100-year flood, the trends remain consistent. The blue bars representing reduced-speed road segments show a clear temporal peak in both cases, while red lines indicate a persistent yet relatively low percentage of full road closures.

Subplots (c) and (d) show the number of running passenger cars and buses over the course of the day. A noticeable decrease in both modes of transport is observed during peak hours in the flooded scenarios compared to the normal condition. The disruption pattern is more moderate in the 1-in-10-year scenario but remains significant in the 1-in-50-year case, particularly for public transport services, which appear more sensitive to network disruption.

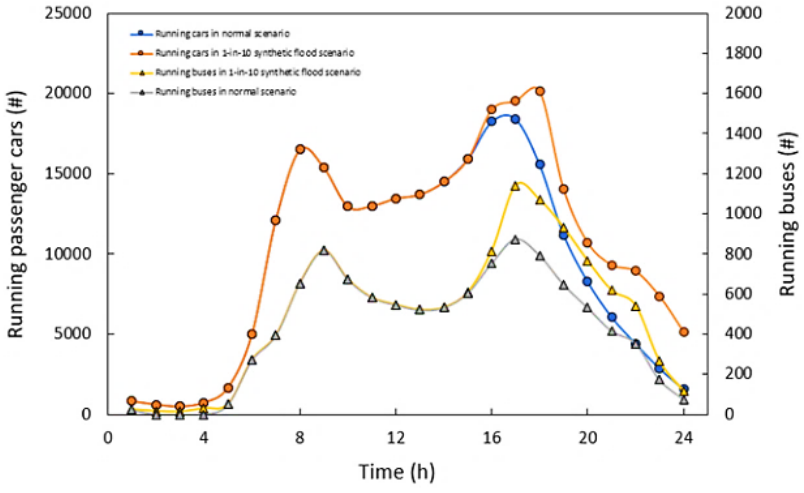
Finally, subplots (e) and (f) present the total trip duration per departure hour under flooded and normal scenarios. The increase in total duration is visible in both cases, especially during the morning and evening peak periods, indicating slower network performance under flood stress. Although the severity of delay is lower than in the 1-in-100-year scenario, the trend of degradation remains consistent.


Closed roads Length (km)
Reduced speed roads length (km)
Closed roads percentage
Reduced speed roads percentage
Length (km)
Percentage (%)
Time

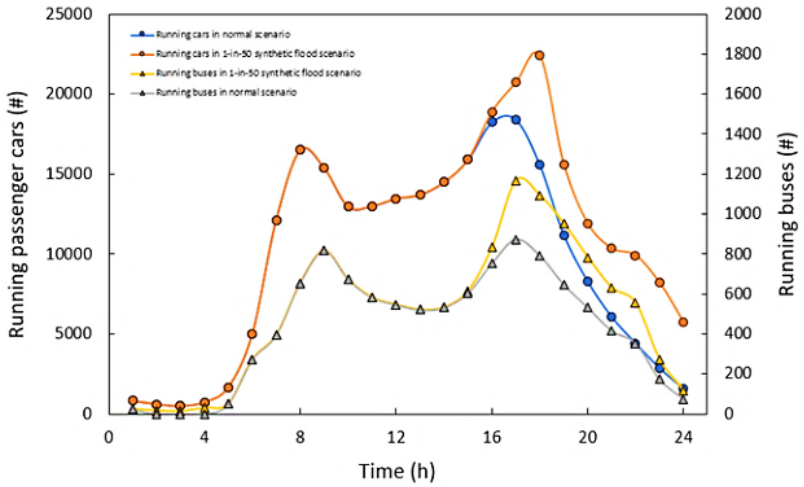
(a)


Closed roads Length (km)
Reduced speed roads length (km)
Closed roads percentage
Reduced speed roads percentage
Length (km)
Percentage (%)
Time

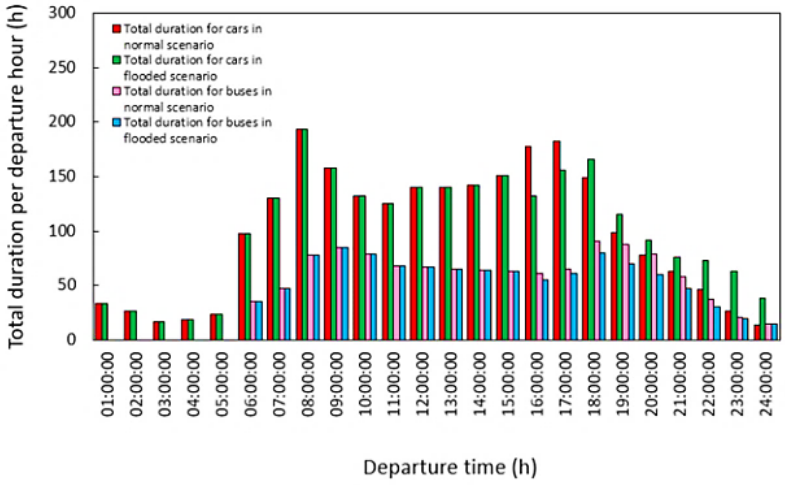
(b)


Running cars in normal scenario
Running cars in 1-in-10 synthetic flood scenario
Running buses in 1-in-10 synthetic flood scenario
Running buses in normal scenario
Running passenger cars (#)
Running buses (#)
Time (h)

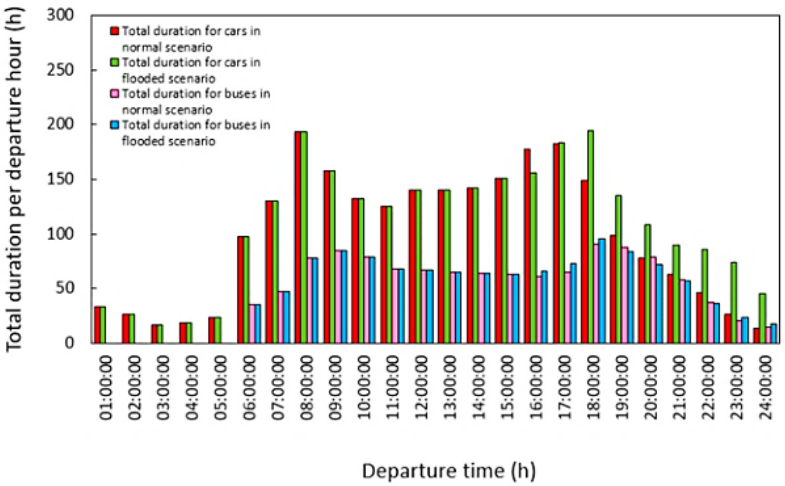
(c)



(d)



(e)



(f)

Figure 4.19. Road length and percentage of closed roads or speed-reduced roads, and percentage of closed bus routes over the flooding time for a) 1-in-10 and b) 1-in-50 year synthetic flood; running vehicles over time for c) 1-in-10 and d) 1-in-50 year synthetic flood; average trip duration per departure hour for e) 1-in-10 and f) 1-in-50 year synthetic flood.

In addition to the operational indicators presented earlier, Table 4.4 quantifies the indirect traffic costs associated with the 1-in-10 and 1-in-50 synthetic flood scenarios, compared to the base scenario. These costs include the value of passenger hours lost and the resulting monetary costs due to travel time delay time and emissions. The results show that the total indirect cost rises sharply from £79,468 in the base case to £251,646 under the 1-in-10-year scenario and to £374,889 in the 1-in-50-year case, corresponding to relative increases of 217% and 372%, respectively. This significant rise in cost with decreasing flood return period highlights the economic vulnerability of the network even under more frequent but less extreme events.

Table 4.4. Indirect traffic cost of 1-in-10 and 1-in-50 synthetic scenarios on the main roads of Tyne and Wear region, UK.

Parameter	Base scenario		1-in-10 scenario		1-in-50 scenario	
	Cars	Bus	Cars	Bus	Cars	Bus
PHD (h)	-		11,482	5,136	19,684	7,548
C_{time} (£)	0	0	116,083	51,925	199,005	76,310
C_e (£)	79,468	0	83,638	0	99,574	0
Total cost (£)	79,468		251,646		374,889	
Relative increase (%)	-		217%		372%	

Overall, the sensitivity analysis confirms that the transport network remains vulnerable across a range of flood severities. The consistent patterns observed—though with varying intensity—suggest that even more frequent, moderate floods can lead to considerable disruption, emphasizing the need for resilient transport planning across all hazard levels.

4.8. CONCLUSION

This chapter has demonstrated a comprehensive methodology for assessing the indirect costs and traffic impacts of flood-induced disruptions in an urban road network, with a focus on both private cars and public buses. The Tyne and Wear region, characterized by its dense road infrastructure and high exposure to pluvial flooding, served as an ideal case study to apply and validate the proposed integration framework. Using dynamic simulations integrated with real flood and traffic data, the study reveals several important findings that carry implications for transport resilience planning and public transport operations under climate-related disruptions.

The 1-in-100-year synthetic flood scenario, used as the baseline extreme event, showed that up to 68% of the main road network experienced speed reductions and around

30% faced full closure at the flood's peak. These disruptions led to significant increases in vehicle travel time and congestion, particularly during peak traffic hours. A consistent recovery pattern was observed over time, but certain parts of the network remained impaired well into the evening, demonstrating the slow dissipation of flood effects.

Although buses represented a smaller share of total traffic, their operational characteristics—fixed routes, scheduled departures, and lack of rerouting flexibility—resulted in considerable delays and reduced network coverage during flooding. Unlike cars that adapt through dynamic rerouting, buses remained stuck in congestion, leading to reduced trip distances and prolonged presence in the network.

More importantly, after converting vehicle-hours of delay into person-hours using realistic occupancy factors (25 passengers per bus), the analysis revealed that buses contributed substantially to the overall economic loss. In the 1-in-100-year flood scenario, buses were responsible for 8,781 person-hours of delay, leading to a cost of £88,776 in time lost—despite not contributing to emissions due to the assumption of full electrification. This highlights the amplified societal cost of delayed public transport, even under optimistic environmental assumptions.

Flooding not only increased trip duration but also affected total route length. Passenger cars were found to take longer detours, resulting in increased kilometers travelled. In contrast, buses under flood conditions covered shorter distances due to their inability to complete routes or make progress through blocked or congested areas. This mismatch further underscores the inflexibility of public transport systems during urban floods.

Indirect traffic costs rose from £79,468 under normal conditions to £360,519 under the 1-in-100-year flood—representing a 354% increase. Buses accounted for over 63% of this increase, despite being fewer in number. Sensitivity analysis showed similar trends for 1-in-50 and 1-in-10-year floods, with relative increases of 372% and 217%, respectively. These results confirm that even less severe, more frequent floods carry substantial economic consequences for both transport users and operators.

The simulation results were validated using multiple independent datasets, including traffic count records from 2012 and 2023, rainfall data from five meteorological

stations, and real-world observations from the Toon Monsoon event. The simulated outputs closely matched recorded traffic flows, and GEH statistics remained well below acceptable thresholds across multiple sites, reinforcing the credibility of the integrated flood-traffic modelling framework.

Spatial correlation analysis revealed that traffic cost increases are not always co-located with areas of highest flood depth. For cars, there was no statistically significant linear relationship between cost increase and flood depth, while for buses, a moderate negative correlation was found. However, traffic volume changes showed a strong positive correlation with cost increase in both cases, indicating that network congestion, not just flood exposure, is a primary driver of indirect traffic costs.

Overall, this chapter demonstrates that road network disruptions due to urban flooding have profound effects not only on physical mobility but also on economic and societal levels—particularly for public transportation systems. The insights gained emphasize the need to incorporate public transit considerations into flood resilience planning and highlight the value of dynamic, integrated models for understanding and mitigating transport impacts under climate stress. Future work should explore more adaptive bus operation strategies, passenger behavioural responses, and real-time system management under extreme weather scenarios.

CHAPTER 5

RESILIENCE ASSESSMENT AND MITIGATION MEASURES

5.1. INTRODUCTION

This chapter presents the dynamic resilience assessment of the main roads network in Tyne and Wear region under the synthetic flood scenarios induced by a two-hour rainfall event. It then proceeds to identify the most critical segments of the network through targeted analysis. Finally, the potential impact of proposed mitigation measures on network performance and resilience is evaluated.

5.2. RESILIENCE QUANTIFICATION

As discussed in the Methodology chapter, in this research, a dynamic approach was adopted for resilience assessment. Unlike conventional snapshot-based approaches that assess resilience at a single peak moment, this research captures the temporal evolution of network resilience throughout the flood's impact period. Separate resilience profiles are generated for cars and buses, reflecting their differing levels of routing flexibility. While cars are able to reroute dynamically in response to flooded links, buses typically follow fixed routes and are more vulnerable to prolonged disruptions. Therefore, all metrics are calculated independently for each vehicle class.

As an example, and to illustrate the network's resilience calculation at lowest value, metric values are given in Table 5.1 to Table 5.4 for the hour of maximum impact—defined as the time when the network experiences the greatest traffic disruption (i.e., the lowest overall performance compared to normal conditions). The compliance matrix converts each performance value to a binary indicator by comparing it with its predefined threshold: 1 indicates the metric meets or exceeds the threshold, and 0 indicates it does not. The partial resilience index is then the percentage of metrics with value 1 under each flood category.

Table 5.1. Performance matrix for Tyne and Wear main roads network for cars at the hour of maximum impact (17:00)

Metrics	**Flood category**		
	L	**M**	**H**
Safety	1	0.87	0.41
Accessibility	1	0.63	0.58
Reliability	0.68	0.37	0.09
Efficiency	0.73	0.53	0.05

Table 5.2. Compliance matrix for Tyne and Wear main roads network for cars at the hour of maximum impact (17:00)

Metrics	**Flood category**			**Partial resilience index**
	L	**M**	**H**	
Safety	1	0	0	33%
Accessibility	1	1	1	100%
Reliability	0	0	0	0%
Efficiency	0	1	0	33%
Capacity to cope with the given flood category	50%	50%	25%	Resilience = 42%

Table 5.3. Performance matrix for Tyne and Wear main roads network for buses at the hour of maximum impact (17:00)

Metrics	**Flood category**		
	L	**M**	**H**
Safety	1	0.78	0.34
Accessibility	1	0.67	0.12
Reliability	0.59	0.29	0.07
Efficiency	0.27	0.27	0.27

Table 5.4. Compliance matrix for Tyne and Wear main roads network for buses at the hour of maximum impact (17:00)

Metrics	**Flood category**			**Partial resilience index**
	L	**M**	**H**	
Safety	1	0	0	33%
Accessibility	1	1	0	66%
Reliability	0	0	0	0%
Efficiency	0	0	1	33%
Capacity to cope with the given flood category	50%	25%	25%	Resilience = 33%

The temporal variations of each metric—as well as the overall resilience score—are illustrated in two time-series plots (see Figure 5.1 and Figure 5.2). Specifically, Figure 5.1 illustrates the evolution of network resilience metrics for cars, and Figure 5.2 presents the corresponding trends for buses.

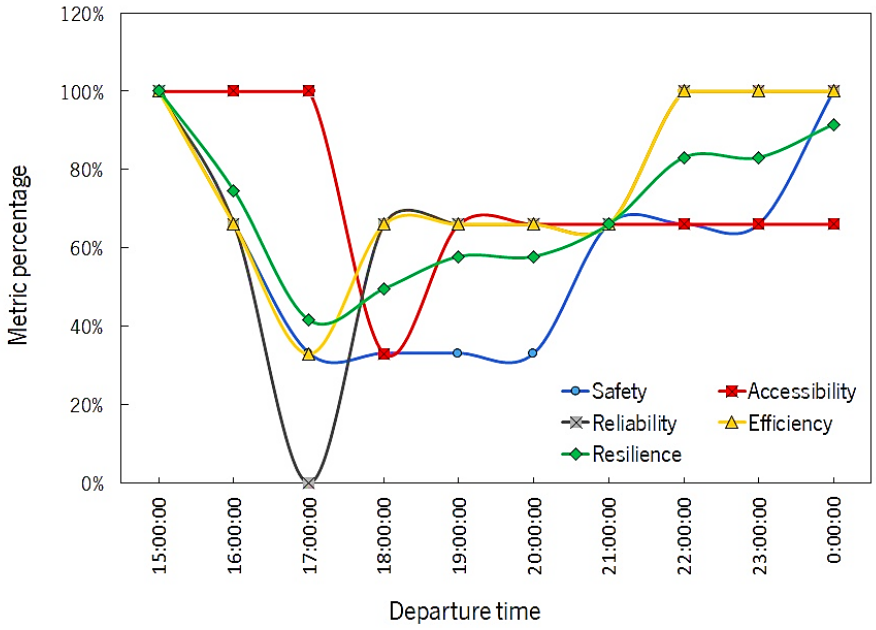


Figure 5.1. Evolution of network resilience metrics for car users

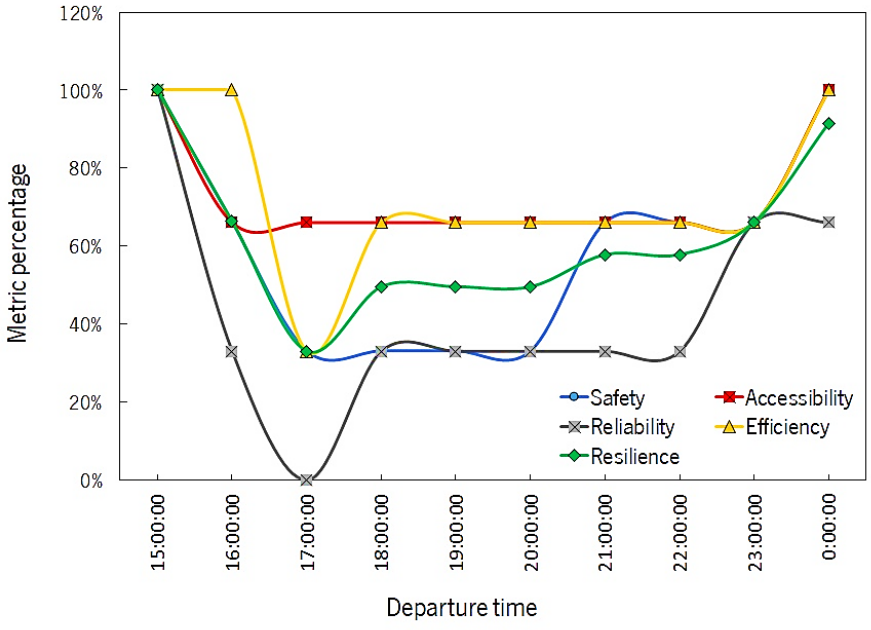


Figure 5.2. Evolution of network resilience metrics for bus users

For car users (Figure 5.1), all metrics experience a sharp initial decline immediately after the onset of disruption (around 16:00), reflecting the combined effects of flooded road segments, reduced route availability, and increased congestion due to diversions. The

largest drop is observed in reliability, which falls to approximately 60%, indicating significant variability and delays in travel times compared to normal conditions. Safety and accessibility also decrease but to a lesser extent, suggesting that although some routes remain physically safe and connected, their travel times become considerably less predictable. Efficiency follows a similar pattern to reliability but remains slightly higher, showing that the geometric efficiency of available routes is partly preserved despite the disruption. After reaching the minimum point around 18:00 h, all metrics recover gradually as floodwaters recede and road availability improves.

For buses (Figure 5.2), the disruption impact is more severe, particularly for accessibility and performance, which drop to below 50% at the lowest point (around 18:00 h). This sharper decline reflects the greater vulnerability of fixed-route services to road closures and delays; detours or loss of critical road segments can disproportionately disrupt bus operations compared to private vehicles. Reliability for bus users also exhibits a significant decrease, reaching its lowest value earlier in the disruption period and recovering more slowly than in the car network. This is consistent with the compounded effect of traffic congestion and the reduced operational flexibility of buses. Safety remains relatively high, similar to the car network, indicating that the majority of bus routes are not directly exposed to unsafe flood depths but are still affected indirectly through network congestion and rerouting. The resilience index for buses thus shows a deeper trough and a slower recovery slope compared to cars, highlighting the need for targeted adaptation measures for public transport services.

Comparing the two Figure 5.1 and Figure 5.2, it is evident that while both vehicle classes follow the same overall temporal pattern—initial sharp decline followed by gradual recovery—buses experience a greater magnitude of loss in accessibility and efficiency, slower recovery rates across most metrics, and a resilience curve with a longer lag before returning to near-normal values.

These results confirm that although the road network as a whole begins to regain functionality within a few hours after peak flooding, public transport services remain more disrupted for a longer period. This underscores the importance of incorporating mode-specific resilience strategies into flood risk management.

Finally, for each hour of the flood event, a resilience score is computed by integrating the weighted values of the two vehicle class flows. The overall resilience of the main roads network over the disruption time is shown in Figure 5.3.

As shown in Figure 5.3, the overall network resilience—calculated by weighting the resilience of cars and buses according to their respective traffic flows—exhibits a marked decline immediately after the onset of flooding, dropping from its pre-disruption level of 100% to approximately 38% at the lowest point around 17:00. This decrease reflects the combined effects of reduced accessibility, degraded reliability, and diminished efficiency across both vehicle classes. Following this trough, the network demonstrates a gradual recovery, with resilience steadily increasing as floodwaters recede and traffic conditions stabilise, reaching around 90% by midnight. The recovery pattern indicates that while the main road network is capable of regaining most of its operational functionality within several hours, some residual disruption persists beyond the peak flood period.

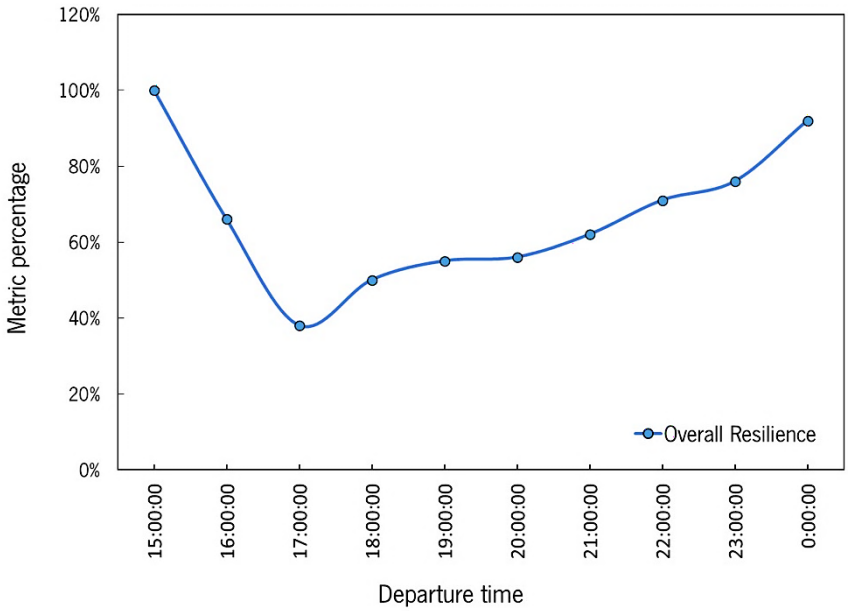


Figure 5.3. Overall resilience of the network over time.

The hourly resilience values are then analysed to quantify the rate of degradation (Decline Rate) and the rate of recovery (Recovery Rate), thereby offering a more comprehensive and time-sensitive representation of network resilience. Based on the results shown in Figure 5.3, the network experienced a decline rate of approximately 31% per hour, indicating a rapid loss of functional performance in the initial stages of the disruption. In contrast, the recovery rate was approximately 7.4% per hour, reflecting a much slower

restoration of network functionality as flood conditions subsided. This asymmetry between the speed of degradation and recovery highlights the network's vulnerability to sudden flood-induced failures and the extended time required to return to near-normal operational conditions. Such a disparity underscores the importance of proactive resilience measures that can slow down the rate of decline and accelerate recovery following extreme events.

5.3. MOST CRITICAL PARTS OF THE NETWORK

To improve the resilience of the network and reduce the indirect costs of flooded traffic, it is necessary to identify the best location for interventions. However, during a hazard event, identifying priority intervention areas requires a more comprehensive approach. An effective method involves using a matrix that integrates both hazard severity and exposure levels, allowing for the identification of critical road links [126]. Table 5.5 presents a matrix-based approach that combines the maximum flood depth from the 1-in-100-year return period (hazard) with the average normal traffic flow (exposure) to assess the criticality of road segments. This scenario represents the most disruptive conditions. The ranking is performed separately for passenger cars and buses, offering a comparative analysis of their respective impacts. Figure 5.4 illustrates the application of this matrix to the Tyne and Wear region, highlighting high-risk areas (marked in red circles and green rectangles) where both vulnerability and traffic flows are elevated for cars and buses, respectively. This analysis pinpoints the top three road links within the network for cars and buses, separately. In order of criticality are

For cars:

- A: A1058 (Jesmond Road, section of the coast road in Newcastle);
- B: A167 (Central motorway east of Newcastle); and
- C: A1 (bypassing Newcastle to the west).

For buses:

- A: A1058 (Jesmond Road, section of the coast road in Newcastle);
- B: A184 (bypassing Gateshead to the west); and
- C: A193 (New bridge street).

Table 5.5. The assessment of road link criticality is based on the severity of the hazard and the level of vehicle exposure. Road links are then classified into four categories: N (negligible), L (low criticality), M (medium criticality), and H (high criticality). (adopted from [13]).

(a)		Exposure (Number of cars/day)			
		Minor 0 - 20000	Moderate 20001 - 40000	Major 40001 - 60000	Severe >60000
Flood depth (m)	Minor (0 - 0,1)	N	L	L	M
	Moderate (0,1 – 0,2)	L	L	M	M
	Major (0,2 – 0,3)	L	M	M	H
	Severe (>0,3)	M	M	H	H
(b)		Exposure (Number of buses /day)			
		Minor 0 - 200	Moderate 201- 400	Major 401 - 600	Severe >600
Flood depth (m)	Minor (0 - 0,1)	N	L	L	M
	Moderate (0,1 – 0,2)	L	L	M	M
	Major (0,2 – 0,3)	L	M	M	H
	Severe (>0,3)	M	M	H	H



Figure 5.4. Critical Roads for cars and buses in Tyne and Wear main roads network.

5.4. INDIRECT COSTS REDUCTION AND RESILIENCE IMPROVEMENT BY MITIGATION MEASURES

Mitigation strategies play a crucial role in enhancing the resilience of transportation networks by addressing vulnerabilities in critical locations. In this study, traditional engineering mitigation measures are employed to reinforce key segments of the network.

According to Pregnolato *et al.* [55], one of the primary mitigation strategies involves 'hardening' critical road links to make them resistant to flood events. This can be achieved through the road elevation which means raising the level of vulnerable road segments to prevent inundation, or drainage system improvements that enhance stormwater drainage infrastructure to mitigate flood accumulation, or usage of runoff storage tanks that means installing underground or roadside tanks to temporarily store excess water. In the simulation process, hardened links are assumed to function as they would under normal, undisrupted conditions. Consequently, their free-flow speed should be maintained as the baseline scenario throughout the entire disrupted simulation period.

Four different mitigation scenarios were simulated to test their effectiveness in indirect costs reduction and improving network resilience. These scenarios involved implementing interventions separately, first at critical locations along passenger car routes, then bus routes, and then both car and bus routes. As shown in Figure 5.4, the most critical road for cars and buses is the same (A1058).

Table 5.6. Results of the mitigation scenarios

Label	Return period	Adoptation	Total indirect cost (£)	Minimum resilience
NA-0	No flood	No adaptation	-	100%
NA-100	100-years	No adaptation	360,519	38%
HC-100	100-years	Harden all 3 critical roads for cars	337,102	47%
HB-100	100-years	Harden all 3 critical roads for buses	339,764	43%
HC&B-100	100-years	Harden the most critical road for both cars & buses	338,348	41%
HA-100	100-years	Harden all 5 critical roads for cars & buses	316,763	57%

The results of the simulated mitigation scenarios (Table 5.6) demonstrate that hardening critical road links can yield measurable improvements in network resilience during extreme flood events. Under the baseline 100-year flood scenario without adaptation (NA-100), the

total indirect cost is £360,519, corresponding to the minimum resilience score of 38%. Implementing targeted hardening for the three most critical passenger car routes (HC-100) slightly reduces indirect costs to £337,102 and improves the minimum resilience to 47%. Similarly, reinforcing the three most critical bus routes (HB-100) reduces costs to £339,764 and raises resilience to 43%, suggesting that car-focused interventions have a greater influence on overall network performance than bus-focused ones. Interestingly, hardening only a single critical road that is shared by both cars and buses (HC&B-100) produces nearly identical indirect costs (£338,343) and minimum resilience (41%) to the bus-only intervention, despite requiring significantly fewer link upgrades. This highlights the importance of pre-intervention analysis: upgrading a single strategically located link can yield similar benefits to more extensive interventions, but at a potentially much lower implementation cost. The most comprehensive approach—reinforcing all five critical roads for both modes (HA-100)—offers the highest benefit, reducing costs to £316,763 and increasing minimum resilience to 57%. Overall, these results emphasize that while broader interventions deliver the greatest gains, targeted and well-prioritized upgrades can achieve cost-effective resilience improvements.

5.5. CONCLUSION

This chapter presented a dynamic resilience assessment of the main road network in Tyne and Wear under synthetic flood scenarios, identifying the most critical links for both passenger cars and buses, and evaluating the effectiveness of targeted engineering mitigation measures. The results confirmed that flooding causes a rapid degradation in network performance, with a significantly faster decline rate (31% per hour) than recovery rate (7.4% per hour). While both vehicle classes exhibited similar temporal resilience patterns, buses experienced greater losses in safety and reliability, and slower recovery, underscoring their higher vulnerability to fixed-route disruptions.

The criticality analysis, integrating hazard severity and traffic exposure due to the 1-in-100-year synthetic flood, revealed that the A1058 is the most critical link for both cars and buses, with other high-priority links differing between modes. This mode-specific prioritisation demonstrates the importance of considering heterogeneous travel behaviour and operational constraints in resilience planning.

Mitigation scenario simulations showed that hardening critical road links can lead to measurable improvements in resilience and reductions in indirect costs. While comprehensive interventions (HA-100) yielded the highest minimum resilience gain (57%), targeted improvements such as upgrading a single shared critical link (HC&B-100) achieved similar resilience outcomes to more extensive bus-only interventions, but with potentially lower implementation costs. This finding highlights the value of pre-intervention analysis in identifying cost-effective strategies that maximise benefits with minimal resource expenditure.

Future work should focus on several key areas. First, integrating economic evaluation with lifecycle cost analysis of interventions could better inform investment decisions. Second, extending the methodology to include active transport modes and freight movements would offer a broader understanding of multi-modal network resilience. Third, considering dynamic adaptation strategies—such as temporary bus re-routing, adaptive traffic signal control, or staged hardening—could reveal more flexible and scalable mitigation pathways. Finally, validating the resilience assessment framework using empirical post-event traffic and flood data would strengthen its applicability for operational decision-making and long-term infrastructure planning.

Overall, the findings of this chapter reinforce the necessity of mode-specific, evidence-based resilience strategies and the benefits of targeted, prioritised interventions for optimising the functionality of transport networks under extreme flood conditions.

CHAPTER 6

CONCLUSIONS

6.1. INTRODUCTION

This chapter synthesises the key outcomes of the research, integrating the results from the methodology, modelling, and analysis presented in previous chapters. The study aimed to enhance understanding of transport network vulnerability and resilience under pluvial flooding by combining hydrodynamic and traffic simulation models in a novel, dynamic integration framework.

The main roads network of Tyne and Wear (UK) served as the case study, providing a realistic and complex urban context in which to apply and test the developed framework. The research brought together flood hazard modelling using CityCAT and traffic simulation using SUMO, resulting in the development of a dynamic CityCAT–SUMO integration tool that enables time-dependent analysis of disruption impacts and recovery patterns.

A major methodological innovation was the explicit modelling of two distinct vehicle classes — passenger cars and buses — to assess whether omitting buses, as is common in literature, meaningfully affects resilience and indirect cost estimations. Alongside this, the study developed a dynamic resilience assessment methodology capable of capturing both the rate of functional degradation and the rate of recovery, while also quantifying indirect cost.

6.2. CONTRIBUTIONS TO RESEARCH DOMAIN

This research makes several key contributions to the literature and practice of transport resilience assessment:

1. Development of a dynamic integration tool
    - Created a fully functional CityCAT–SUMO integration workflow, enabling automated transfer of spatial–temporal flood hazard data into a traffic simulation environment.
    - The tool supports link-by-link, time-dependent hazard inputs, allowing simulation of realistic network disruptions over multi-hour events.
2. Dynamic resilience assessment methodology
    - Introduced a resilience evaluation approach that captures temporal evolution rather than static peak impacts, including decline rate and recovery rate metrics.
    - Applied the method to four resilience dimensions: safety, accessibility, reliability, and efficiency.
3. Two-vehicle-class (passenger and public transport) modelling
    - Modelled and analysed passenger cars and buses separately to capture their distinct resilience profiles and operational vulnerabilities.
    - Demonstrated that buses — due to fixed routing and lower operational flexibility — face greater accessibility and efficiency losses and slower recovery than cars.
4. Indirect cost quantification linked to resilience
    - Integrated indirect cost modelling (value of time + CO_2 emissions) with resilience analysis for each vehicle class.
    - Showed how resilience loss directly translates to monetary losses, with different cost contributions from cars and buses.
5. Hazard–exposure criticality mapping
    - Developed a matrix approach combining flood depth severity with average traffic flows to rank critical road links for each vehicle class.
    - Enabled targeted mitigation strategies to be designed based on mode-specific vulnerability.

6. Scenario-based adaptation evaluation
    - Tested multiple hardening strategies, from targeted single-link upgrades to full multi-link reinforcement and compared their resilience and cost benefits.
    - Showed that strategic single-link upgrades can, in some cases, achieve nearly the same benefits as more extensive and expensive interventions.

Table 6.1 presents the updated mapping between literature gaps and this research's contributions.

Table 6.1. Research gaps identified from literature and how this study addressed them

Research gap	How this research addressed it	Relevant chapters
Lack of open-source integrated dynamic modelling between flood hazard and traffic simulation tools.	Developed a CityCAT–SUMO integration tool enabling link-level, time-varying hazard inputs into traffic simulation.	Ch. 3–4
Predominance of static resilience assessment methods.	Designed and applied a dynamic resilience framework with degradation and recovery rate metrics over the disruption period.	Ch. 3, Ch. 5
Limited analysis of multiple vehicle classes.	Modelled cars and buses separately, quantifying resilience and cost impacts for each, and showing implications of ignoring buses.	Ch. 4–5
Insufficient link between hazard severity and exposure in identifying network vulnerabilities.	Applied hazard–exposure criticality mapping for cars and buses separately to identify top critical links.	Ch. 5
Limited evaluation of cost-effective mitigation.	Tested targeted vs. broad hardening scenarios and identified cases where targeted interventions matched broader strategies.	Ch. 5

6.3. SYNTHESIS OF FINDINGS

The integration of CityCAT and SUMO enabled the creation of a realistic simulation environment in which flooding effects were applied dynamically to the road network. This produced more realistic representations of how traffic conditions evolve during and after storm compared to static approaches. Key findings include:

- Buses are more vulnerable in accessibility and efficiency metrics, and their recovery is slower than that of cars.

- Indirect costs are mode-dependent — while car users contribute more to total costs due to their larger share of trips, bus disruptions cause significant societal impacts by reducing public transport accessibility.
- Critical link identification revealed that some links are shared in importance between cars and buses, meaning that hardening them can benefit both modes simultaneously.
- Mitigation strategies must be informed by hazard–exposure analysis to avoid unnecessary expenditure on low-priority links.

6.4. CONCLUSIONS

Detailed conclusions have been provided throughout the preceding chapters, each addressing specific aspects of the research. This section consolidates the key findings, summarizing the main conclusions drawn from this study in direct relation to the research objectives:

- Review of current methods and frameworks for traffic assessment in flooded transport networks

The state-of-the-art review in Chapter 2 provided a comprehensive examination of existing approaches, including topological, statistical, and simulation-based methods. The review highlighted the limitations of static analyses and the absence of detailed, time-varying integration between hydrodynamic and traffic simulation models. It also identified the frequent omission of certain transport modes (notably buses) from resilience assessments, despite their potential vulnerability. These findings underscored the need for a dynamic, multimodal, and integrated modelling framework.

- Development of a dynamic integration tool for resilience assessment

Chapters 3 and 4 presented the development of a dynamic integration tool that links the CityCAT hydrodynamic flood model with the SUMO traffic microsimulation model. This tool automatically transfers time-varying, link-specific flood depth data to the traffic simulation environment, enabling realistic, hour-by-hour disruption modelling. The integration supports the evaluation of network performance under evolving flood conditions and is adaptable to other networks and hazard types.

- Validation of the integrated framework with real flood event data

The framework was validated using the Toon Monsoon event (June 28, 2012) in the Tyne and Wear region. Comparison with observed data from the Traffic and Accident Data Unit (TADU) showed that the model could accurately reproduce the spatial and temporal patterns of disruption. Empirical speed–depth relationships were implemented to ensure realistic vehicle behaviour under flood conditions. The validated framework demonstrates high applicability for resilience planning in flood-prone urban regions.

- Differential impacts of flooding on passenger cars and buses

A major novelty of this research was the explicit modelling of two vehicle classes—passenger cars and buses—to assess whether excluding buses, as commonly done in literature, leads to significant underestimation of disruption impacts. Results confirmed that buses, due to fixed routes and lower rerouting flexibility, experience greater accessibility losses, higher travel time increases, and slower recovery than cars. Even partial flooding along bus corridors caused notable increases in indirect costs. This finding challenges the assumption that buses can be ignored in flood resilience analysis of road networks.

- Dynamic resilience assessment and indirect cost quantification

Chapter 5 introduced a dynamic resilience methodology that accounts for both the rate of functional degradation and the rate of recovery over the disruption period. This approach was applied to multiple metrics (safety, accessibility, reliability, and efficiency) for each vehicle class. The framework was extended to include indirect cost analysis, quantifying time-related costs and CO_2 emission costs under each scenario. Results revealed a clear relationship between resilience loss and monetary loss, and highlighted mode-specific cost contributions.

- Evaluation of targeted and network-wide adaptation strategies

Multiple hardening scenarios were tested, from single critical-link reinforcement to full multi-link upgrades. Hazard–exposure mapping identified critical roads for each vehicle class. Results showed that, in some cases, targeted single-link reinforcement can deliver

similar resilience and cost benefits to more extensive interventions, offering a cost-effective alternative. This demonstrates the importance of pre-intervention analysis to prioritise adaptation measures based on both hazard severity and traffic exposure.

6.5. LIMITATIONS AND FUTURE WORK SUGGESTIONS

This final section highlights the limitations of certain approaches implemented in this thesis and proposes potential directions for future research. The recommendations aim to refine and expand the methods developed in this study, addressing existing constraints while encouraging further exploration of complementary and emerging perspectives. By identifying areas for improvement and extension, this section provides a foundation for advancing research on transport network resilience, fostering more comprehensive and robust analytical frameworks in future studies.

- Scope of hazard types

  While this research focused exclusively on pluvial flooding, the developed dynamic integration tool — combining the CityCAT hydrodynamic model with the SUMO microscopic traffic simulator — has the flexibility to be applied to other hazard types, such as fluvial flooding, storm surges, or even non-weather-related disruptions like wildfires and earthquakes. Extending the framework to multi-hazard scenarios would require defining appropriate hazard-disruption relationships (e.g., temperature-induced rail buckling) and incorporating their temporal dynamics into the simulation.

- Multimodal transport representation

  A novel feature of this work was the explicit inclusion of public transport (buses) as a separate vehicle class in the dynamic flood–traffic modelling process. This allowed quantification of bus-specific vulnerabilities and their contribution to overall indirect costs and network resilience. However, other public transport modes (e.g., rail, metro, ferries) were not included. Expanding the model to capture the resilience of a fully multimodal transport system would provide a more comprehensive assessment, especially in urban contexts where interdependencies between modes are significant.

- Adaptation strategy diversity

This thesis examined hard engineering interventions such as road hardening and elevation, applying them in different combinations to critical links. The results showed that optimising interventions through targeted selection can achieve similar resilience gains with fewer treated links, reducing costs. Future research could explore combined adaptation portfolios that integrate both hard engineering and nature-based solutions — such as green infrastructure, permeable pavements, and urban wetlands — to achieve cumulative and sustainable resilience improvements.

- Integration of structural and functional damage assessments

The resilience evaluation here was based on network functionality loss (e.g., reduced speed, closures) without explicitly modelling structural damage to infrastructure. Future studies should integrate structural fragility analysis with network performance modelling to capture both physical damage and functional disruption. Such a holistic approach would more accurately reflect the cascading impacts of extreme events and guide prioritisation of interventions.

- Dynamic resilience analysis extension

This research assessed resilience dynamically across the disruption period, providing time-varying resilience curves for different vehicle classes. However, recovery dynamics were simplified and assumed constant once floodwaters receded. Incorporating more detailed, hazard-specific recovery models — including partial reopening of links, staged drainage improvements, or real-time traffic management — would enhance the realism of the resilience assessment.

- Indirect cost estimation refinement

Indirect costs in this study were computed for both passenger cars and buses, using travel time increases and value-of-time assumptions. These estimates could be further refined by integrating real economic data from operators, incorporating passenger load factors, and extending the scope to include freight costs and environmental externalities (e.g., emissions).

- Model calibration and transferability

While the framework was validated using the 2012 Toon Monsoon event in Tyne and Wear, its transferability to other regions depends on local data availability and calibration. Future research should apply and validate the tool in diverse geographical contexts, especially in data-scarce regions, to test its robustness and identify data-minimal configurations.

BIBLIOGRAPHY

[1] S. Re, Natural catastrophes and man-made disasters in 2011, Sigma. (2011).

[2] B. Evans, A.S. Chen, S. Djordjević, J. Webber, A.G. Gómez, J. Stevens, Investigating the Effects of Pluvial Flooding and Climate Change on Traffic Flows in Barcelona and Bristol, Sustainability. 12 (2020) 2330.

[3] A. Kadaverugu, K.V. Gorthi, N.R. Chintala, Impacts of Urban Floods on Road Connectivity-A Review and Systematic Bibliometric Analysis, Curr. World Environ. 16 (2021) 575.

[4] S. Tachaudomdach, K. Arunotayanun, A. Upayokin, A systematic review of the resilience of transportation infrastructures affected by flooding, in: Proc. Asia-Pacific Conf. Intell. Med. 2018 Int. Conf. Transp. Traffic Eng. 2018, 2018: pp. 176–182.

[5] A. Rebally, C. Valeo, J. He, S. Saidi, Flood Impact Assessments on Transportation Networks: A Review of Methods and Associated Temporal and Spatial Scales. Front. Sustain, Cities. 3 (2021) 732181.

[6] M. Bruneau, S.E. Chang, R.T. Eguchi, G.C. Lee, T.D. O'Rourke, A.M. Reinhorn, M. Shinozuka, K. Tierney, W.A. Wallace, D. Von Winterfeldt, A framework to quantitatively assess and enhance the seismic resilience of communities, Earthq. Spectra. 19 (2003) 733–752.

[7] P. Suarez, W. Anderson, V. Mahal, T.R. Lakshmanan, Impacts of flooding and climate change on urban transportation: A systemwide performance assessment of the Boston Metro Area, Transp. Res. Part D Transp. Environ. 10 (2005) 231–244.

[8] Z.Y. Jasour, A.C. Reilly, G.L. Tonn, C.M. Ferreira, Roadway flooding as a bellwether for household retreat in rural, coastal regions vulnerable to sea-level rise, Clim. Risk Manag. 36 (2022) 100425.

[9] R.K. Pachauri, L. Mayer, Intergovernmental Panel on Climate Change, Climate Change 2014, Synthesis Report, IPCC Geneva, Switz. (2014).

[10] E. Hooper, L. Chapman, A. Quinn, Investigating the impact of precipitation on vehicle speeds on UK motorways, Meteorol. Appl. 21 (2014) 194–201.

[11] S.D. Drobot, C. Benight, E.C. Gruntfest, Risk factors for driving into flooded roads, Environ. Hazards. 7 (2007) 227–234.

[12] V. Murray, K.L. Ebi, IPCC special report on managing the risks of extreme events and disasters to advance climate change adaptation (SREX), J Epidemiol Community Heal. 66 (2012) 759–760.

[13] M. Pregnolato, A. Ford, V. Glenis, S. Wilkinson, R. Dawson, Impact of climate change on disruption to urban transport networks from pluvial flooding, J. Infrastruct. Syst. 23 (2017) 4017015.

[14] R. Zhou, H. Zheng, Y. Liu, G. Xie, W. Wan, Flood impacts on urban road connectivity in southern China, Sci. Rep. 12 (2022) 16866.

[15] Y. He, S. Thies, P. Avner, J. Rentschler, The Impact of Flooding on Urban Transit and Accessibility, (2020).

[16] Z. Wang, N. Zhou, J. Wang, Using Hopkinson pressure bar to perform dynamic tensile tests on SFRC at medium strain rates, Mag. Concr. Res. 64 (2012) 657–664.

[17] R. Faturechi, E. Miller-Hooks, Travel time resilience of roadway networks under disaster, Transp. Res. Part B Methodol. 70 (2014) 47–64.

[18] P. Apivatanagul, R. Davidson, B. Blanton, L. Nozick, Long-term regional hurricane hazard analysis for wind and storm surge, Coast. Eng. 58 (2011) 499–509.

[19] F.J. Shahdani, M. Santamaria-Ariza, H.S. Sousa, M. Coelho, J.C. Matos, Assessing Flood Indirect Impacts on Road Transport Networks Applying Mesoscopic Traffic Modelling: The Case Study of Santarém, Portugal, Appl. Sci. 12 (2022) 3076.

[20] S. Webb, Concrete jungle: How much of the surface area of the UK is taken up by roads? Does anything eat wasps?, Profile Books, London, 2005.

[21] J.-P. Rodrigue, The geography of transport systems, Routledge, 2020.

[22] L.-Z. Mao, H.-G. Zhu, L.-R. Duan, The social cost of traffic congestion and countermeasures in Beijing, in: Sustain. Transp. Syst. Plan, Des. Build, Manag. Maint., 2012: pp. 68–76.

[23] E. Dalziell, A. Nicholson, Risk and impact of natural hazards on a road network, J. Transp. Eng. 127 (2001) 159–166.

[24] E. Zio, Critical infrastructures vulnerability and risk analysis, Eur. J. Secur. Res. 1 (2016) 97–114.

[25] I.G. Kasmalkar, K.A. Serafin, Y. Miao, I.A. Bick, L. Ortolano, D. Ouyang, J. Suckale, When floods hit the road: Resilience to flood-related traffic disruption in the San Francisco Bay Area and beyond, Sci. Adv. 6 (2020) eaba2423.

[26] M. Borowska-Stefańska, M. Kowalski, S. Wiśniewski, The Measurement of Mobility-Based Accessibility—The Impact of Floods on Trips of Various Length and Motivation, ISPRS Int. J. Geo-Information. 8 (2019) 534.

[27] T. Ahmad, A.C. Pandey, A. Kumar, Impact of 2014 Kashmir flood on land use/land cover transformation in Dal lake and its surroundings, Kashmir valley, SN Appl. Sci. 2 (2020) 681.

[28] I.G. Kasmalkar, K.A. Serafin, J. Suckale, Integrating urban traffic models with coastal flood maps to quantify the resilience of traffic systems to episodic coastal flooding, MethodsX. 8 (2021) 101483.

[29] Y. Alabbad, J. Mount, A.M. Campbell, I. Demir, Assessment of transportation system disruption and accessibility to critical amenities during flooding: Iowa case study, Sci. Total Environ. 793 (2021) 148476.

[30] B. Hankin, I. Craigen, W. Rogers, J. Morphet, A. Bailey, M. Whitehead, Flood risk to the strategic road network in England, in: E3S Web Conf., EDP Sciences, 2016: p. 10001.

[31] N. Chen, S. Yao, C. Wang, W. Du, A method for urban flood risk assessment and zoning considering road environments and terrain, Sustainability. 11 (2019) 2734.

[32] J. Hackl, J.C. Lam, M. Heitzler, B.T. Adey, L. Hurni, Estimating network related risks: A methodology and an application in the transport sector, Nat. Hazards Earth Syst. Sci. 18 (2018) 2273–2293.

[33] L.S. Smith, Q. Liang, Towards a generalised GPU/CPU shallow-flow modelling tool,

Comput. Fluids. 88 (2013) 334–343.

[34] S. Loreti, E. Ser-Giacomi, A. Zischg, M. Keiler, M. Barthelemy, Local impacts on road networks and access to critical locations during extreme floods, Sci. Rep. 12 (2022) 1552.

[35] R. Vacondio, A. Dal Palù, P. Mignosa, GPU-enhanced finite volume shallow water solver for fast flood simulations, Environ. Model. Softw. 57 (2014) 60–75.

[36] V. Glenis, V. Kutija, C.G. Kilsby, A fully hydrodynamic urban flood modelling system representing buildings, green space and interventions, Environ. Model. Softw. 109 (2018) 272–292.

[37] J. Sohn, Evaluating the significance of highway network links under the flood damage: An accessibility approach, Transp. Res. Part A Policy Pract. 40 (2006) 491–506.

[38] J. Gao, S. V Buldyrev, H.E. Stanley, S. Havlin, Networks formed from interdependent networks, Nat. Phys. 8 (2012) 40–48.

[39] A.C. Testa, M.N. Furtado, A. Alipour, Resilience of coastal transportation networks faced with extreme climatic events, Transp. Res. Rec. 2532 (2015) 29–36.

[40] S. Dong, X. Gao, A. Mostafavi, J. Gao, Modest flooding can trigger catastrophic road network collapse due to compound failure, Commun. Earth Environ. 3 (2022) 38.

[41] K. Barker, J.E. Ramirez-Marquez, C.M. Rocco, Resilience-based network component importance measures, Reliab. Eng. Syst. Saf. 117 (2013) 89–97.

[42] M.J. Anderson, D.A.F. Kiddle, T.M. Logan, The underestimated role of the transportation network: Improving disaster & community resilience, Transp. Res. Part D Transp. Environ. 106 (2022) 103218.

[43] J. Barceló, J. Casas, D. García, J. Perarnau, Methodological notes on combining macro, meso and micro models for transportation analysis, in: Work. Model. Simul., Citeseer, 2005: pp. 1–40.

[44] E.J. Moore, W. Kichainukon, U. Phalavonk, Maximum flow in road networks with speed-dependent capacities-application to Bangkok traffic., Songklanakarin J. Sci.

Technol. 35 (2013).

[45] H. Chang, M. Lafrenz, I.-W. Jung, M. Figliozzi, D. Platman, C. Pederson, Potential impacts of climate change on flood-induced travel disruptions: a case study of Portland, Oregon, USA, in: Geogr. Clim. Chang., Routledge, 2013: pp. 231–245.

[46] J. Yin, D. Yu, Z. Yin, M. Liu, Q. He, Evaluating the impact and risk of pluvial flash flood on intra-urban road network: A case study in the city center of Shanghai, China, J. Hydrol. 537 (2016) 138–145.

[47] P. Singh, V.S.P. Sinha, A. Vijhani, N. Pahuja, Vulnerability assessment of urban road network from urban flood, Int. J. Disaster Risk Reduct. 28 (2018) 237–250.

[48] S. Shabou, I. Ruin, C. Lutoff, S. Debionne, S. Anquetin, J.-D. Creutin, X. Beaufils, MobRISK: a model for assessing the exposure of road users to flash flood events, Nat. Hazards Earth Syst. Sci. 17 (2017) 1631–1651.

[49] W. Wang, S. Yang, J. Gao, F. Hu, W. Zhao, H.E. Stanley, An Integrated Approach for Assessing the Impact of Large-Scale Future Floods on a Highway Transport System, Risk Anal. 40 (2020) 1780–1794.

[50] K. Pyatkova, A.S. Chen, S. Djordjević, D. Butler, Z. Vojinović, Y.A. Abebe, M. Hammond, Flood impacts on road transportation using microscopic traffic modelling techniques, in: Simulating Urban Traffic Scenar., Springer, 2019: pp. 115–126.

[51] K.L. Knight, G. Hou, A.S. Bhaskar, S. Chen, Assessing the Use of Dual-Drainage Modeling to Determine the Effects of Green Stormwater Infrastructure on Roadway Flooding and Traffic Performance, Water. 13 (2021) 1563.

[52] K. Pyatkova, A.S. Chen, D. Butler, Z. Vojinović, S. Djordjević, Assessing the knock-on effects of flooding on road transportation, J. Environ. Manage. 244 (2019) 48–60.

[53] D. Li, X. Zhu, G. Huang, H. Feng, S. Zhu, X. Li, A hybrid method for evaluating the resilience of urban road traffic network under flood disaster: An example of Nanjing, China, Environ. Sci. Pollut. Res. 29 (2022) 46306–46324.

[54] A. Pérez-Morales, F. Gomariz-Castillo, P. Pardo-Zaragoza, Vulnerability of transport networks to multi-scenario flooding and optimum location of emergency

management centers, Water. 11 (2019) 1197.

[55] M. Pregnolato, A. Ford, S.M. Wilkinson, R.J. Dawson, The impact of flooding on road transport: A depth-disruption function, Transp. Res. Part D Transp. Environ. 55 (2017) 67–81.

[56] W. Wang, S. Yang, H.E. Stanley, J. Gao, Local floods induce large-scale abrupt failures of road networks, Nat. Commun. 10 (2019) 2114.

[57] Y. Alabbad, I. Demir, Understanding flood risk in public transit systems: Insights from accessibility and vulnerability analysis in Iowa, Int. J. Disaster Risk Reduct. (2025) 105615.

[58] T. Zhu, H. Li, Y. Wu, Y. Jiang, J. Pan, Z. Dai, Resilience Assessment of Urban Bus–Metro Hybrid Networks in Flood Disasters: A Case Study of Zhengzhou, China, Sustainability. 17 (2025) 4591.

[59] F. Ma, F. Liu, K.F. Yuen, P. Lai, Q. Sun, X. Li, Cascading failures and vulnerability evolution in bus–metro complex bilayer networks under rainstorm weather conditions, Int. J. Environ. Res. Public Health. 16 (2019) 329.

[60] L. Huang, H. Huang, Y. Wang, Resilience analysis of traffic network under emergencies: a case study of bus transit network, Appl. Sci. 13 (2023) 8835.

[61] S. Mudigonda, K. Ozbay, B. Bartin, Evaluating the resilience and recovery of public transit system using big data: Case study from New Jersey, J. Transp. Saf. Secur. 11 (2019) 491–519.

[62] Y. Zhang, S.T. Ng, A hypothesis-driven framework for resilience analysis of public transport network under compound failure scenarios, Int. J. Crit. Infrastruct. Prot. 35 (2021) 100455.

[63] A. Kermanshah, S. Derrible, Robustness of road systems to extreme flooding: using elements of GIS, travel demand, and network science, Nat. Hazards. 86 (2017) 151–164.

[64] N. Yadav, S. Chatterjee, A.R. Ganguly, Resilience of urban transport network-of-networks under intense flood hazards exacerbated by targeted attacks, Sci. Rep. 10

(2020) 10350.

[65] Y. Xing, J. Lu, S. Chen, S. Dissanayake, Vulnerability analysis of urban rail transit based on complex network theory: a case study of Shanghai Metro, Public Transp. 9 (2017) 501–525.

[66] T. Papilloud, M. Keiler, Vulnerability patterns of road network to extreme floods based on accessibility measures, Transp. Res. Part D Transp. Environ. 100 (2021) 103045.

[67] Y. Yang, S.T. Ng, S. Zhou, F.J. Xu, H. Li, Physics-based resilience assessment of interdependent civil infrastructure systems with condition-varying components: A case with stormwater drainage system and road transport system, Sustain. Cities Soc. 54 (2020) 101886.

[68] H. Baroud, K. Barker, J.E. Ramirez-Marquez, C.M. Rocco, Inherent costs and interdependent impacts of infrastructure network resilience, Risk Anal. 35 (2015) 642–662.

[69] H. Ishibashi, M. Akiyama, D.M. Frangopol, S. Koshimura, T. Kojima, K. Nanami, Framework for estimating the risk and resilience of road networks with bridges and embankments under both seismic and tsunami hazards, Struct. Infrastruct. Eng. 17 (2020) 494–514.

[70] O. Moura Rezende, A.B. Ribeiro da Cruz de Franco, A.K. Beleño de Oliveira, A.C. Pitzer Jacob, M. Gomes Miguez, A framework to introduce urban flood resilience into the design of flood control alternatives, J. Hydrol. 576 (2019) 478–493.

[71] O.M. Rezende, F.M. Miranda, A.N. Haddad, M.G. Miguez, A framework to evaluate urban flood resilience of design alternatives for flood defence considering future adverse scenarios, Water. 11 (2019) 1485.

[72] M.T.S. Aghababaei, S.B. Costello, P. Ranjitkar, Measures to evaluate post-disaster trip resilience on road networks, J. Transp. Geogr. 95 (2021) 103154.

[73] T.M. Logan, M.J. Anderson, A.C. Reilly, Risk of isolation increases the expected burden from sea-level rise, Nat. Clim. Chang. 13 (2023) 397–402.

[74] M. Loli, G. Kefalas, S. Dafis, S.A. Mitoulis, F. Schmidt, Bridge-specific flood risk assessment of transport networks using GIS and remotely sensed data, Sci. Total Environ. 850 (2022) 157976.

[75] A. Anisha, A. Jacob, R. Davis, S. Mangalathu, Fragility functions for highway RC bridge under various flood scenarios, Eng. Struct. 260 (2022) 114244.

[76] N. Zhang, A. Alipour, A multi-step assessment framework for optimization of flood mitigation strategies in transportation networks, Int. J. Disaster Risk Reduct. 63 (2021) 102439.

[77] J.Y. Lee, H.J. Moon, T.I. Kim, H.W. Kim, M.Y. Han, Quantitative analysis on the urban flood mitigation effect by the extensive green roof system, Environ. Pollut. 181 (2013) 257–261.

[78] T. Sarmah, S. Das, Urban flood mitigation planning for Guwahati: A case of Bharalu basin, J. Environ. Manage. 206 (2018) 1155–1165.

[79] S.A. Mitoulis, S.A. Argyroudis, M. Loli, B. Imam, Restoration models for quantifying flood resilience of bridges, Eng. Struct. 238 (2021) 112180.

[80] M. Pregnolato, A. Ford, C. Robson, V. Glenis, S. Barr, R. Dawson, Assessing urban strategies for reducing the impacts of extreme weather on infrastructure networks, R. Soc. Open Sci. 3 (2016) 160023.

[81] S. Starita, M.P. Scaparra, J.R. O'Hanley, A dynamic model for road protection against flooding, J. Oper. Res. Soc. 68 (2017) 74–88.

[82] L.A.P. Jardim Gonçalves, S. Ferreira, P.J.G. Ribeiro, Assessing Urban Mobility Resilience: An Exploratory Approach Using Hazard-Based Duration Models, Electronics. 13 (2024) 4220.

[83] J. Li, Y. Zhou, Optimizing risk mitigation investment strategies for improving post-earthquake road network resilience, Int. J. Transp. Sci. Technol. 9 (2020) 277–286.

[84] M. Goerigk, K. Deghdak, P. Heßler, A comprehensive evacuation planning model and genetic solution algorithm, Transp. Res. Part E Logist. Transp. Rev. 71 (2014) 82–97.

[85] A. Kashyap, D. Ghose, P.P. Menon, P.B. Sujit, K. Das, UAV aided dynamic routing of

resources in a flood scenario, in: 2019 Int. Conf. Unmanned Aircr. Syst., IEEE, 2019: pp. 328–335.

[86] X. He, H. Zheng, S. Peeta, Model and a solution algorithm for the dynamic resource allocation problem for large-scale transportation network evacuation, Transp. Res. Procedia. 7 (2015) 441–458.

[87] S. Bretschneider, A. Kimms, Pattern-based evacuation planning for urban areas, Eur. J. Oper. Res. 216 (2012) 57–69.

[88] P. Lertworawanich, Highway network restoration after the great flood in Thailand, Nat. Hazards. 64 (2012) 873–886.

[89] T. Zhao, Y. Zhang, Transportation infrastructure restoration optimization considering mobility and accessibility in resilience measures, Transp. Res. Part C Emerg. Technol. 117 (2020) 102700.

[90] M. Akiyama, D.M. Frangopol, H. Ishibashi, Toward life-cycle reliability-, risk-and resilience-based design and assessment of bridges and bridge networks under independent and interacting hazards: emphasis on earthquake, tsunami and corrosion, Struct. Infrastruct. Eng. 16 (2020) 26–50.

[91] D.K. Devendiran, S. Banerjee, A. Mondal, Impact of climate change on multihazard performance of river-crossing bridges: Risk, resilience, and adaptation, J. Perform. Constr. Facil. 35 (2021) 4020127.

[92] C. Iliadis, V. Glenis, C. Kilsby, Representing buildings and urban features in hydrodynamic flood models, J. Flood Risk Manag. 17 (2024) e12950.

[93] Ordnance Survey. OS Terrain 5 [Internet]. Southampton: Ordnance Survey; [cited 2026 Mar 26]. Available from: https://www.ordnancesurvey.co.uk/products/os-terrain-5, (n.d.).

[94] A.W. Warrick, Soil water dynamics, Oxford University Press, 2003.

[95] C. Bourdarias, M. Ersoy, S. Gerbi, A mathematical model for unsteady mixed flows in closed water pipes, Sci. China Math. 55 (2012) 221–244.

[96] N.C. Council, Summer 2012 flooding in Newcastle upon Tyne, Total Res. Tech. Serv.

Report. Newcastle City Counc. (2013).

[97] R. Robson, A., and Duncan, Flood estimation handbook, Centre for Ecology and Hydrology, Wallingford, U.K, 1999.

[98] OpenStreetMap contributors, OpenStreetMap contributors. Planet dump [Internet]. Cambridge: OpenStreetMap Foundation; 2017 [cited 2026 Mar 26]. Available from: https://www.openstreetmap.org, (n.d.).

[99] DLR. Routes from observation points – SUMO documentation [Internet]. Cologne: German Aerospace Center (DLR); [cited 2026 Mar 26]. Available from: https://sumo.dlr.de/docs/Demand/Routes_from_Observation_Points.html, (n.d.).

[100] TransitFeeds. Association of Train Operating Companies – GTFS feed [Internet]. n.p.: TransitFeeds; [cited 2026 Mar 26]. Available from: https://transitfeeds.com/p/association-of-train-operating-companies/284, (n.d.).

[101] DLR. GTFS import – SUMO tools documentation [Internet]. Cologne: German Aerospace Center (DLR); [cited 2026 Mar 26]. Available from: https://sumo.dlr.de/docs/Tools/Import/GTFS.html, (n.d.).

[102] DLR. Automatic routing – SUMO documentation [Internet]. Cologne: German Aerospace Center (DLR); [cited 2026 Mar 26]. Available from: https://sumo.dlr.de/docs/Demand/Automatic_Routing.html, (n.d.).

[103] Wikipedia. Dijkstra's algorithm [Internet]. San Francisco: Wikimedia Foundation; [cited 2026 Mar 26]. Available from: https://en.wikipedia.org/wiki/Dijkstra%27s_algorithm, (n.d.).

[104] P. Bocchini, D.M. Frangopol, T. Ummenhofer, T. Zinke, Resilience and sustainability of civil infrastructure: Toward a unified approach, J. Infrastruct. Syst. 20 (2014) 4014004.

[105] UK Department for Transport (DfT), TAG data book (Transport Analysis Guidance), 2023.

[106] F.& R.A. (Defra) UK Department for Environment, Air quality appraisal: damage cost guidance, 2023.

[107] E. Arango, M. Nogal, M. Yang, H.S. Sousa, M.G. Stewart, J.C. Matos, Dynamic thresholds for the resilience assessment of road traffic networks to wildfires, Reliab. Eng. Syst. Saf. 238 (2023) 109407.

[108] L.-G. Mattsson, E. Jenelius, Vulnerability and resilience of transport systems–A discussion of recent research, Transp. Res. Part A Policy Pract. 81 (2015) 16–34.

[109] M. Nogal, O.M. Nápoles, A. O'Connor, Structured expert judgement to understand the intrinsic vulnerability of traffic networks, Transp. Res. Part A Policy Pract. 127 (2019) 136–152.

[110] Wikipedia. Tyne and Wear [Internet]. San Francisco: Wikimedia Foundation; [cited 2026 Mar 26]. Available from: https://en.wikipedia.org/wiki/Tyne_and_Wear, (n.d.).

[111] Department for Transport Department for Transport annual report and accounts 2022 to 2023. Available at: https://www.gov.uk/government/publications/dft-annual-report-and-accounts-2022-to-2023/department-for-transport-annual-report-and-accounts-2022-to-202, (2023).

[112] Nexus. Transport for Tyne and Wear [Internet]. Newcastle upon Tyne: Nexus; [cited 2026 Mar 26]. Available from: https://www.nexus.org.uk/, (n.d.).

[113] N.G. Wright, C. Thorne, Delivering and evaluating multiple flood risk benefits in blue-green cities, (2014).

[114] T.I.D. (TRADS), Traffic and Accident Data Unit (TRADS). Hourly traffic flows dashboard [Internet]. London: Department for Transport; [cited 2026 Mar 26]. Available from: https://tinyurl.com/gbaadtdashboard, Https://Tinyurl.Com/Gbaadtdashboard. (n.d.).

[115] Geofabrik. Tyne and Wear – OpenStreetMap data download [Internet]. Karlsruhe: Geofabrik GmbH; 2023 [cited 2026 Mar 26]. Available from: https://download.geofabrik.de/europe/united-kingdom/england/tyne-and-wear.html, (n.d.).

[116] Department for Transport. Bus open data service downloads [Internet]. London: UK Government; 2024 [cited 2026 Mar 26]. Available from: https://data.bus-

data.dft.gov.uk/downloads/, (n.d.).

[117] Environment Agency. Hydrology data explorer [Internet]. London: Environment Agency; [cited 2026 Mar 26]. Available from: https://environment.data.gov.uk/hydrology/explore, (n.d.).

[118] Department for Transport. Road traffic statistics: Region 11 [Internet]. London: UK Government; [cited 2026 Mar 26]. Available from: https://roadtraffic.dft.gov.uk/regions/11, (n.d.).

[119] Department for Transport. Department for Transport annual report and accounts 2022 to 2023 [Internet]. London: UK Government; 2023 [cited 2026 Mar 26]. Available from: https://www.gov.uk/government/publications/dft-annual-report-and-accounts-2022-to-2023/, (n.d.).

[120] Environment Agency Hydrology Data Explorer. Available at: https://environment.data.gov.uk/hydrology/explore, (2026).

[121] D. Han, M. Bray, Automated Thiessen polygon generation, Water Resour. Res. 42 (2006).

[122] A. Robson, D. Reed, Flood estimation handbook: statistical procedures for flood frequency estimation, Centre for Ecology and Hydrology, 2008.

[123] UK Department for Transport (DfT), Annual bus statistics: year ending March 2023 (revised), 2023.

[124] Liu Y, Ford A, Dawson RJ, Pyatkova K, Tang J, Wan Y, Yang S. Flood impact on urban transport networks considering the flooding propagation [Internet]. Rochester: SSRN; 2024 [cited 2026 Mar 26]. Available from: https://dx.doi.org/10.2139/ssrn.5007414, (n.d.).

[125] ChronicleLive. Readers' memories of the Great Storm 2012 [Internet]. Newcastle upon Tyne: Reach plc; [cited 2026 Mar 26]. Available from: https://www.chroniclelive.co.uk/news/history/gallery/readers-memories-great-storm-2012-13256642, (n.d.).

[126] M. LARSEN, K.A. Pihl, The Blue spot model-development of a screening method to

assess flood risk on highways, Rep. Danish Road Dir. (2010).